A THEORETICAL AND EXPERIMENTAL STUDY OF THE MECHANISM OF AXOPLASMIC CONVECTION IN NERVE FIBERS DRIVEN BY PERISTALTIC SURFACE WAVES

BY

ROBERT JOHN BIONDI

A DISSERTATION

PRESENTED IN PARTIAL FULFILLMENT OF

THE REQUIREMENTS FOR THE DEGREE

OF

DOCTOR OF ENGINEERING SCIENCE IN MECHANICAL ENGINEERING

AT

NEWARK COLLEGE OF ENGINEERING

Newark, New Jersey
1971

ABSTRACT

In the study of cell biology, investigators have found that substances which are produced within the cell nucleus are sometimes found throughout the cell at points distant from the site of production. In the case of nerve cells (neurons), this is particularly dramatic because of the unusual elongated geometry of these cells.

A neuron possesses a cylindrical tubular extension called an "axon" or "axis cylinder" which is characterized by a large length-to-diameter ratio (10^3-10^6). The existence of a continuous proximo-distal flow of axoplasm within these cylindrical axons has now been demonstrated by numerous investigators. In this study, engineering techniques are employed to explore the role of microperistalsis as a possible driving mechanism for this axoplasmic flow.

An experimental technique for injecting axons (5-10 microns-diameter) with micropipettes under visual microscopic control has been perfected. A new technique for microcapillary tube viscometric measurements applicable to micro samples of biological materials is presented. Using these techniques, a flow curve has been obtained for the axoplasmic substance. The results of these experiments indicate that axoplasm behaves as a highly viscous, pseudoplastic material. No evidence of significant time-dependent thixotropic or viscoelastic effects was apparent.

A theoretical analysis of the peristaltic pumping of pseudo-plastic fluids at low Reynolds numbers by means of an infinite

train of sinusoidal peristaltic waves is presented. Results are shown as a series of pump characteristic curves involving the geometrical properties of the wave and the flow properties of the pseudoplastic fluid as parameters. Data obtained from experiments performed on a plane, two-dimensional model are used to confirm the theoretical results.

Cinemicrographic evidence reported in the literature describing waves traveling over the surface of axons in culture is discussed. A study of the geometrical properties of the peristaltic waves taken from these motion picture data is presented.

The viscometric data obtained from axoplasm are used to establish system resistance curves for axons idealized as uniform cylindrical tubes. These data are correlated with the theoretical pump characteristic curves to determine an expected flow rate. A comparison between the theoretical flow rates and the observed axonal flow rates gives quantitative support to the hypothesis that peristalsis is the mechanism for axoplasmic flow. In addition, it is shown that the peristaltic pumping of a pseudoplastic fluid depends only on the geometrical properties of the peristaltic waves and the flow behavior index of the fluid. For this case of axoplasm, this indicates that the theoretical flow speed of axoplasm is independent both of the consistency of the axoplasmic material and the diameter of the axon.

A THEORETICAL AND EXPERIMENTAL STUDY OF THE MECHANISM OF AXOPLASMIC CONVECTION IN NERVE FIBERS DRIVEN BY PERISTALTIC SURFACE WAVES

BY

ROBERT JOHN BIONDI

FOR

DEPARTMENT OF MECHANICAL ENGINEERING

NEWARK COLLEGE OF ENGINEERING

FACULTY COMMITTEE

APPROVED:

NEWARK, NEW JERSEY

MARCH 1971

To my wife, Tina,

to make up in a small way for her patience and understanding

ACKNOWLEDGMENTS

I am deeply indebted to my research advisor, Professor Martin J. Levy, for his guidance and direction throughout this study. I wish to express my sincere appreciation to Professor Paul A. Weiss for providing both his laboratory facilities at The Rockefeller University and financial support for this research. Doctor Weiss' overall guidance was an invaluable help in the completion of this research. I would like, also, to thank the many people, both at Newark College of Engineering and at The Rockefeller University, who offered their helpful assistance throughout this work.

TABLE OF CONTENTS

LIST OF FIGURES

PAGE

LIST OF TABLES

SYMBOLS

a	mean halfwidth of passage (two-dimensional geometry); or, mean radius (axisymetric geometry), ft.
b	half amplitude of peristaltic wave, ft.
c	wave speed, ft./sec.
D	capillary diameter, ft.
e	internal energy, Btu./lb.
D_j	mass diffusion coefficient of jth component, $ft.^2/sec.$
h	transverse coordinate of wall, ft.
h_j	partial enthalpy of jth component, Btu./lb.
k	thermal conductivity, $Btu./hr.-ft.-^oF.$
K	consistency index, $lb.-sec.^m/ft.^2$
L	capillary length, ft.
m_j	mass concentration of jth component, lb./lb.
n	flow behavior index, dimensionless
P	pressure, $lb./ft.^2$
ΔP	pressure difference across length of capillary, $lb./ft.^2$
ΔP_λ	pressure rise per wavelength, $lb./ft.^2$
q	volume flow rate observed in wave reference frame (flow per unit width between axis and wall - two-dimensional geometry; total flow in duct - axisymetric geometry), $ft.^3/sec.$
Q	instantaneous local flow rate observed in laboratory reference frame; or, capillary volume flow rate, $ft.^3/sec.$

$\bar{Q}$ time-mean volume flow rate observed in laboratory reference frame, ft.^{3}/sec.

r transverse coordinate in wave reference frame (axisymetric geometry), ft.

R transverse coordinate in laboratory reference frame (axisymetric geometry), ft.

t time, sec.

T period of wave,sec. or temperature, $^{\circ}F$

u longitudinal velocity in wave reference frame; or longitudinal velocity in capillary tube, ft./sec.

U longitudinal velocity in laboratory reference frame, ft./sec.

v transverse velocity in wave reference frame, ft./sec.

V transverse velocity in laboratory reference frame ft./sec., or, average, theoretical axonal flow speed, mm./day

W mechanical work, Btu/sec.

x Longitudinal coordinate in wave reference frame, ft.

X Longitudinal coordinate in laboratory reference frame, ft.

y transverse coordinate in wave reference frame, ft.

Y transverse coordinate in laboratory reference frame, ft.

z dimensionless wavelength

θ dimensionless time-mean volume flow rate (two-dimensional geometry)

η efficiency of peristaltic pump, dimensionless

λ wavelength, ft.

m_o number of waves per unit length, ft.$^{-1}$

$\textcircled{H}$	dimensionless time-mean volume flow rate (axisymetric geometry)
μ	Newtonian viscosity, lb.-sec./ft.^{2}
μ_a	apparent viscosity for non-Newtonian fluids, lb.-sec./ft.^{2}
τ	shear stress, lb./ft.^{2}
ρ	fluid density, lb./ft.^{3}
ϕ	wave amplitude ratio, dimensionless
Re_Y	Reynolds number, dimensionless

Subscripts

t	total
w	wall
λ	per wavelength

1. INTRODUCTION

1.1 The Neuron: The Nerve Fiber

The universal cellular unit of the nervous system is the neuron. Geometrically, the neuron is an unusual cell. It is a highly asymetrical structure in which the cytoplasm, surrounding the cell nucleus with its chromosomes and working genes, lies at one end of an extremely elongated protoplasmic process called an axon. (See diagram in Figure 1.) The other end of the axon connects with another nerve cell

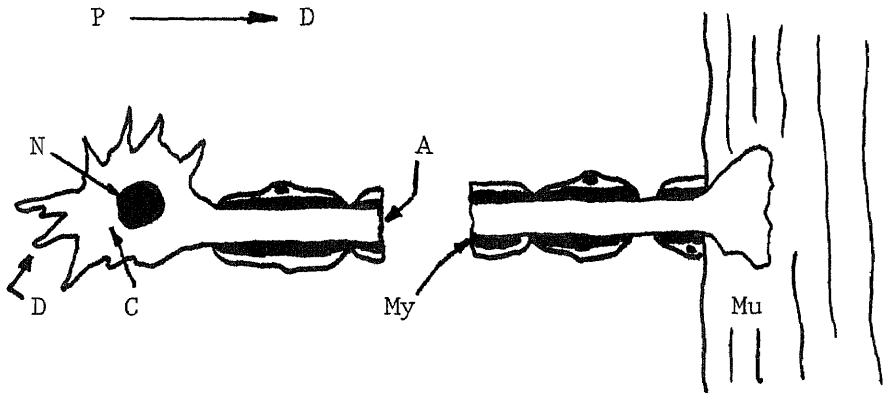

C	Cell Body	My	Myelin Sheath
N	Nucleus	Mu	Muscle Fiber
A	Axon	D	Dendrite

P D Proximo-distal Direction

Figure 1 Schematic of a Neuron

in brain, spinal cord, or ganglia, or with non-nervous cells of muscle, skin or glands. Shorter extensions from the massive bulk of the eccentric neuronal cell body, called dendrites, link the neuronal unit with other nerve cells of the vast network of central connections. The axons are lined by accessory sheath cells with or without an intermediate layer of myelin. The proximo-distal direction refers to the direction from the cell body to the peripheral termination of the axon. (Ref. 1)

Morphologically, each neuron is in contact (synapse) through its processes with other neurons so that each neuron is an interconnecting segment in the network of the entire nervous system. Functionally, each neuron is an integrator, conductor, and transmitter of coded information. (Ref. 2)

Most of the biological experiments described in this paper involved the use of frog sciatic nerves, the largest of the peripheral nerves. A peripheral nerve is a composite structure consisting of a large number of nerve fibers, additional supporting cells, and connective tissue. Figure 2 shows a schematic of a cross sectional cut through a peripheral nerve. Small groups of individual nerve fibers (axons), along with their associated sheath cells, are encapsulated into fascicles by a connective tissue called perineurium. The individual nerve fibers are insulated from each other and conduct impulses independently. Groups of fascicles are in turn encapsulated by an outer connective tissue called an epineurium. (Ref. 2)

From an engineering standpoint, the cylindrical axon is characterized by a very large length to diameter ratio. The diameter of the axon is of the order of several microns whereas the axon may range from several millimeters to more than a meter in length. The whole complex (axon plus lining of myelin and accessory sheath cells) is often called a nerve fiber, although it is not really a fiber, but a tube, the lumen of which is occupied by the cylindrical column of axoplasm. (Ref. 1) Figure 3 shows a photograph of a number of axons which have been teased apart from a frog sciatic nerve. The tubular nature of the axon is clearly evident in this photograph.

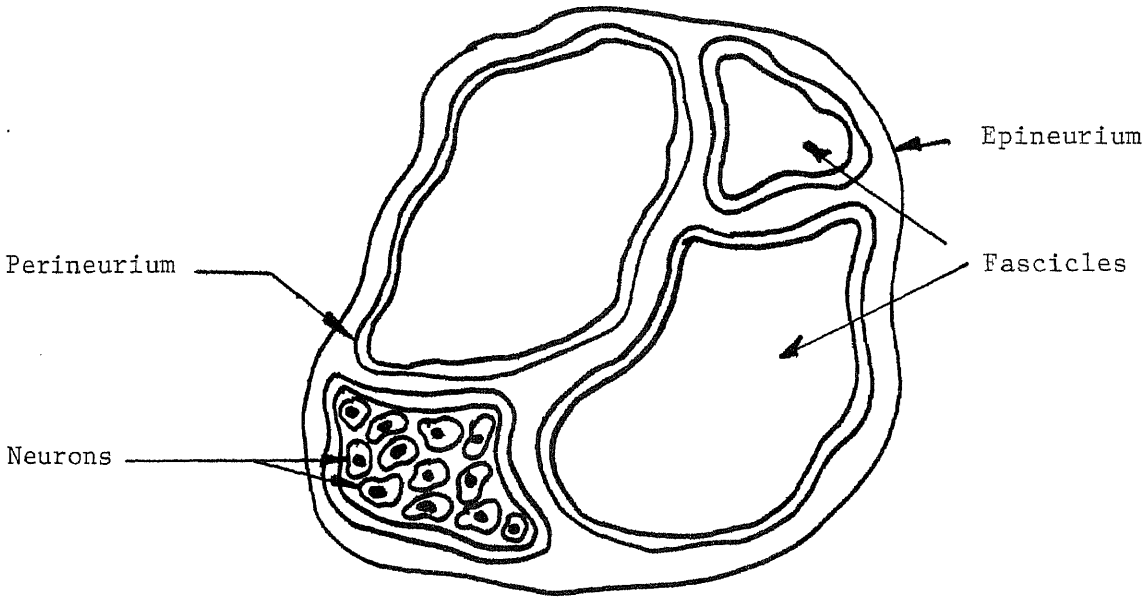

Figure 2 Schematic of Cross Sectional Cut Through Peripheral Nerve

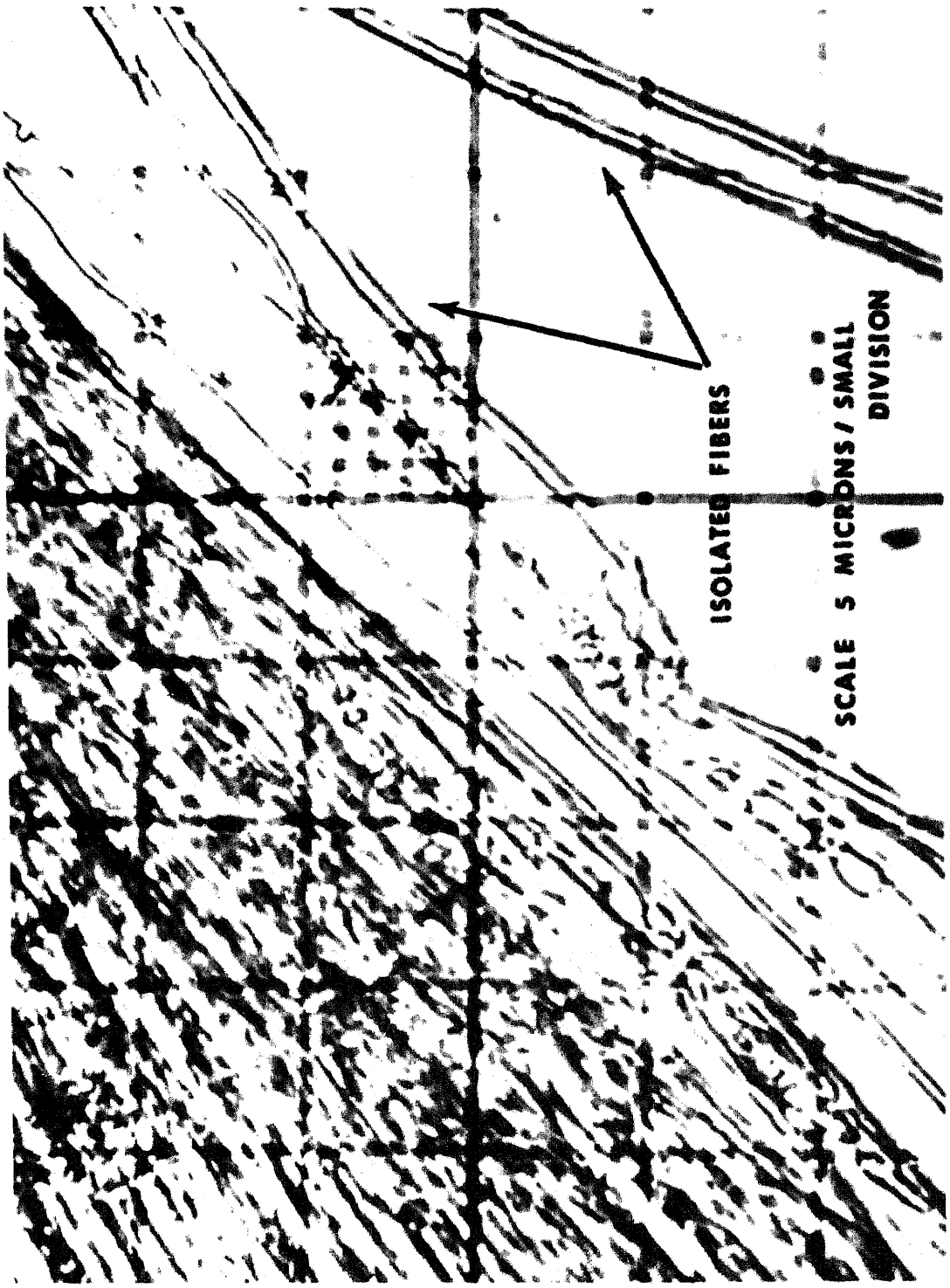

Figure 3 Photograph of Axons Separated From a Nerve Bundle

An electron-micrograph study of the fine structure of axoplasm (the protoplasmic substance contained within the axon) indicates that, from an engineering standpoint, it may be considered to be a composite matrix of materials of different consistency which is both inhomogeneous and anisotropic to some degree.

1.2 Flow of Axoplasm: Experimental Evidence

The concept of a continuous flow of axoplasm emerged from the observation that surplus axoplasm accumulates on the proximal side of a chronic nerve restriction, followed by a corresponding reduction in the nerve fiber diameter on the distal side of the restriction. The first descriptions of this phenomenon were published in 1943 by Weiss[3] and Weiss and Davis[4]. In 1948, Weiss and Hiscoe[5] presented the results of their now classical experiments with constricted nerves. They systematically introduced the partial constriction of living nerves and reported the morphological changes which took place. In particular, they described a swelling of the axon and various structural deformations of the axoplasm which appeared at the proximal side of a sudden narrowing of the cross section of the axon. They attributed this local swelling to the accumulation of axoplasm which flows continuously down the axon. Weiss and Hiscoe removed the constriction and found that the "bolus" of accumulated material moved down the axon at a speed of approximately 1.0 mm./day. Weiss and Cavanaugh[6] studied the effects of nerves constricted for long periods of time (up to one year). Refer to Weiss (Ref. 7) for a detailed history of the study of axonal flow.

The first attempts to record axonal flow with radioactive tracers were undertaken in Weiss' laboratories by Shepherd[8] (1951) and independently by Samuels et al[9] (1951). The latter group demonstrated a general shift of radioactivity in ^{35}P-labeled nerves. These results were confirmed by the work of Ochs and Burger[10] (1958). Waelsch[11] (1958), using ^{14}C-amino acids as labels, demonstrated the progressive proximo-distal shift of proteins in nerves by chemical identification. Droz and Leblond[12] demonstrated that ^{3}H-leucine-marked protein in rabbit sciatic nerves shifts in the proximo-distal direction at a rate of the order of 1.0 mm./day. Since that time many investigators have employed tracer methods to measure various properties of axonal flow. (See Ref. 13 for summary.) Significantly, even with these more sophisticated techniques, their measurements of axonal flow speeds are in reasonably close agreement with Weiss' original estimate of 1.0 mm. per day.

Weiss and Pillai[14] presented further evidence of axoplasmic flow. They studied the distribution of small cytoplasmic bodies, mitochondria, at various positions along an axon in a constricted nerve. They presented electron microscopic evidence that the mitochondria, which are apparently carried downstream passively by the flowing axoplasm, tended to accumulate in great numbers in the stagnant regions proximal to a constriction in the axon.

Weiss[15] postulated that this axoplasmic convection was necessary in order to supply the very long axon with the macromolecular

constituents which are manufactured in the cell body and which undergo a continuous degradation in the axon. Weiss felt that these must be continuously replenished from a localized central source in the cell body.

1.3 Driving Mechanism For Axoplasmic Flow

Since the existence of axoplasmic flow had been demonstrated and estimates of the flow rates had been obtained, a considerable effort was spent in an attempt to determine the mechanism for such a flow. Young[16] suggested that a hydrostatic pressure within the cell body, osmotically generated, might force the axoplasm in the distal direction. One may, however, rule out this possibility by a straightforward calculation. With the microscopic diameters of the axons and the extremely high viscosity of the axoplasm, inordinately high pressure differences would be required to force the fluid at the observed flow rates.

Weiss and Hiscoe[5] first speculated on the possibility that the driving mechanism might be related to a traveling surface deformation or microperistaltic wave moving over the surface of the axon. The observation of rhythmic pulses sweeping over the surfaces of certain eggs and tissue cells (Weiss[15]) encouraged the attempt to record cinemicrographically evidence of such surface activity in axons. Weiss, Taylor, and Pillai[17] (1962) presented direct cinemicrographic evidence of regular peristaltic waves in the surface of

mature nerve fibers. Intercostal nerves with their ganglion cells attached, excised from young mice, were placed in special culture chambers and kept alive for a week or longer. Portions of the nerve were stripped of their perineurium and the nerve fibers teased apart sufficiently to study the individual fibers under high power phase contrast microscopy. Time-lapse motion pictures revealed remarkably regular peristaltic surface deformations traveling in the proximo-distal direction. The waves exhibited a regular period of approximately 16 minutes.

Figure 4 shows a sequence of frames taken from Weiss' cinemicrographic data. The peristaltic wave (see arrows) may be readily seen moving along the surface of the axon.

The source of the energy for this peristaltic surface activity has not been identified. Weiss[18] has speculated that the Schwann cell may be contributing the metabolic energy for the mobility of the axon surface. Weiss states that the actual mobile mechanism must be located somewhere in the myelin sheath or the axolemma or perhaps in a cooperative process between the lipid layers and the special windings of the sheath cell protoplasm sandwiched between them. Assuming the Davson-Danielli biochemical model of a cell surface, Weiss[19] presented a hypothetical model of how a combined lipid-protein array, surrounding an incompressible content, could act as a mechanism for a peristaltic drive for cells in general.

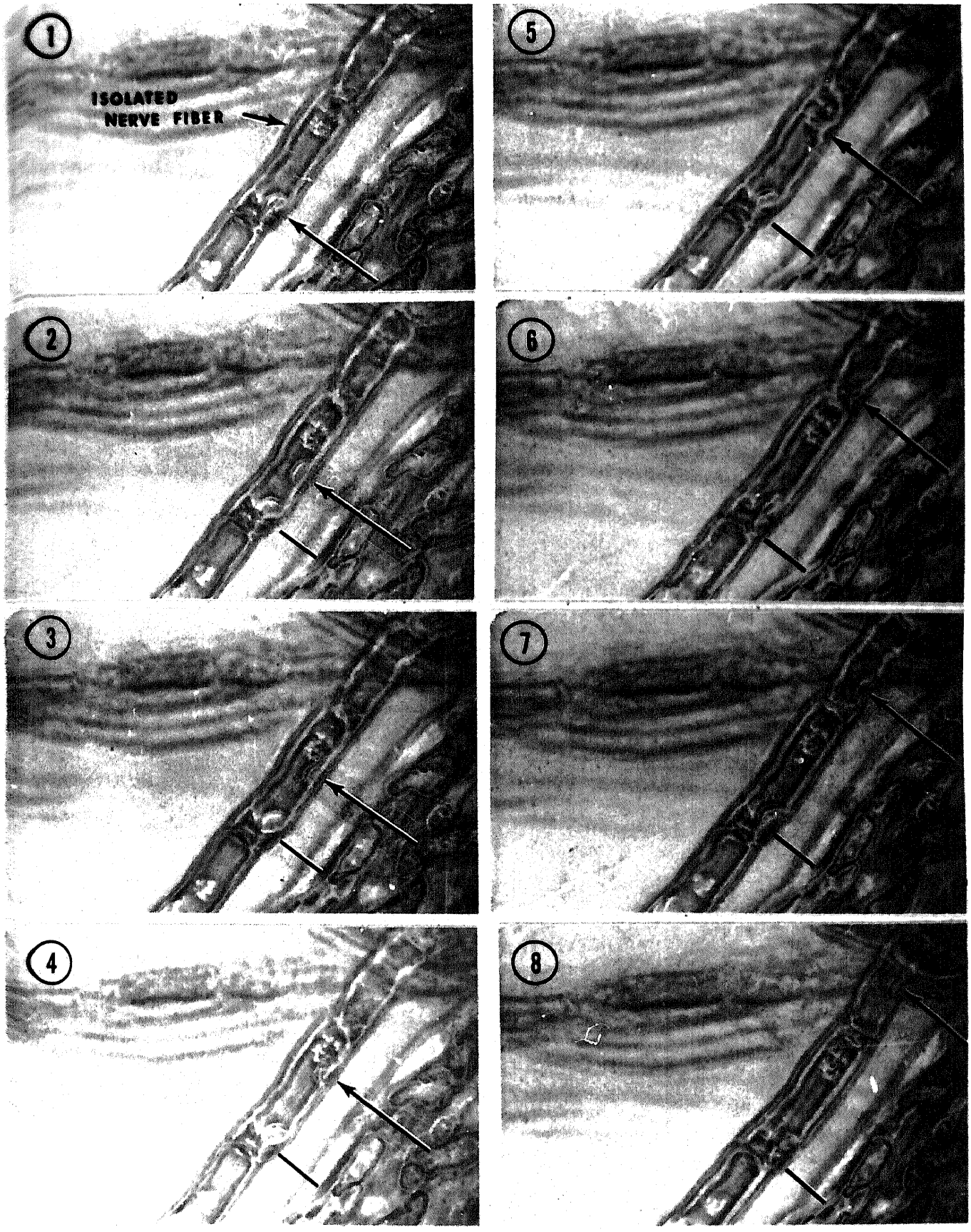

Figure 4 Peristaltic Wave in the Surface of an Axon in Culture

1.4 Statement of the Problem

The existence of axoplasmic flow has been clearly verified by a number of investigators. Measurements of the flow rates in axons by a number of authors using a variety of experimental methods has been reasonably consistent. In addition, the presence of regular surface deformations (microperistaltic waves) on the surfaces of living axons has been recorded. The major aim of the research presented in this paper was to investigate the role of peristalsis in forcing the flow of axoplasm.

In order to study this question, two separate approaches were taken; the rheological properties of axoplasm were investigated; and, an analytic and experimental study of peristaltic pumping was undertaken. In Chapter 2, viscometric data for axoplasm obtained from microcapillary tube experiments are presented. Conclusions about the fluid dynamic properties of the axoplasm are drawn from these data. In Chapter 3, a theoretical analysis of peristaltic pumping of a pseudoplastic fluid with long wavelengths at low Reynolds numbers is presented. Results of experiments performed on a large-scale, two dimensional model are used to verify the theoretical analysis. In Chapter 4, data concerning the geometrical properties of the peristaltic waves in axons are given. The viscometric data obtained for axoplasm are used to establish system resistance curves for axons idealized as uniform cylindrical tubes. These data are correlated with the theoretical pump characteristic curves to determine an expected flow rate. A comparison between the theoretical flow rates

and the observed axonal flow rates gives quantitative support to the hypothesis that peristalsis is the mechanism for axoplasmic flow.

2. EXPERIMENTAL DETERMINATION OF THE FLOW PROPERTIES OF AXOPLASM

2.1 Preliminary Experiments

In this study, microperistalsis is explored as a possible driving mechanism for axoplasmic flow. In order to derive a mathematical model for peristaltic pumping, an investigation of the rheological properties of the axoplasm was first undertaken. Several experimental procedures which may be used to make quantitative viscometric measurements are described below.

In order to avoid the experimental difficulties involved in working with a nerve fiber whose diameter is of the order of a few microns, the first experimental attempts to obtain viscometric data were performed on composite nerve bundles. A series of experiments were conducted involving the use of the high speed centrifuge to study the relative motion of cytoplasmic inclusions through the axoplasm. The movement of these bodies, mitochondria, determined by their distribution in the axon before and after centrifugation, may then be related to the viscosity of the surrounding medium. Sciatic nerves, excised from adult rats, were mounted in a gelatin medium and centrifuged at 1000 g for up to 30 minutes. The nerves were then fixed, stained, and serially sectioned and the sections examined for the presence of mitochondria. The results after centrifugation showed no unusual distribution of mitochondria. This can probably be traced to the very high viscosity of the axoplasm and the small density difference between the mitochondria and the surrounding medium.

A second series of experiments involved attempts to force the flow of axoplasm by compressing the entire nerve bundle. Weiss [18] had been able to photograph artificially produced convection of axoplasm using a device developed by Rosenberg [20] which is shown schematically in figure 5. The device is used as follows. A nerve is placed between the lower glass plate and the thin, flexible glass cover slip. A pressure applied in the upper chamber deflects the cover slip slightly and gently compresses the nerve bundle. Knowing the applied pressure, the deflection of the circular plate may be calculated from elasticity theory. Weiss and Taylor were able to tease apart the nerve bundle and cinemicrographically record the forced flow in the individual axons.

Several experiments similar to these were performed using the sciatic nerve of the rat. Although these compression tests were quite satisfactory as a means of externally forcing the flow, they did not prove feasible for making quantitative viscometric measurements. It was not possible to estimate accurately the compression of the individual fibers during the compression of the whole nerve bundle.

It became apparent that, in spite of the experimental difficulties, additional attempts to obtain viscometric data should be based on experiments performed directly on the individual nerve fibers. Two such experiments are now described.

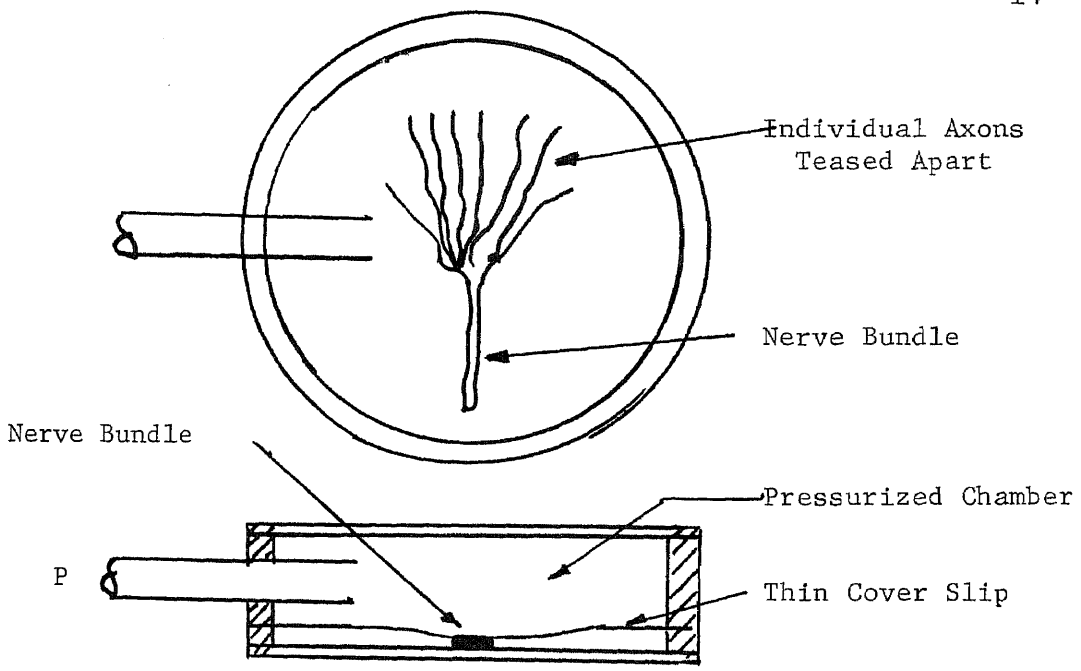

Figure 5 Schematic of Nerve Cell Compression Device

2.2 Microinjection Experiments

The determination of rheological properties involves measuring a deformation or flow in response to an applied force. In working with cells of micron dimensions, the application of an external pressure to deform the fluid appears to be a feasible way to apply an accurately measureable force. In practice, this limits the viscometric experiments to those tests in which the fluid is forced through a channel by an external pressure. This may be done in either of two ways: The axoplasm may be pushed through the axonal "tube" by forcing another fluid into the axon under pressure; or, the axoplasm may be extruded from the axon and drawn into a capillary tube under a negative pressure. The tube used to inject

the axon or to draw in the axoplasm must be of the order of 1 micron in diameter. (See Section 2.8).

DeRenyi[21] and Peterfi [22] first described a microsurgical technique for inserting micropipettes into axons. Electrophysiologists now routinely insert into nerve fibers with very fine micropipettes (less than .5 microns) to record electrical impulses. However, rarely do they inject nerve fibers under visual microscopic control. In general, electrophysiologists inject an entire nerve bundle with a microelectrode and they use electrical measurements to indicate when an individual fiber has been penetrated. Weiderheilm et al.[23] have injected 30 micron diameter arterioles with micropipettes under microscopic control to record pressure measurements. Injecting the axon under visual control is essential to making viscometric measurements since the displacement of axoplasm is measured in response to an applied force.

The experimental technique for injecting and manipulating individual axons under microscopic control was perfected as a tool for making quantitative viscometric measurements. This procedure is briefly described below. A detailed description of the apparatus and the procedure may be found in Sections 2.8 and 2.9.

A nerve preparation (frog sciatic nerve in paraffin oil with fibers teased apart sufficiently to separate the individual axons) was placed on a glass slide under the microscope. A micropipette (tip

diameter approximately 1 micron) was filled with methyl salicylate and placed in the micromanipulator. Using the micromanipulator to move the micropipette accurately in the three coordinate directions, the pipette was used as a "microspear" to penetrate an axon. An external pressure was then applied to the pipette to force the methyl salicylate into the axon and displace the axoplasm. (See figures 6 and 7). In figure 7, methyl salicylate may be seen entering the nerve fiber and displacing the axoplasm. Methyl salicylate, a light oil, is immiscible with the axoplasm. With careful inspection it is also possible to follow the movement of inclusions in the axoplasm.

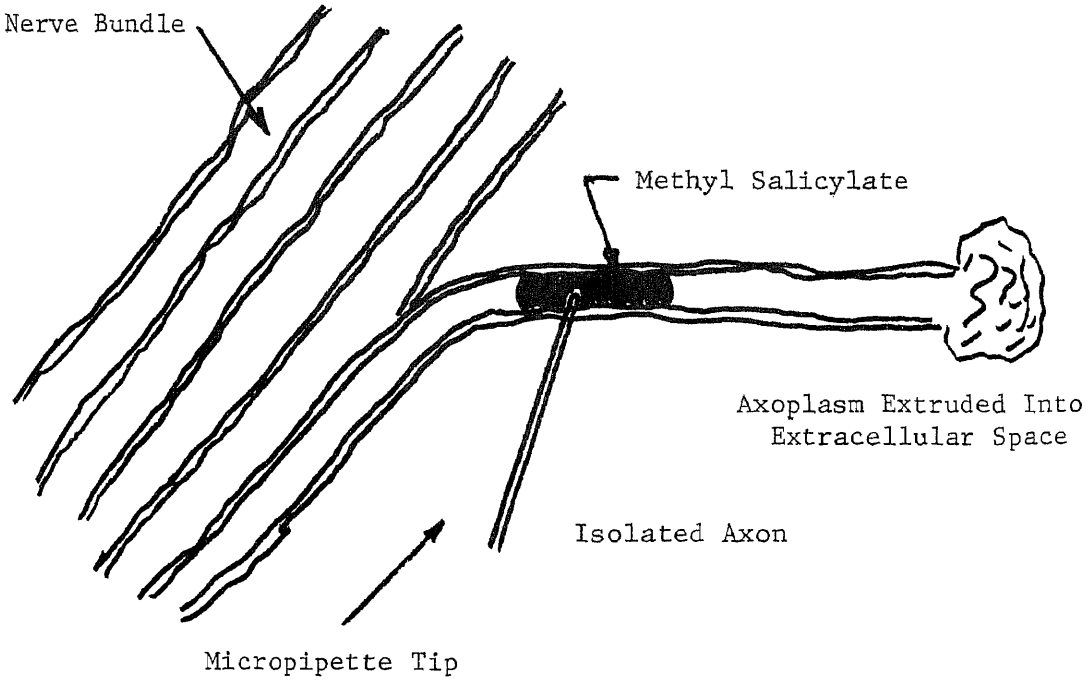

Figure 6 Schematic of Axon Impaled by a Micropipette

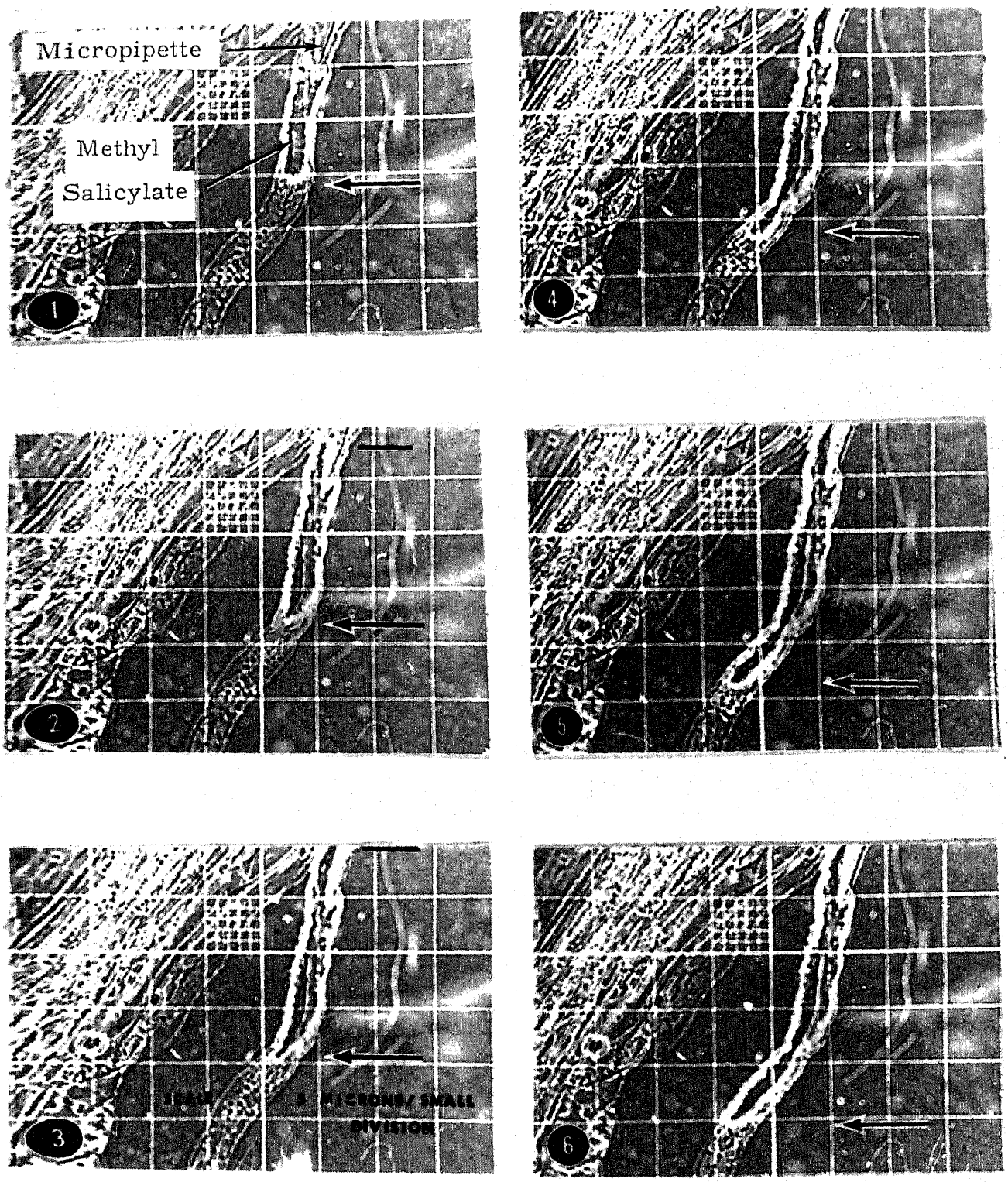

Figure 7 Oil Injected By Micropipette Displacing Column of Axoplasm

Although this type of injection experiment may be used to obtain viscometric data, the difficulties involved in the technique do not make it a practical tool for such measurements. In order to displace the axoplasm, it is necessary that the free end of the axon be open to the extracellular space as shown in the schematic. Quite often this was not the case. Apparently, the axonal membrane seals off the axon from the extracellular space within a short time. In addition, it was very difficult to keep the tip of the micropipette within the axon throughout the duration of the test. Both of these difficulties may be avoided with the microcapillary experimental technique described in Section 2.3.

The ability to inject substances into axons may, however, prove to be of value in studying axoplasmic flow in vivo. Some preliminary tests involving the injection of substances into intact nerve fibers in anesthetized frogs has shown the feasibility of such experiments. A great deal more work remains to be done in this area.

2.3 Microcapillary Tube Experiments

In order to avoid the difficulties inherent in the microinjection techniques, a method of drawing a small quantity of axoplasm into a microcapillary tube has been developed. By carefully rolling the flexible tip of a micropipette over the surface of an isolated nerve fiber, a small amount of fluid (100-200 cubic microns) is extruded from an

axon. The tip of the micropipette is then placed into the pool of axoplasm. A vacuum is applied to the pipette to draw the axoplasm into the microcapillary. A detailed description of this experimental procedure is presented in Section 3.9.

The composite photograph in figure 8 shows the axoplasm being drawn into a micropipette. The position of the meniscus may be seen advancing into the pipette. Notice the small pool of axoplasm at the tip of the pipette. Each small division of the reticule is 12.5 microns.

It was necessary to employ a long working distance objective lens. This was the limiting factor in obtaining very high magnifications. It was not possible to use a high enough magnification to determine the shape of the advancing meniscus.

A method of obtaining viscometric data from this relatively direct experimental procedure is presented in Section 2.4.

2.4 Viscometric Data From The Rabinowitsch-Mooney Equations For Capillary Tube Flow

In this section, a method for obtaining viscometric data from the microcapillary tube experiments is presented.

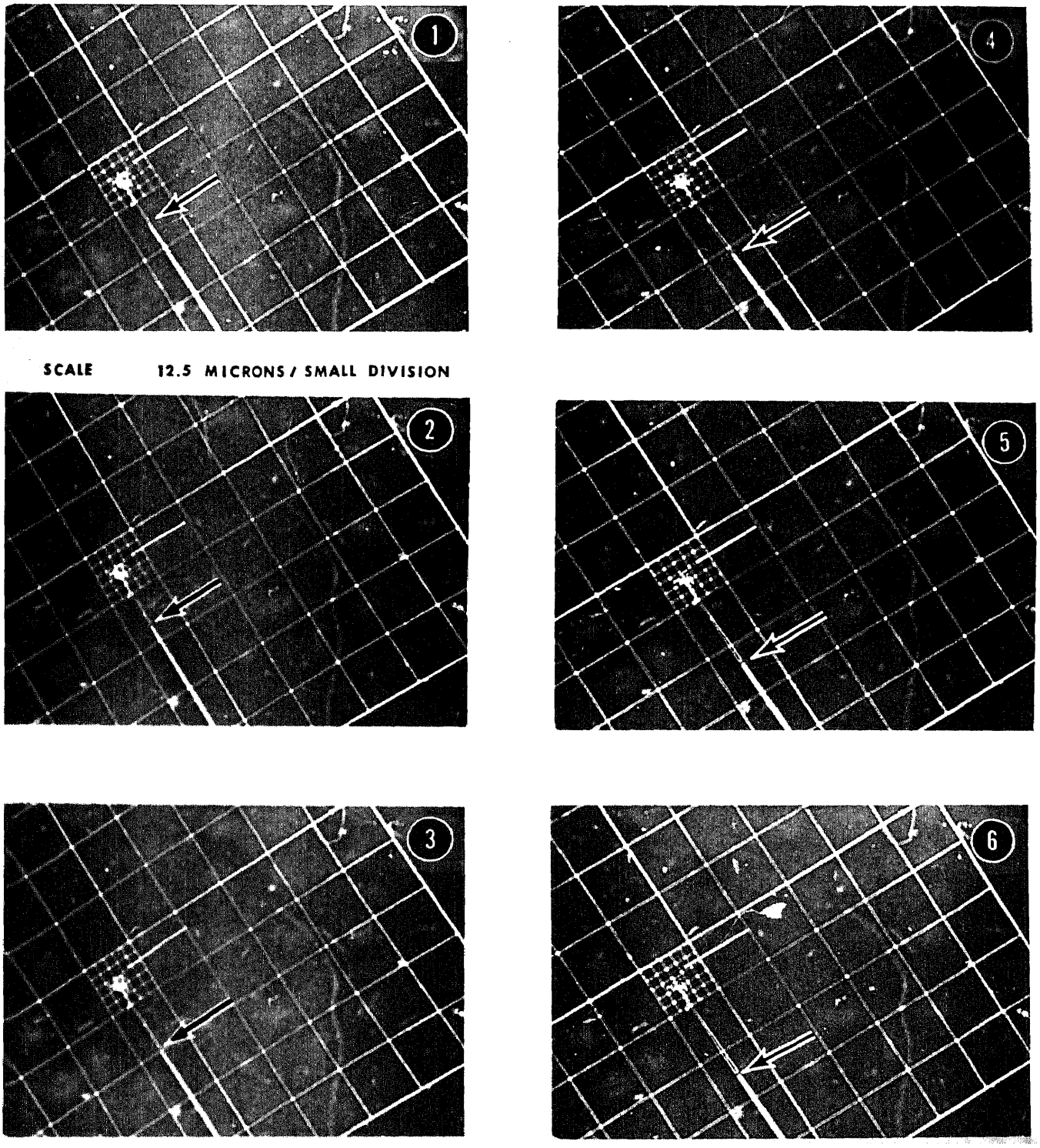

Figure 8 Film Sequence Showing Pool of Axoplasm Being Drawn Into a Micropipette

Consider a flow through a uniform cylindrical tube of radius R. Assume: 1. The fluid is in steady laminar flow; 2. The fluid is time-independent (this assumption essentially rules out thixotropic and viscoelastic fluids); and, 3. There is no slip between the fluid and the walls of the tube. If these assumptions are satisfied, the Rabinowitsch-Mooney equations derived in Appendix D may be used to relate the shear stress to the shear rate in the fluid. This relationship, known as the flow curve, establishes the rheological properties of time-independent fluids.

$$\tau_w = D\Delta P/4L \tag{2-1}$$

$$-\left.\frac{du}{dr}\right)_w = \frac{8V}{D}\left(\frac{3}{4}+\frac{1}{4}\,\frac{d(\ln(8V/D))}{d(\ln(D\Delta P/4L))}\right) \tag{2-2}$$

where τ_w is the shear stress at the wall and $-\left.\frac{du}{dr}\right)_w$ is the shear rate at the tube wall. In general the capillary diameter D, the capillary length L, the pressure difference across the capillary ΔP and the flow speed V may be measured or calculated for a given experiment. The parameters $D\Delta P/4L$ and $8V/D$ are plotted on logarithmic coordinates. From the slope of this curve at each point, the shear rate may be calculated from equation (2-2). The flow curve, the plot of τ_w versus $-\left.\frac{du}{dr}\right)_w$ establishes both the type and

degree of non-Newtonian behavior.

Consider the experiment of drawing a small quantity of axoplasm into a micropipette (figure 9) as described in Section 2.3.

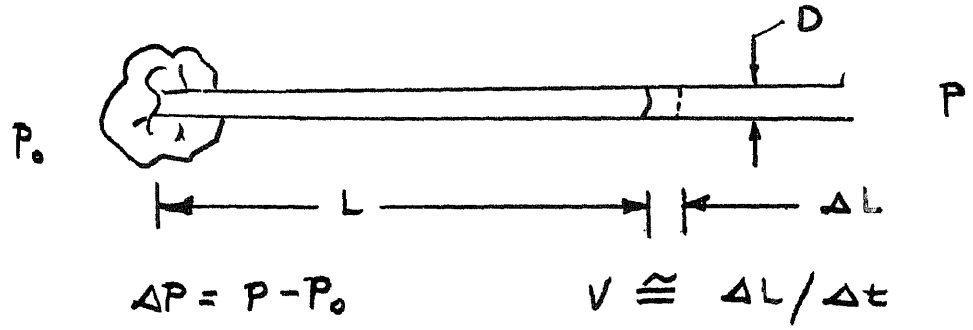

Figure 9 Schematic of Axoplasm Being Drawn Into a Micropipette

At a given time t the meniscus is at some position L. At some small increment in time Δt later, the meniscus has advanced to $L + \Delta L$. The flow speed V at this point is approximately equal to $\Delta L / \Delta t$. Thus the shear stress $D \Delta P / 4L$ and the apparent shear rate $8V/D$ may be calculated at t and L. Before the Rabinowitsch-Mooney equations may be applied, however, it is necessary to carefully consider each of the assumptions involved in the derivation.

The first assumption of steady flow is only approximately satisfied. As the fluid is drawn into the tube, it is continuously decelerated. For a constant pressure difference ΔP, as the capillary length increases, the pressure gradient dP/dL or $\Delta P/L$ continuously decreases. However, if the capillary length L is sufficiently long and a

sufficiently small time interval Δt is considered, the movement of the meniscus ΔL will be very small compared to the length. Thus the change in the pressure gradient over the time interval will be small and it may be reasonable to neglect the deceleration of the fluid.

More importantly, the viscous forces acting on the fluid completely predominate over the inertial forces. Because of the small capillary diameters and the high viscosity of the fluid, the Reynolds numbers for the flow are of the order of 10^{-5} or less. Thus it appears reasonable to completely neglect inertial effects.

In order to test this assumption and the ability of this simplified capillary tube experiment to yield meaningful data, various Newtonian and non-Newtonian fluids were tested by drawing then into the microcapillary tubes. The flow curves were then calculated from these tests. Since the properties of the fluids could be established by standard large-scale viscometric techniques, the flow curves could be compared with those from the microcapillary tests. The results indicated that the simplified microcapillary tests were able to predict the actual flow curves for both the Newtonian and non-Newtonian fluids to within 25%. These results are presented in detail in Section 2.6.

The second assumption requires that the fluid be time-independent. This essentially rules out thixotropic or viscoelastic fluids. A standard method to test for time-dependent behavior involves running a

series of flow curves with a number of different diameter capillary tubes. If the fluid is time-dependent, the data will correlate into a series of curves according to the diameter, whereas, if the fluid is time-independent, the test data will plot as a single curve.[43] The results of the axoplasm tests for a number of different capillary diameters are presented in Section 2.5. Although there is considerable scatter in the data, a multiple regression analysis did not show evidence of a significant, diametral dependence. The second assumption appears to be reasonably well satisfied.

In order to test the ability of the microcapillary test to predict time-dependent behavior, data was taken on a known thixotropic fluid (sodium carboxymethylcellulose -- CMC 1.5%) with various diameter microcapillary tubes. The results, which are presented in Section 2.6, exhibit the expected diametral dependence.

The third assumption requires that the fluid does not slip at the walls of the capillary. A standard test for the evidence of fluid slip involves running a series of flow curves with various diameter capillaries. If there is evidence of fluid slip, the results will plot as a series of curves depending on the diameter. If the fluid does not slip at the tube wall, the results should correlate as a single curve. This test is the same as that used to detect thixotropic behavior. Time-dependent behavior may be distinguished from the effects of fluid slip by running a series of curves at various capillary lengths. Time-dependent fluids will exhibit a dependence

on the length, whereas, the effect of fluid slip is independent of the length of the capillary.

As was discussed above, no evidence of a significant dependence on the length or diameter of the microcapillary was found. In addition, it should be noted that axoplasm, like many cytoplasms, adheres reasonably well to glass surfaces.

In addition, the assumption is made that the meniscal resistance may be neglected with respect to the resistance due to the viscous forces. There is a resistance to motion associated with the meniscus at the head of a fluid column which is related to the complex interactions between the fluid and a solid surface. Meniscal resistance is a "sticking" effect which depends both on the properties of the fluid and on the nature and condition of the solid surface in contact with the fluid. Meniscal resistance presents a source of error in tube viscometry because it is indistinguishable from true resistances arising within the liquid. Jacobs [24,25] discusses meniscal resistance as a source of error in blood viscometry. Mardles [26] conducted experiments to measure the meniscal resistance. He found that it was essentially independent of the viscosity of the fluid and that it increased appreciably as the capillary diameter decreased. Mardles ran some experiments with plates spaced apart a distance of 3 microns.

Since the meniscal resistance is essentially independent of the fluid viscosity, as the viscosity increases, the error introduced by

the meniscal resistance becomes appreciably less significant[26]. At a shear rate of 100 $sec.^{-1}$ (center of test range), the apparent viscosity of 1.2% CMC is approximately 400 c.p. The microcapillary tube experiments yielded results approximately 22% higher than those obtained using the Cannon-Fenske viscometers. Similarly, test run on a viscous silicone oil (μ = 5,000 c.p.) predicted a viscosity approximately 14% higher than the actual viscosity. For the shear rates encountered in the microcapillary tube experiments, the apparent viscosity of axoplasm is of the order of 160,000 c.p. or approximately 30 times the viscosity of silicone oil. These results suggest that the error in neglecting the effects of meniscal resistance should be small.

It is also assumed that the effects of capillarity may be neglected. Although the microcapillary diameters are small, the apparent viscosity of the axoplasm is sufficiently large that there is no noticeable tendency of the meniscus to either advance or recede under the influence of capillarity. This was demonstrated by drawing a small amount of axoplasm into a micropipette with a strong vacuum. With the pressure equalized, no tendency of the meniscus to advance or recede was recorded.

It is assumed that the taper of the capillary tube has a negligible effect on the results of the experiment. As may be seen in figure 18, the micropipette is slightly tapered approaching the tip. Measurement of the taper shows that it usually falls between ½ and 1

degree. The test results appeared to correlate best when an average value of the diameter was used.

Finally, the assumption is made that the axoplasm is not substantially affected during the test. In general, it is very difficult to perform a biological experiment without in some way affecting the material during the test. Attempts to evaluate the degree to which the axoplasm has been altered are discussed in Section 2.7.

2.5 Presentation of Viscometric Data For Axoplasm

Results of the microcapillary tube experiments for axoplasm are presented in figure 10 as a plot of shear stress versus apparent shear rate. The microcapillary diameters are distinguished by different symbols for the data points. The data appears to correlate as a straight line with a slope equal to 0.41. Notice that there is no evidence of a significant diametral dependence.

A linear plot of the shear stress $D\Delta P/4L$ versus apparent shear rate $4Q/\pi R^3$ or $8V/D$ on logarithmic coordinates with a slope less than 1.0 is characteristic of pseudoplastic fluids. Mathematically, pseudoplastic fluids obey a power law relationship between the shear stress and the shear rate which is given by

$$\tau_{yx} = K \left| \frac{\partial u}{\partial y} \right|^{m-1} \frac{\partial u}{\partial y} \qquad (2\text{-}3)$$

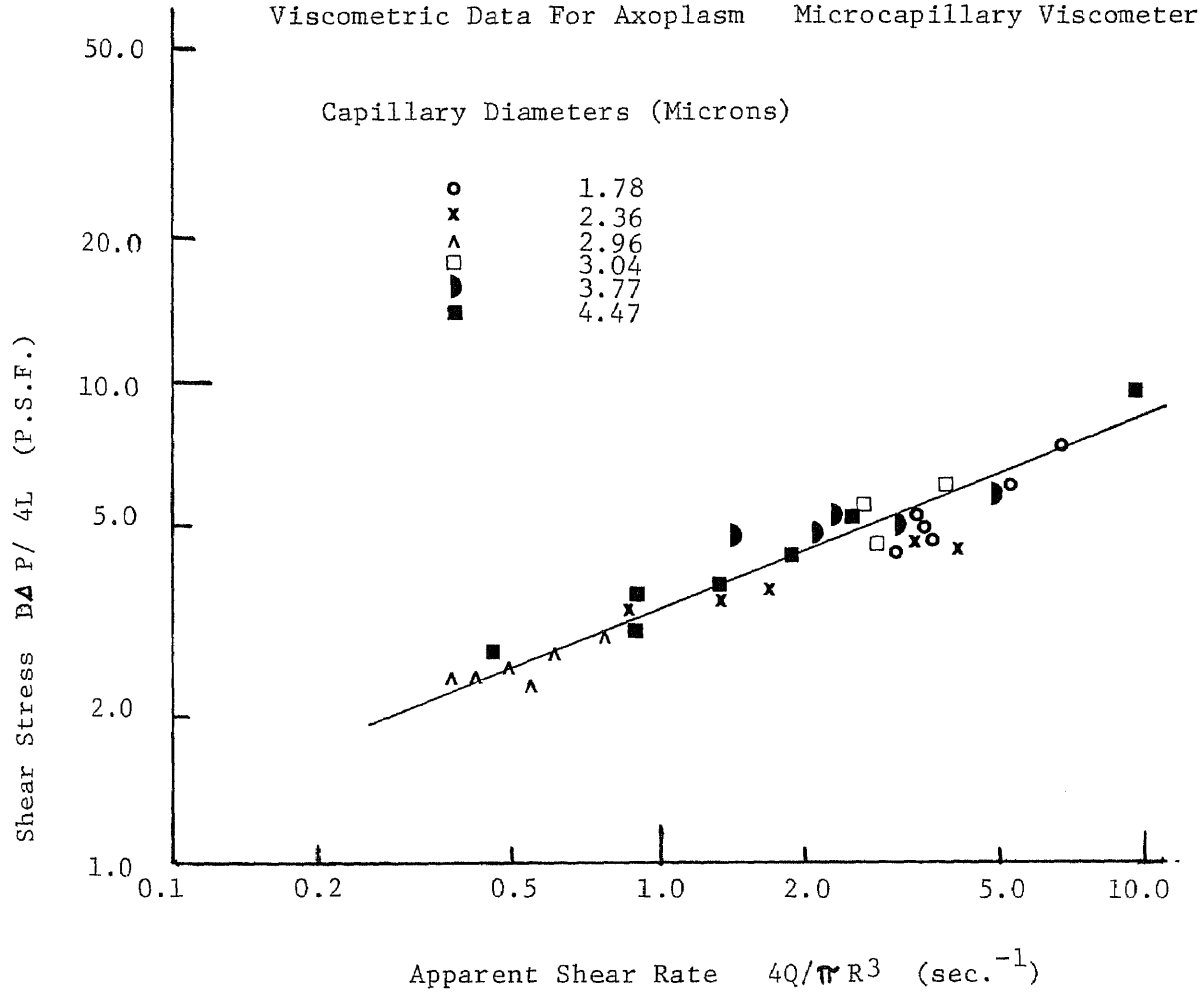

Figure 10 Plot of Shear Stress Versus Apparent Shear Rate for Axoplasm

where n (flow behavior index) is given by the slope of the curve shown in figure 10 and K (consistency index) $= K' / \left(\frac{3n+1}{n}\right)^n$ where K' is given by the intercept in figure 10 at an apparent shear rate of 1.0. A lower value of n indicates an increasing degree of pseudoplasticity. Pseudoplastic fluids exhibit a shear rate "thinning", that is, a decrease in apparent viscosity at increasing shear rates. The apparent viscosity is usually defined by the relationship

$$\mu_a \equiv \tau_{yx} / \left(\partial u / \partial y\right) \tag{2-4}$$

Thus the apparent viscosity of a pseudoplastic fluid is given by

$$\mu_a = K \left| \frac{\partial u}{\partial y} \right|^{n-1} \tag{2-5}$$

Since $n < 1.0$, the apparent viscosity μ_a decreases as the shear rate $\left| \frac{\partial u}{\partial y} \right|$ increases. By comparison, a thixotropic fluid exhibits a similar shear rate thinning; but, unlike a pseudoplastic fluid, a thixotropic fluid exhibits a reversible time-dependent change in viscosity at a constant rate of shear.

From figure 10, the flow behavior index n taken from the slope of the curve is equal to 0.41. The value of the consistency index K is found to be 2.98 lb.- sec.^{n}/ ft.^{2}. Using these two values, the apparent viscosity of axoplasm at a shear rate of .05 sec.$^{-1}$ is approximately 17.45 lb.- sec./ft.^{2} or 0.834 x 10^6 centipoise.

By comparison, the viscosity of water at $20^{o}C$ is 1.0 c.p. At $20^{o}C$ the viscosity of heavy machine oil is approximately 5×10^{2} c.p.; the viscosity of glycerine is approximately 1.5×10^{3} c.p. The viscosity of polyethylene glycol 6000 which has a consistency of a grease is approximately 10^{5} c.p.

2.6 Test of Microcapillary Techniques Using Known Newtonian, Pseudoplastic and Thixotropic Fluids

In order to examine the validity of the method described in Section 2.3, the flow curves for several Newtonian and non-Newtonian fluids were determined using microcapillary tubes and the results were compared to flow curves established in large-scale tests. A series of various diameter Cannon-Fenske viscometers were used to accurately establish the flow curves for each test fluid. A small sample of the test fluid was then placed on a glass slide under the microscope and a series of tests were run drawing the fluid into microcapillaries. A comparison of the results are presented in figures 11 to 14.

Figure 11 shows the results of microcapillary tube experiments using a Newtonian oil (G.E. Silicone Oil 5000 c.s.) as the test fluid. Notice that the curve of shear stress versus shear rate is linear with a slope equal to 1.0 as expected for a Newtonian fluid. The viscosity, given by the intercept of the curve at a shear rate of 1.0, is equal to .136 lb.-sec./ft.^{2}. This result is approximately 14%

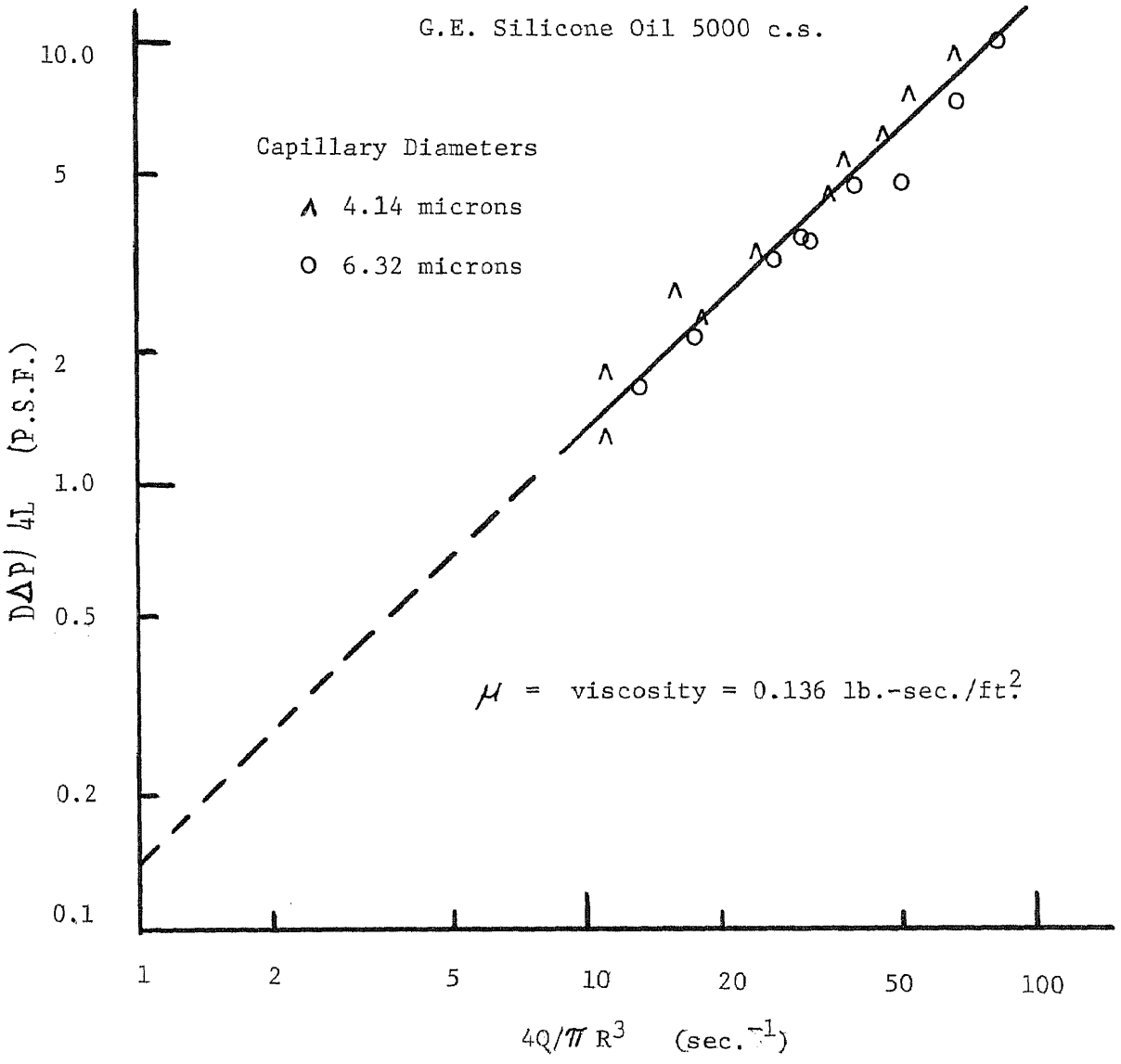

Figure 11 Logarithmic Plot of Shear Stress Versus Shear Rate

higher than the results obtained using the Cannon-Fenske viscometers. This may be attributed to the meniscal resistance which was discussed above.

Figure 12 shows the results of the microcapillary tests of a pseudoplastic fluid (1.2% sodium carboxymethylcellulose). Different symbols for the data points indicate different capillary lengths. The solid line is the result of large scale tests using the Cannon-Fenske viscometers. Notice that the results of the microcapillary tests corrected for capillarity are in generally good agreement with the large scale tests although the data appear to plot approximately 22% higher. This is probably the result of a meniscal resistance. The apparent viscosity of the CMC is somewhat lower than the viscosity of the silicone oil; thus the effect of a meniscal resistance would probably be more evident.

Figure 13 shows the results for a thixotropic fluid (1.5% CMC) obtained using the Cannon-Fenske viscometers. Notice that the data correlate as a series of curves according to the diameter of the capillary. This is characteristic of thixotropic behavior. Figure 14 shows the results of microcapillary tests. The length to diameter ratios were maintained the same as those in the large scale tests in figure 13. Notice that the evidence of a diametral dependence is detected in the microcapillary tests as well.

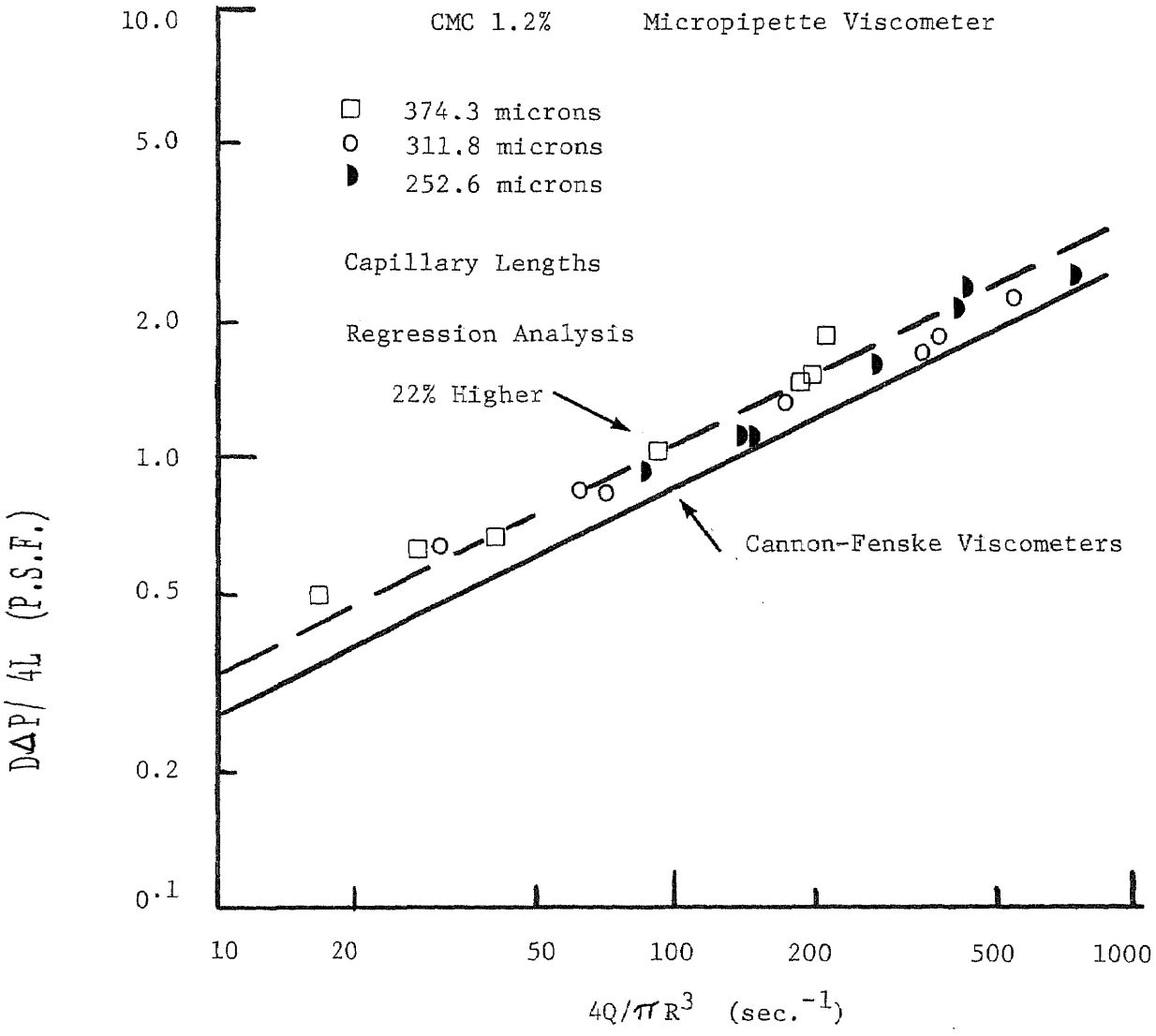

Figure 12 Logarithmic Plot of Shear Stress Versus Apparent Shear Rate

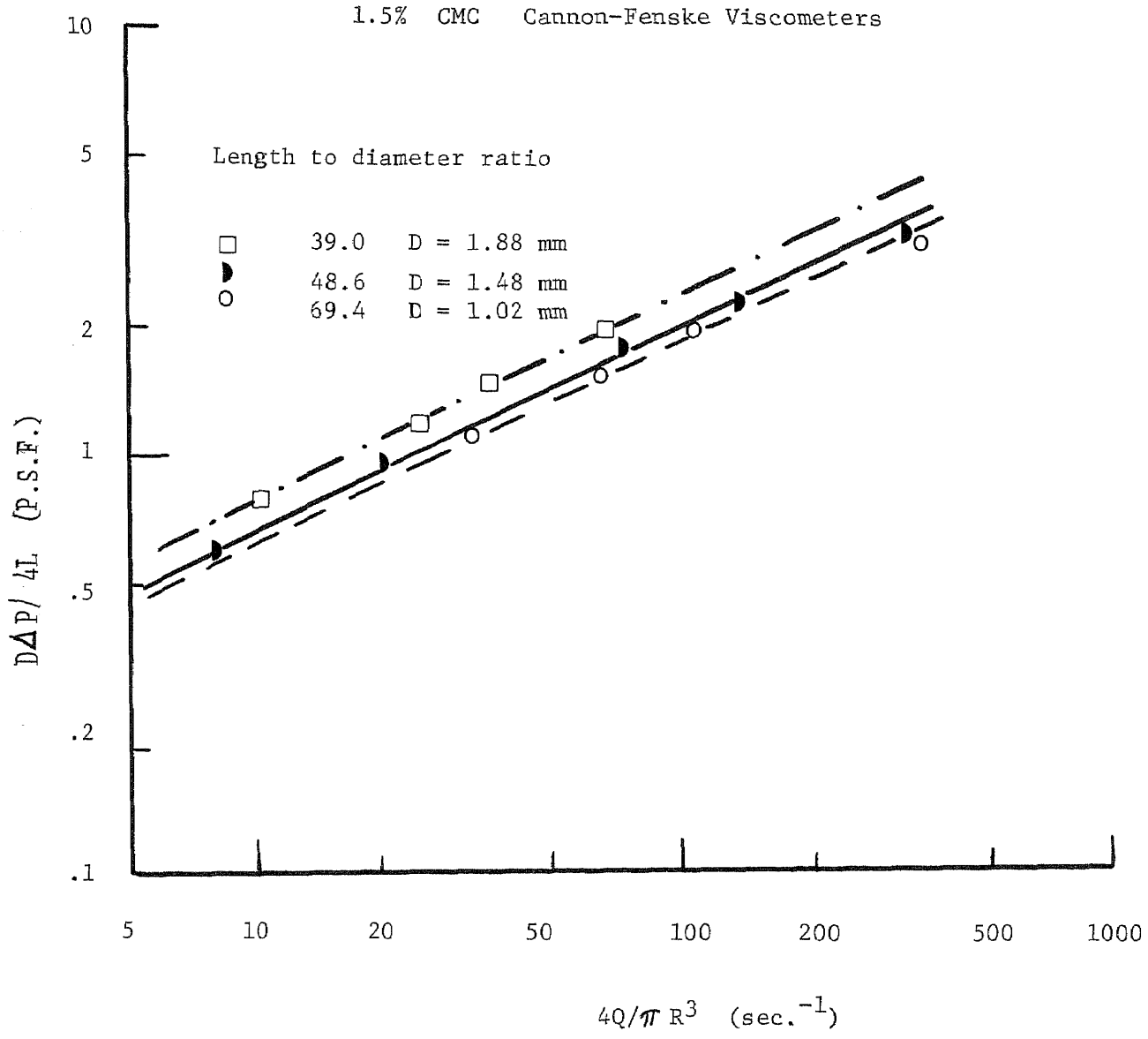

Figure 13 Logarithmic Plot of Shear Stress Versus Apparent Shear Rate

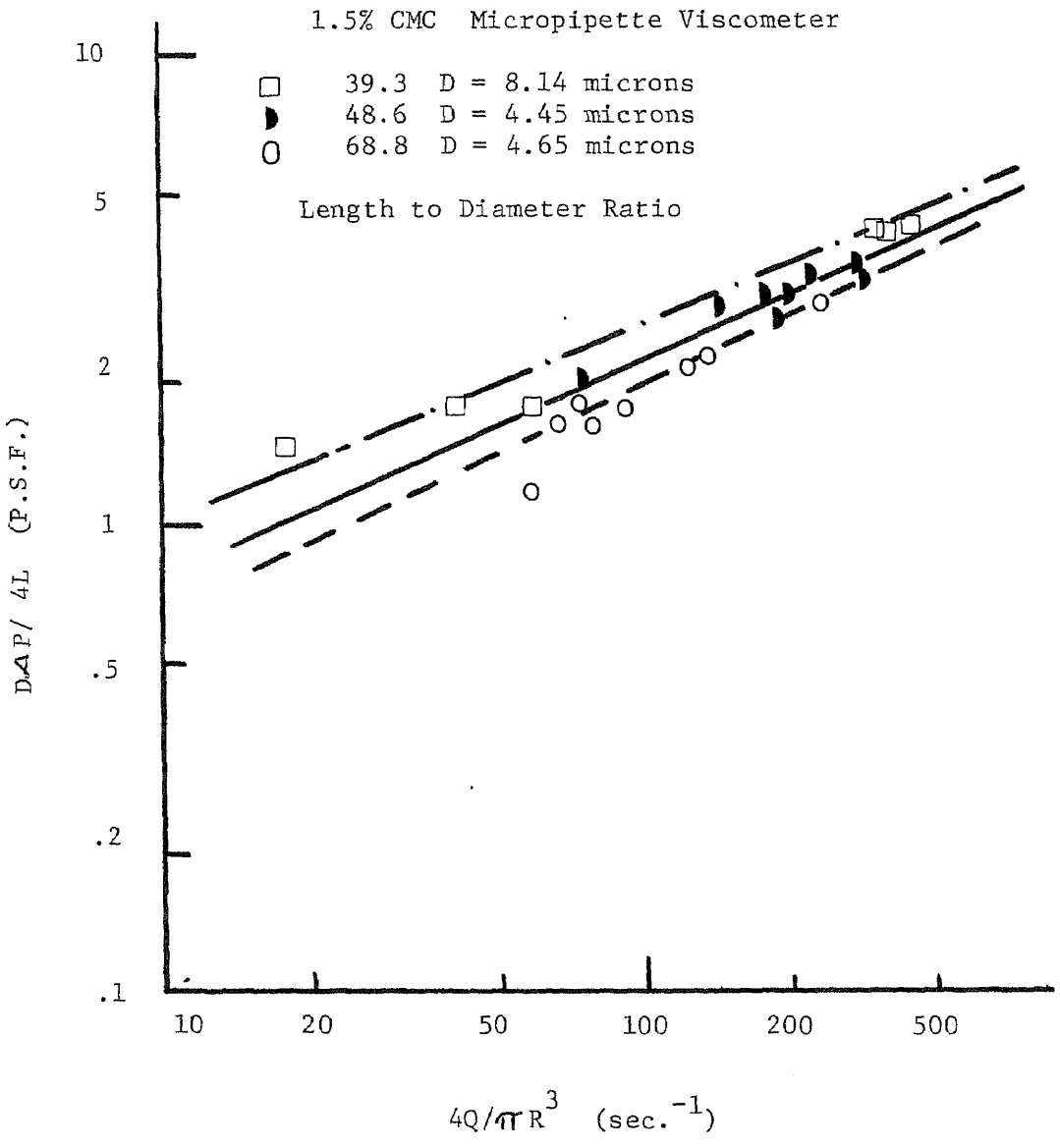

Figure 14 Logarithmic Plot of Shear Stress Versus Apparent Shear Rate

The curves presented above show that the results of the microcapillary tests compare very favorably with the results of large scale tests provided the apparent viscosity of the fluid is sufficiently high to minimize the effects of any meniscal resistance.

2.7 Electron Microscopic Structure of the Axon

Although axoplasm has been treated as a uniform, homogeneous substance in order to study its gross fluid properties, it is quite apparent that it is a highly complex material. Electron microscopic pictures of axonal fine structure prove that axoplasm is a complex system of heterogeneous materials of different consistency. This matrix contains longitudinal microtubules (approximately 240 A^{o} diameter) and 100 A^{o} wide neurofilaments as well as cytoplasmic organelles (mitochondria and endoplasmic reticulum). This inhomogeneous and anisotropic nature of axoplasm has been disregarded.

A number of attempts were made to obtain electron microscopic pictures of axoplasm which had been extruded from an axon, in order to compare these with the electron microscopic pictures of axonal fine structure. Such a comparison might have been used to estimate the degree to which axoplasm is altered during the extrusion process. Fernandez-Moran[27] describes experimental techniques for preparing and sectioning ultra small tissue samples. However, the experimental difficulties involved in maintaining visual contact with such a small quantity of material through the elaborate preparation required for electron microscopic sectioning thwarted our efforts to obtain such pictures. This question is left open for future work.

2.8 Description of Test Apparatus

The test apparatus consisted of the following components: a Zeiss phase contrast microscope, a motor-driven Bolex 16mm movie camera, a micromanipulator, micropipettes, and a system to apply and record external pressures. Refer to the photographs in figures 15 and 16.

A micromanipulator is a device used to hold and precisely position a micropipette. A micropipette is held in the chuck of a cantilevered arm of the micromanipulator which may be advanced or retracted for course positioning. Accurate movement of the pipette in the three coordinate directions may be obtained by turning three separate micrometer dials. One of the dials is a micro-micrometer which permits movements of the pipette as small as 1 micron. The micromanipulator is mounted on a heavy steel base and isolated from the supporting table by rubber mounts to minimize vibrations. In general, while a slight vibration of the instruments was present, it did not prove to be a major problem.

A Zeiss phase contrast microscope was used for these experiments although most of the movie sequences were made using bright field. A camera was mounted on a tripod above the third ocular tube of the microscope. A calibrated reticule was placed in this ocular to provide an accurate dimension reference in the movie sequences. For most of the experiments, a 12.5x ocular lens and a 16x long working distance objective lens were used. Higher magnification reduced the size of the field and a lower

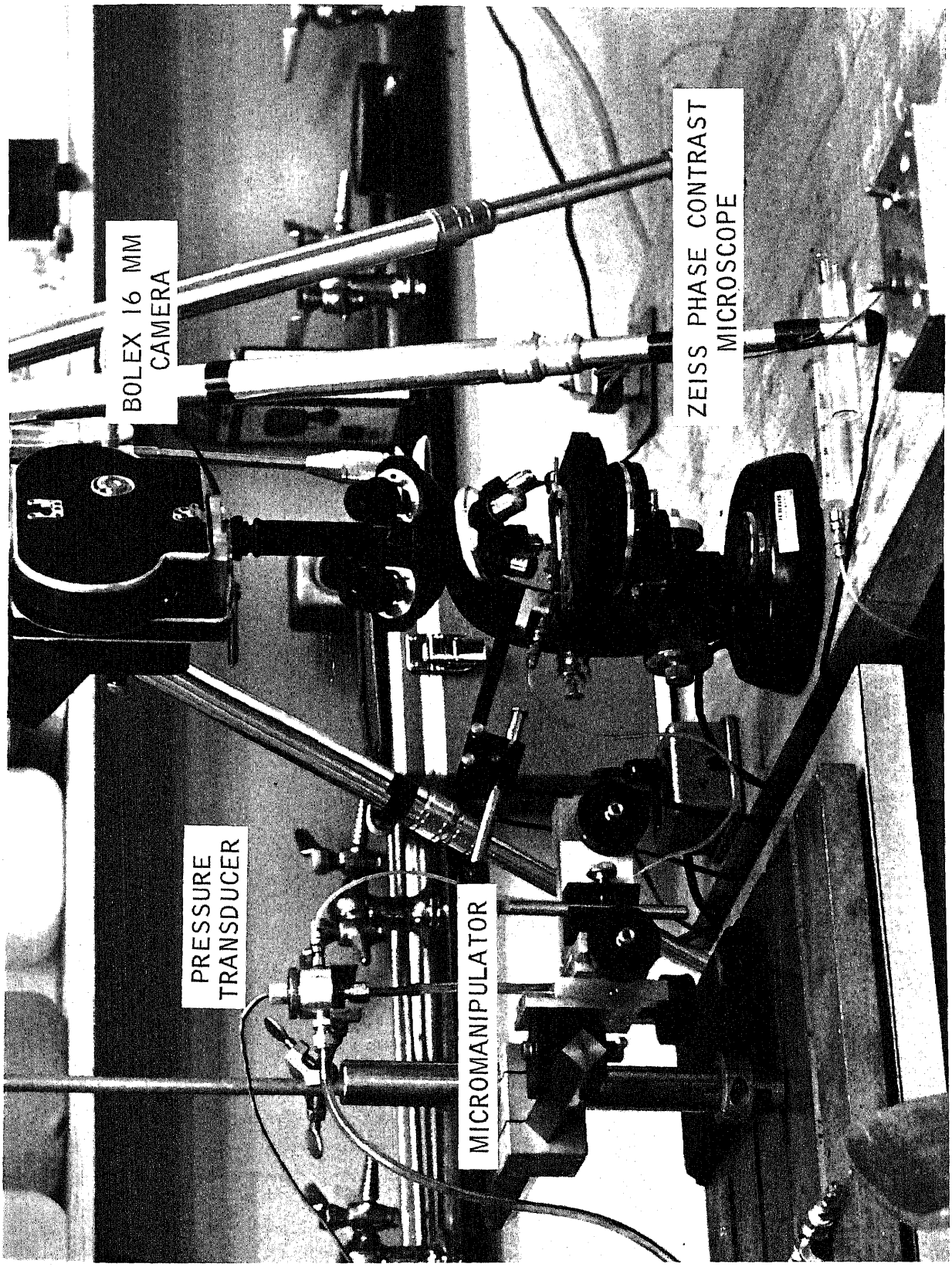

Figure 15 Photograph of Test Apparatus

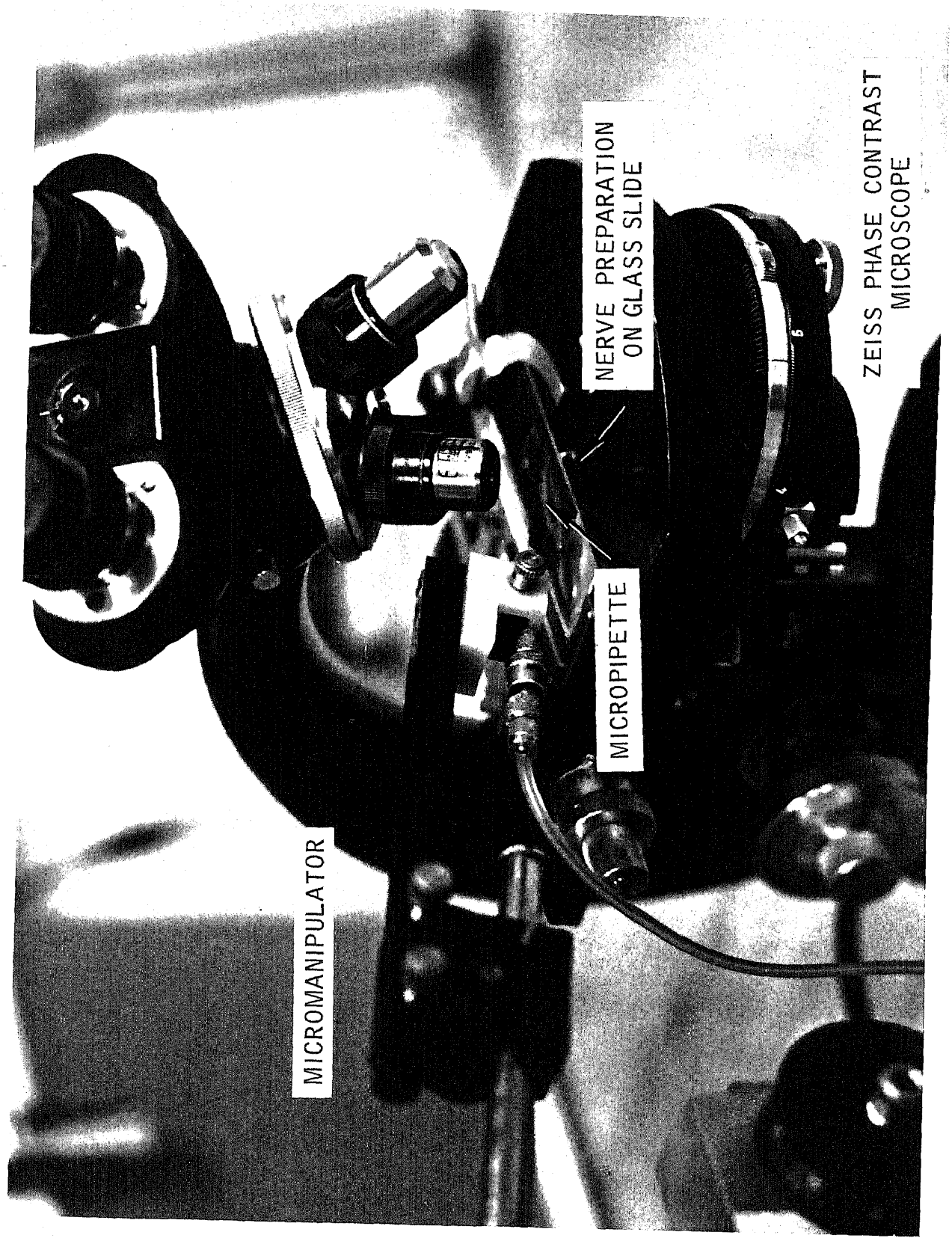

Figure 16 Photograph of Test Apparatus

magnification caused difficulties in making measurements on the films.

A Bolex 16mm motor-driven camera was used at 12 frames per second with Kodak Tri-X Reversal film. All the experiments were performed under visual control, with the lens of the camera and the ocular lens in focus simultaneously. This was done by setting the camera lens at infinity and by locating the surface of the lens at the focal point of the ocular in the third tube. Light intensity was regulated by adjusting the microscope diaphragm.

Figure 17 shows a photograph of a micropipette. A micropipette is made by heating a 2 mm glass capillary tube and simultaneously pulling the two ends in a micro-forge. The capillary will draw out to an extremely fine tip with an outer diameter usually less than 1 micron. The end of the pipette is sealed in this procedure but may be opened by carefully breaking a small fragment from the tip. It was often possible to obtain micropipettes with open tips as small as $\frac{1}{2}$ micron in diameter. The tip of a micropipette, shown in figure 18, is relatively rugged and quite flexible and can be bent into a 180^{o} arc without breaking.

A quick disconnect compression fitting with teflon seat was used to connect the glass micropipette through a plastic tube to the pressure supply. Using appropriate bleeds, the high pressure air and the vacuum systems could be used to supply a pressure from 40 psig to

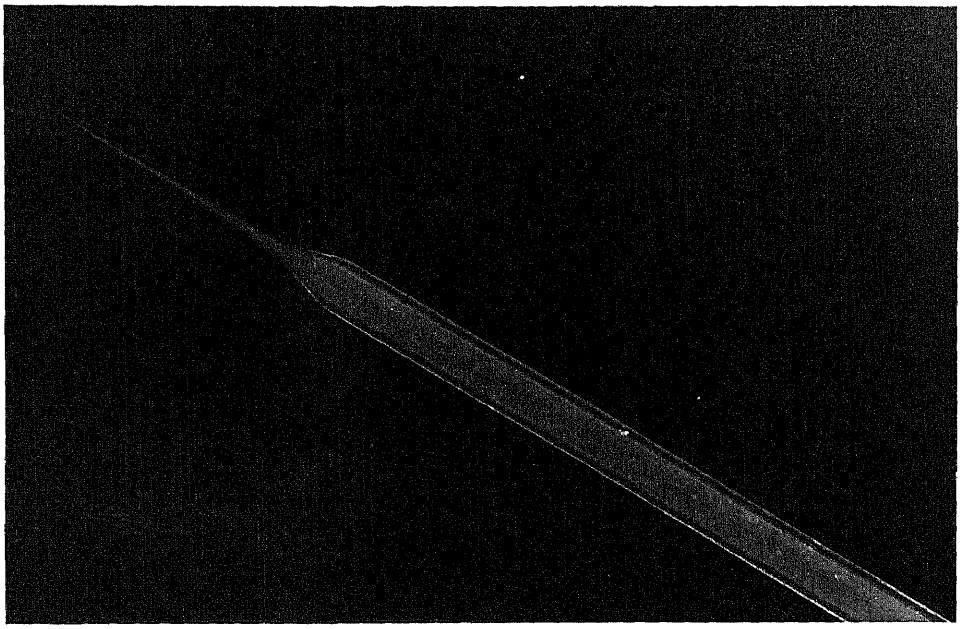

Figure 17 Photograph of a Glass Capillary Formed Into a Micropipette

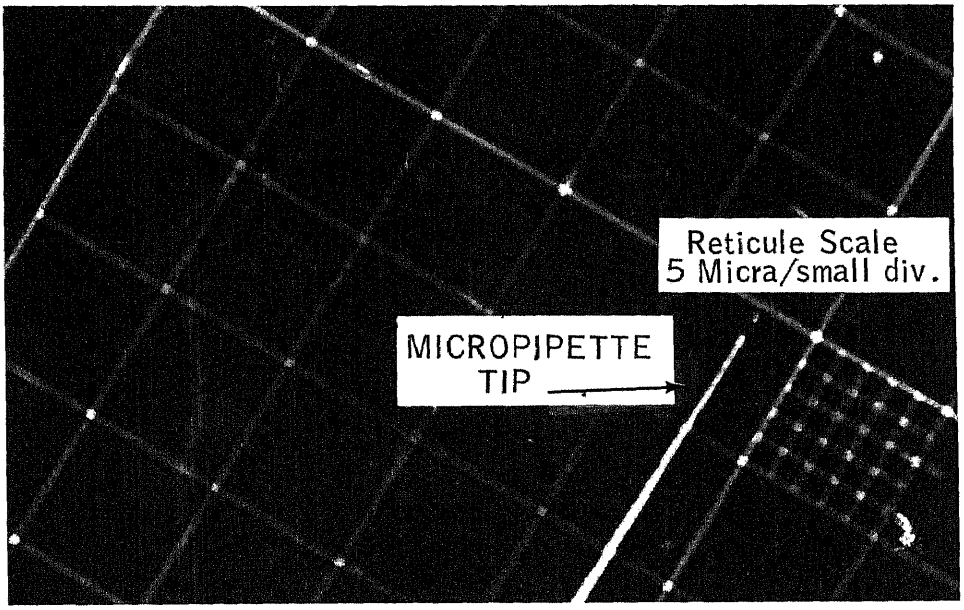

Figure 18 Photograph of Tip of Micropipette

20 in.Hg.vacuum. The pressure was sensed by a pressure transducer and read out on a calibrated bridge amplifier.

A Vanguard Motion Analyzer was used to record data from the movie films. The instrument indexes the film frame by frame. The 16mm frame is magnified 10x at the screen and the analyzer is equipped with micrometer advanced movable cross hairs which allow measurements in thousands of an inch at the screen. (A distance of 1 micron corresponded to a movement of the cross hairs .0078 in. at the surface of the screen.)

Additional information about the test apparatus is presented in Appendix F.

2.9 Description of Test Procedure

A teased nerve was prepared as follows. An adult frog (rana pipiens) was sacrificed and the sciatic nerve was excised from a point in the lower back to the knee (slightly below the point where the nerve bifurcates into the peroneal and the tibial nerves). The excised nerve was immediately placed in paraffin oil. (Paraffin oil was chosen because it is an effective medium in short term experiments for sealing off the nerve fibers from the atmosphere and, in addition, its high viscosity retards the free mobility of the teased nerve fibers.) Using a very fine forceps, the epineurium and perineurium were carefully

stripped off with a minimum of disruption to the axons. Two fine dissecting needles were then used to gently spread apart the axons on a glass slide into small groups of bundles. Although most of the axons remained in these small bundles, a number of individual fibers could usually be found. Figure 3 shows three individual axons near a large bundle of fibers. This procedure usually required approximately 1/2 hour.

A small quantity of axoplasm may be extruded as follows. An individual axon which has been severed at one end from the nerve bundle is located by carefully inspecting the nerve preparation. Using the micromanipulator, the tip of a micropipette is placed above and perpendicular to the axon. The micropipette is then lowered until it depresses the axon. Since the pipette tip is quite flexible, there is little liklihood of the tip breaking. The pipette tip is then used as a "rolling pin" to extrude a small amount of axoplasm. The axon is moved in a direction perpendicular to the micropipette by advancing the microscope stage, figure 19.

In general, the excised nerve fibers remain fully viable in the paraffin oil for at least 8 hours after the animal has been sacrificed. On the other hand, axoplasm which has been extruded into the extracellular space definitely appears to change character with time. After several hours, it becomes quite rigid and it may begin to change

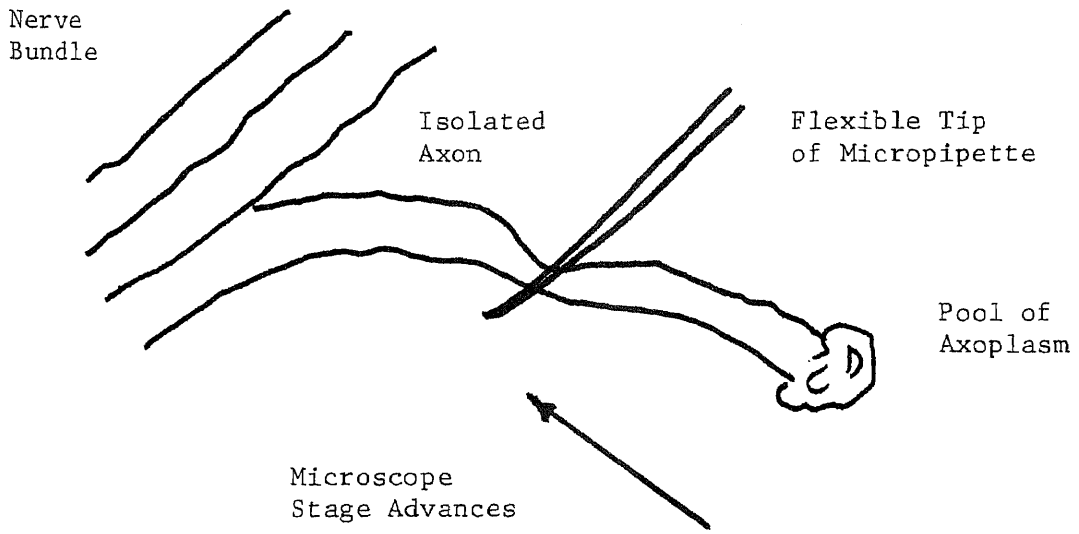

Figure 19 Schematic of Procedure To Extrude Axoplasm From a Nerve Fiber

properties soon after it is squeezed from the axon. Therefore, it is essential that the axoplasm be drawn into the micropipette immediately after it is extruded. Although this was usually accomplished within 1 to 2 minutes, it is possible that slight changes in the physiological properties might be responsible for some of the scatter in the data.

The room temperature during the tests ranged from 22.5°C to 24.5°C. Since there would be some concern about experimenting at room temperature with nerve fibers from a warm blooded animal, a frog, which is a cold blooded animal, was chosen as the test animal. The effect of temperature on the properties of axoplasm has not been explored. However, increasing the temperature would be expected to decrease the value of the consistency index K. The flow behavior index m

should be essentially independent of the temperature.

Several difficulties were encountered which limited the number of usable film sequences. Quite often fragments of myelin or other debris would be mixed in with the axoplasm. These would tend to become lodged in the pipette tip and block the flow of axoplasm. Such fragments were quite difficult to dislodge and the micropipette usually had to be discarded. In many cases both axoplasm and paraffin oil would be drawn into the pipette simultaneously. This occurred most commonly with large diameter micropipettes. Finally, as a result of vibrations, quite often the tip of the pipette would intermittently leave the pool of axoplasm causing both oil and axoplasm to be drawn into the micropipette. Since all of these occurrences could be easily identified, it was not particularly difficult to ascertain which sequences were usable.

The results of an error analysis (Appendix G) indicate that somewhat more scatter might be expected in the axoplasm data than experienced with the silicone oil or CMC data. Unlike CMC or silicone oil, axoplasm is relatively opaque. This resulted in an additional error associated with estimating the position of the pipette tip.

2.10 Qualitative Observations

Weiss [18] observed that the axoplasm appeared to move as a

cohesive semi-solid column. The pseudoplastic nature of the axoplasm agrees with this qualitative observation. The fully developed velocity profile for the flow of a pseudoplastic fluid through a tube takes the shape of a blunted parabola. As the degree of pseudoplasticity increases ($n \rightarrow 0$), the shape approaches that of a plug flow, which agrees with Weiss' observations.

Because of the difficulties in obtaining a measurable sample, there is a scarcity of rheological data for protoplasm. Kamiya [28] and Kamiya and Kuroda [29] have studied velocity profiles in the shuttle streaming of the slime mold Physarum polycephalum which offers the distinct advantage of large masses of protoplasm. Kamiya and Kuroda found that the velocity profile took the form of a truncated parabola, which suggests qualitatively a shear rate thinning fluid. It is significant that two different protoplasms (axoplasm and Physarum polycephalum) have been shown to behave as pseudoplastics by two very different experimental techniques.

3. THEORETICAL AND EXPERIMENTAL ANALYSIS OF PERISTALTIC PUMPING OF PSEUDOPLASTIC FLUIDS WITH LONG WAVELENGTHS AT LOW REYNOLDS NUMBERS

3.1 THEORETICAL ANALYSIS

3.1.1 General Discussion of Peristaltic Pumping

Peristalsis is a transport mechanism for conveying the contents of a channel or tube by means of surface deformations traveling over the tube. Peristaltic pumping is of interest to biologists because it is the mechanism by which the intestines transport their solid and liquid contents and by which fluid is transported through the ureter to the bladder. In this study, it is considered as a possible cause of axoplasmic flow. Commercial peristaltic pumps find application where it is desirable to separate the fluid being pumped from the pumping mechanism. A common type of commercial peristaltic pump employs a rolling member to completely occlude a flexible tube and forces a bolus of fluid forward. Such devices operate as positive displacement pumps by occluding the tube, figure 20.

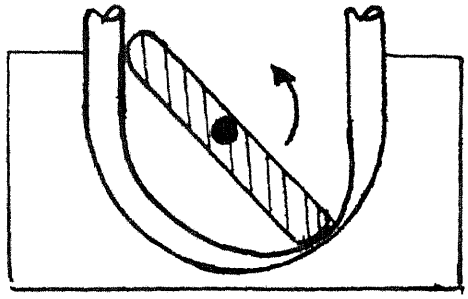

Figure 20 Schematic of Commercial Peristaltic Pump

Since the surface deformations observed in the neurons do not, in most cases, completely occlude the axon, it is of interest to study the properties of peristalsis at smaller wave amplitudes.

Consider a flexible tube connecting two reservoirs as depicted in figure 21.

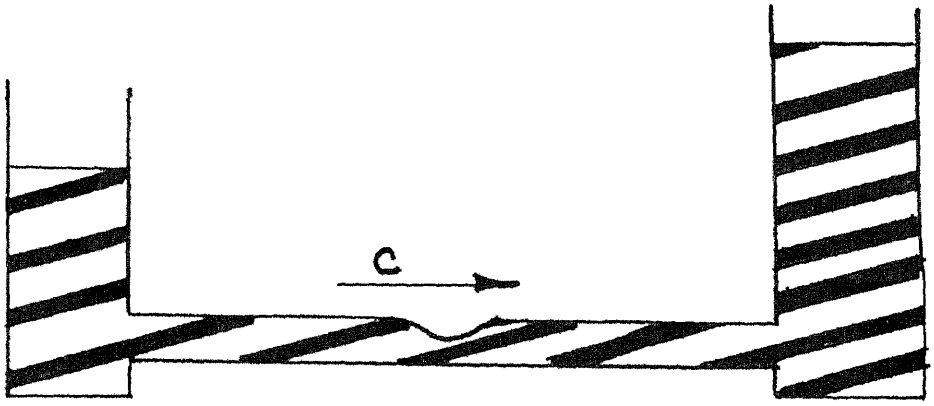

Figure 21 Schematic of a Single Peristaltic Deformation in a Tube

Assume that a surface deformation in a tube is moving to the right at speed C . If the deformation completely occludes the tube, it is obvious that the fluid will be forced into the reservoir on the right. If, on the other hand, the deformation does not completely close off the tube, some of the fluid in the tube will be pushed into the reservoir on the right and some will flow back relative to the wave through the contracted section.

Since the fluid is viscous, the pressure must be higher ahead of the wave than behind it to overcome the viscous losses associated with

the fluid flowing back through the contracted section. Thus the peristaltic wave must produce a rising pressure in the direction of the wave. For a given wave amplitude ratio, the larger the net fluid flow in the direction of the wave, the smaller the reverse flow through the contracted section and hence the smaller the pressure rise produced by the pump. The usual condition in a peristaltic wave is that the fluid in the contracted sections moves opposite to the wave direction, in the reference frame of the wave, and the fluid in the enlarged sections moves in the same direction as the waves.

3.1.2 Results of Previous Investigations

A number of other investigators have studied the problem of peristaltic pumping. Burns and Parkes [30] studied peristaltic pumping at low Reynolds numbers and small wave amplitudes. Fung and Yih [31,32] and Hanin [33] considered the case of arbitrary Reynolds number and small values of the amplitude ratio. In all of these papers the solutions are presented as an expansion in ascending powers of the amplitude ratio and for this reason are limited to small values of ϕ. Since the amplitude ratios observed from motion picture studies of living nerve cells are of the order of 0.5, solutions of this type are, in general, not applicable.

Shapiro, Jaffrin, and Weinberg [34] studied the case of peristaltic pumping of a Newtonian fluid with long wavelengths at low

Reynolds numbers and, most important, with arbitrary amplitude ratios. The results of Shapiro et al, are discussed in some detail below. Latham[35] presented an experimental study of peristaltic pumping using a two-dimensional model to corroborate the analytical results of Shapiro et al. Barton and Raynor [36] expanded the results of Shapiro to cover the case of small wavelengths.

Shapiro considered an infinite train of sinusoidal peristaltic waves of wavelength λ , and amplitude b , traveling at speed c along the surface of a tube of radius a . The tube contains a Newtonian fluid of viscosity μ . Shapiro's work requires the assumption that the appropriate Reynolds number is small enough for the inertial terms in the equations of motion to be neglected and that the ratio of the wavelength to the diameter is large enough for the pressure to be considered uniform over the cross section.

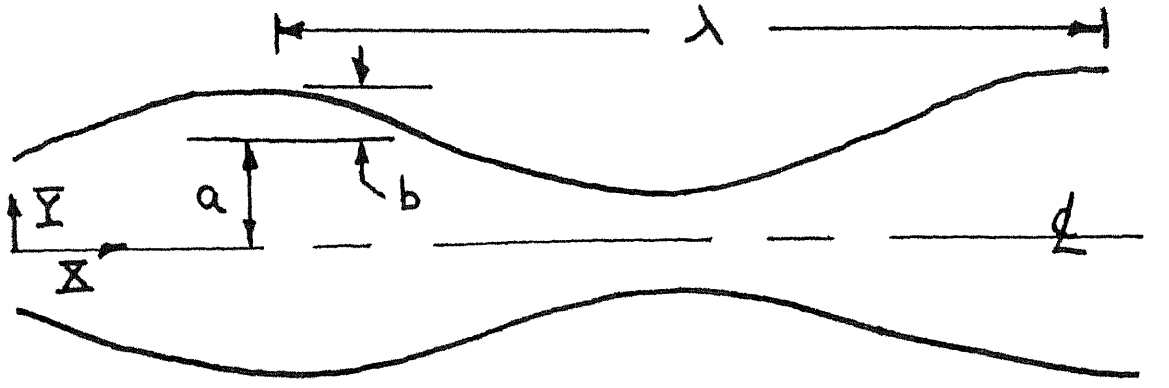

Figure 22 Nomenclature for Infinite Progressive Train of Sine Waves

Shapiro determined a relationship between the pressure rise produced by the peristaltic wave acting as a pump and the time-mean flow rate, shown in equation (3-1). Note that Shapiro obtained the results in closed form, a distinct advantage over previous solutions.

$$\frac{a^2 \Delta P_\lambda}{4\mu c \lambda} = \frac{8\phi^2 (1 - \phi^2/16) - 4\phi (1 - \phi/4)(1 + 3\phi^2/2)}{(1 - \phi^2)^{7/2}} \quad (3\text{-}1)$$

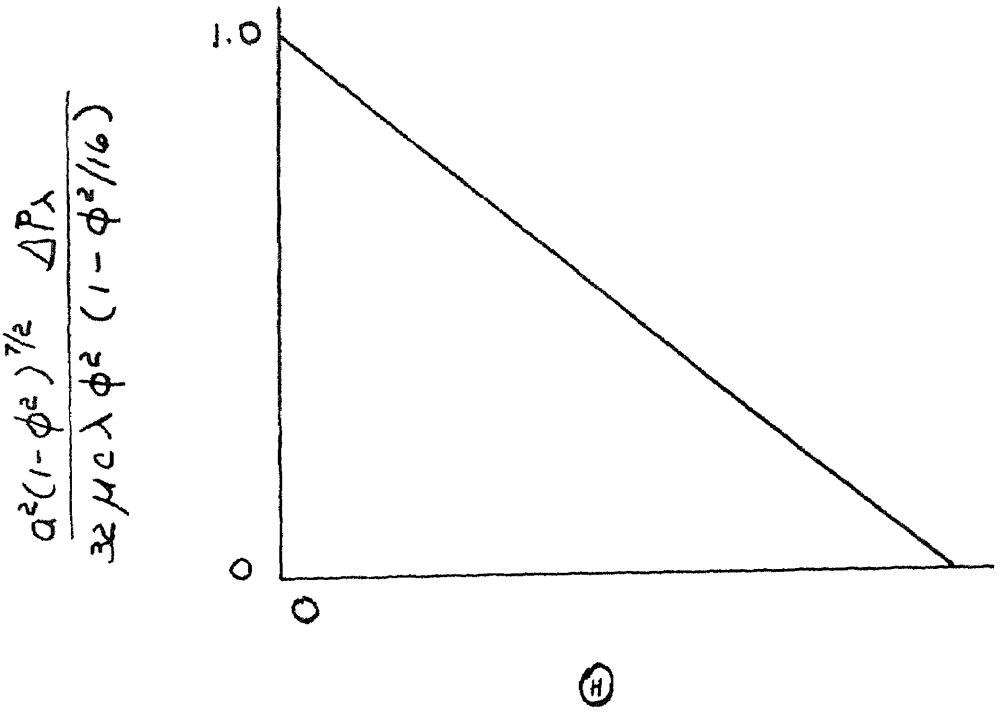

Figure 23 Plot of Dimensionless Pressure Rise vs. Dimensionless Flow Rate

Equation (3-1) is a relationship between the dimensionless pressure rise per wavelength and the dimensionless time-mean flow rate. For fixed values of the wave geometry (a, b, λ, c) and for a constant viscosity μ, the relationship between ΔP_λ and θ is linear, figure 23. This linearity results from the assumption that the Reynolds number approaches zero.

This relationship is similar to a pump head vs. flow characteristic curve. As can be seen from figure 23, the "head" produced by the pump decreases linearity with increasing flow rates. The intercept on the ordinate axis represents the zero-flow or shut-off head condition. The intercept on the abscissa represents the zero head or maximum flow condition.

3.1.3 Peristaltic Pumping of Pseudoplastic Fluids - Two Dimensional Geometry

In sections 3.1.3 and 3.1.4 the gross pumping performance of a pseudoplastic fluid with a peristaltic pump is developed. The details of the analyses presented in these sections may be found in Appendices A and B.

Consider an infinite train of sinusoidal peristaltic waves traveling along the walls of a two-dimensional channel. The problem may be solved in either of two reference frames, the laboratory reference frame

or the reference frame fixed to a moving wave. Since the flow is steady in the reference frame of the wave, the problem is initially solved in this reference frame. Refer to figure (A-1) in Appendix A for the explanation of the nomenclature.

The following assumptions are made:

1. the appropriate Reynolds number is sufficiently small such that the inertial terms in the equations of motion may be neglected;
2. the ratio of the wavelength to the diameter is sufficiently large that the pressure may be considered uniform over each cross section;
3. there is an infinite train of sinusoidal waves with the wall coordinate following the law

$$h = a + b \sin(2\pi x/\lambda) \tag{3-2}$$

(Shapiro [34] has shown that the solution is also valid if the number of waves is finite and integral) and,

4. the fluid is a time-independent pseudoplastic.

The continuity equation for an incompressible fluid becomes

$$\frac{\partial u}{\partial x} + \frac{\partial v}{\partial y} = 0 \tag{3-3}$$

The momentum equation in the x direction in the steady flow wave

coordinate system reduces to

$$\frac{dP}{dx} = -\frac{\partial}{\partial y}(\tau_{yx}) \tag{3-4}$$

The constitutive relationship between the shear stress and the shear rate for a pseudoplastic is given by

$$\tau_{yx} = -K\left|\frac{\partial u}{\partial y}\right|^{n-1}\frac{\partial u}{\partial y} \tag{3-5}$$

The absolute value sign insures that the shear stress and the shear rate always have opposing signs. To remove the absolute value sign, the problem is considered in two regions, one region where $\frac{dP}{dx} \geq 0$ and the distinct region where $\frac{dP}{dx} < 0$.

Using the boundary conditions that

$$\text{at } y = 0 \quad , \frac{\partial u}{\partial y} = 0 \quad \text{and} \tag{3-6}$$

$$\text{at } y = h(x) \, , \quad u = -c \, ,$$

the expressions for the velocity profiles in the wave reference frame may be written in each region

$$u = -c - \left[\frac{n}{n+1}\left(\frac{1}{K}\right)^{\frac{1}{n}}\left(\frac{dP}{dx}\right)^{\frac{1}{n}}\right]\left[h^{\frac{n+1}{n}} - y^{\frac{n+1}{n}}\right] \text{ when } \frac{dP}{dx} \geq 0 \tag{3-7}$$

$$u = -c - \left(\frac{n}{n+1}\left(\frac{1}{k}\right)^{\frac{1}{n}}\left(-\frac{dP}{d\psi}\right)^{\frac{1}{n}}\right)\left(y^{\frac{n+1}{n}} - h^{\frac{n+1}{n}}\right) \quad \text{when} \quad \frac{dP}{d\psi} < 0 \qquad (3\text{-}8)$$

Substituting the expressions for the velocity u into the relationship

$$q = \int_0^{h(\psi)} u\,dy \qquad (3\text{-}9)$$

the volume flow rate through each cross section in the wave reference frame is evaluated in each of the regions

$$q = -ch - \left(\frac{n}{2n+1}\right)\left(\frac{1}{k}\right)^{\frac{1}{n}}\left(\frac{dP}{d\psi}\right)^{\frac{1}{n}}\left(h^{\frac{2n+1}{n}}\right) \quad \text{when} \quad \frac{dP}{d\psi} \geq 0 \qquad (3\text{-}10)$$

$$q = -ch + \left(\frac{n}{2n+1}\right)\left(\frac{1}{k}\right)^{\frac{1}{n}}\left(-\frac{dP}{d\psi}\right)^{\frac{1}{n}}\left(h^{\frac{2n+1}{n}}\right) \quad \text{when} \quad \frac{dP}{d\psi} < 0 \qquad (3\text{-}11)$$

These equations relate q to the pressure gradient $dP/d\psi$. In addition, when $dP/d\psi$ is set equal to zero, they determine the limits of the two regions.

The time-mean flow rate in the laboratory reference frame, $\overline{Q}$, is related to q by the expression

$$\overline{Q} = q + ac \qquad (3\text{-}12)$$

Using equations 3-10 and 3-11 to eliminate the pressure gradient and noting that

$$U = u + c \tag{3-13}$$

the longitudinal velocity in the laboratory reference frame is given by

$$U = \left(\frac{2m+1}{m+1}\right)\left(\frac{bc}{h}\right)\left(\frac{\bar{Q}}{bc} + \sin 2\pi\left(\frac{X-ct}{\lambda}\right)\right)\left(1 - \left(\frac{Y}{h}\right)^{\frac{m+1}{m}}\right) \tag{3-14}$$

The transverse velocity in the laboratory reference frame may be calculated from the continuity relationship

$$V = -\int_0^Y \frac{\partial U}{\partial X}\, dY \tag{3-15}$$

$$V = -\left(\frac{4m+2}{m+1}\right)\left(\frac{\pi b}{\lambda}\right)\cos 2\pi\left(\frac{X-ct}{\lambda}\right)\left\{\frac{\bar{Q}}{ch}\left[\left(\frac{Y}{h}\right)^{\frac{2m+1}{m}} - \left(\frac{Y}{h}\right)\right] - \frac{a}{h}\left[\left(\frac{Y}{h}\right)^{\frac{2m+1}{m}} - \frac{Y}{h}\right] + \left(\frac{m+1}{2m+1}\right)\left(\frac{Y}{h}\right)^{\frac{2m+1}{m}}\right\} \tag{3-16}$$

where $$h = h(X,t) = a + b \sin 2\pi\left(\frac{X-ct}{\lambda}\right)$$

Notice that $U = U(X, Y, t)$ and $V = V(X, Y, t)$. At any given time t and axial position X , the longitudinal velocity profile is proportional to the quantity $\left(1 - \frac{Y}{h}^{\frac{n+1}{n}}\right)$ and takes the shape of a blunted parabola. This is characteristic of pseudoplastic fluids.

The pressure rise per wavelength is defined by

$$\Delta P_\lambda = \int_0^\lambda \left(\frac{dP}{dx}\right) dx \tag{3-17}$$

Solving for the pressure gradient $\frac{dP}{dx}$ in terms of q and substituting into equation 3-17 and using equation 3-12 to relate $\bar{Q}$ and q , the resulting equation gives the relationship between the pressure rise per wavelength and the time-mean flow rate. After performing a number of algebraic manipulations and a change in variables to bring the equation into dimensionless form, the following equation results

$$\left(\frac{n}{2n+1}\right)^n \frac{a^{n+1}\,\Delta P_\lambda}{k\, c^n \lambda\, \phi^n} = -\int_0^{\frac{1}{2\pi}[\sin^{-1}(-\theta)]_1} \left(\frac{(\theta + \sin(2\pi z))}{(1+\phi \sin(2\pi z))^{2n+1/n}}\right)^n dz$$
$$+\int_{\frac{1}{2\pi}[\sin^{-1}(-\theta)]_1}^{\frac{1}{2\pi}[\sin^{-1}(-\theta)]_2} \left(\frac{-(\theta + \sin(2\pi z))}{(1+\phi \sin(2\pi z))^{2n+1/n}}\right)^n dz$$
$$-\int_{\frac{1}{2\pi}[\sin^{-1}(-\theta)]_2}^{1.0} \left(\frac{(\theta + \sin(2\pi z))}{(1+\phi \sin(2\pi z))^{2n+1/n}}\right)^n dz \tag{3-18}$$

where

ΔP_λ = pressure rise per wavelength

a = channel half-width

c = wavespeed

λ = wavelength

b = wave amplitude

ϕ = amplitude ratio = b/a

m = power law exponent

K = power law constant

$\bar{Q}$ = time-mean flow rate

Θ = dimensionless time-mean flow rate = $\bar{Q}/bc$

$\mathcal{J}$ = dimensionless wavelength = π/λ

Equation 3-18 is a pump characteristic curve; it establishes the gross pumping performance of the peristaltic pump by relating the pressure rise produced by the pump to the time-mean flow rate.

Equation 3-18 has been integrated numerically. A digital computer program to accomplish this integration using Simpson's rule has been included in Appendix E. The results of this numerical integration are presented in Section 3.1.5.

As expected, the relationship given in the equation 3-18 reduces to the relationship presented by Shapiro et al[34] for a Newtonian fluid when the power law exponent, m, is equal to 1.0. (Equation 3-1)

3.1.4 Peristaltic Pumping of Pseudoplastic Fluids - Axi-Symetric Geometry

Refer to figure (B-1) in Appendix B for an explanation of the nomenclature.

The four assumptions listed in Section 3.1.3 for the two-dimensional case are also employed for the axi-symetric geometry.

The continuity equation for an incompressible fluid is given by

$$\frac{\partial V}{\partial r} + \frac{V}{r} + \frac{\partial U}{\partial \eta} = 0 \qquad (3\text{-}19)$$

The momentum equation in the axial direction in the steady flow wave coordinate system reduces to

$$\frac{dP}{d\eta} = -\frac{1}{r}\frac{\partial}{\partial r}(r\tau_{r\eta}) \qquad (3\text{-}20)$$

The constitutive relationship between the shear stress and the shear rate for a pseudoplastic is given by

$$\tau_{r\eta} = -K\left|\frac{\partial U}{\partial r}\right|^{n-1}\frac{\partial U}{\partial r} \qquad (3\text{-}21)$$

The absolute value sign insures that the shear stress and the shear rate always have opposing signs. To eliminate the absolute value sign, the problem is considered in two regions, one where $\frac{dP}{d\eta} \geq 0$ and the

distinct region where $\frac{dP}{dx} < 0$.

Using the boundary conditions that

$$\text{at } r = 0, \quad \tau_{rx} = 0 \text{ and}$$
$$\text{at } r = h(x), \quad u = -c, \tag{3-22}$$

the expressions for the velocity profiles in each region in the wave reference frame are written as

$$u = -c - \left[\left(\frac{n}{n+1}\right)\left(\frac{1}{2k}\right)^{\frac{1}{n}} \left(\frac{dP}{dx}\right)^{\frac{1}{n}}\right]\left[h^{\frac{n+1}{n}} - r^{\frac{n+1}{n}}\right] \text{ when } \frac{dP}{dx} \geq 0 \tag{3-23}$$

$$u = -c - \left[\left(\frac{n}{n+1}\right)\left(\frac{1}{2k}\right)^{\frac{1}{n}} \left(-\frac{dP}{dx}\right)^{\frac{1}{n}}\right]\left[r^{\frac{n+1}{n}} - h^{\frac{n+1}{n}}\right] \text{ when } \frac{dP}{dx} < 0 \tag{3-24}$$

Substituting the expressions for the longitudinal velocity u into the relationship

$$q = \int_0^{h(x)} (u)(2\pi r)\, dr \tag{3-25}$$

the volume flow rate through each cross section in the wave reference frame is evaluated in each of the regions

$$q = -\pi h^2 c - \pi \left(\frac{1}{2k}\right)^{\frac{1}{n}} \left(\frac{dP}{dx}\right)^{\frac{1}{n}} \left(\frac{n}{3n+1}\right) h^{\frac{3n+1}{n}} \quad \text{when } \frac{dP}{dx} \geq 0 \tag{3-26}$$

$$q = -\pi h^2 C + \pi \left(\frac{1}{2K}\right)^{\frac{1}{m}} \left(-\frac{dP}{d\chi}\right)^{\frac{1}{m}} \left(\frac{m}{3m+1}\right) h^{\frac{3m+1}{m}} \quad \text{when} \quad \frac{dP}{d\chi} < 0 \qquad (3\text{-}27)$$

These equations relate q to the pressure gradient $\frac{dP}{d\chi}$. In addition, when $dP/d\chi$ is set equal to zero, they determine the limits of the two regions.

The time-mean flow rate in the laboratory reference frame, $\bar{Q}$, is related to q by the expression

$$\bar{Q} = q + \pi a^2 C \left(1 + \phi^2/2\right) \qquad (3\text{-}28)$$

Using equations 3-26 and 3-27 to eliminate the pressure gradient and noting that

$$U = u + c \qquad (3\text{-}29)$$

the longitudinal velocity in the laboratory reference frame U is given by

$$U = \left(\frac{3m+1}{m+1}\right)\left(\frac{q}{\pi} + \frac{h^2}{a^2}\,\frac{\pi a^2 C}{\pi}\right)\left(\frac{1}{h^2}\right)\left(1 - \left(\frac{r}{h}\right)^{\frac{m+1}{m}}\right) \qquad (3\text{-}30)$$

The transverse velocity in the laboratory reference frame V may be calculated from the continuity relationship

$$\frac{1}{r}\frac{\partial}{\partial r}(rV) = -\frac{\partial U}{\partial r} \qquad (3\text{-}31)$$

$$V = \frac{2\pi bc}{\lambda} \cos 2\pi \left(\frac{X-ct}{\lambda}\right) \left\{ \frac{3n+1}{n+1} \frac{q}{\pi h^2 c} \left(\frac{R}{h}\right) - \left(\frac{R}{h}\right)^{\frac{2n+1}{n}} - \frac{3n+1}{n+1} \frac{q}{\pi h^2 c} \left(\frac{R}{h}\right)^{\frac{2n+1}{n}} \right\} \tag{3-32}$$

where $$h = h(X,t) = a + b \sin 2\pi \left(\frac{X-ct}{\lambda}\right)$$

Notice that $U = U(X,R,t)$ and $V = V(X,R,t)$. At any given time t and axial position X, the longitudinal velocity profile is proportional to the quantity $\left(1-R^{\frac{n+1}{n}}\right)$ and takes the shape of a blunted parabola. This is characteristic of pseudoplastic fluids.

The pressure rise per wavelength is defined by

$$\Delta P_\lambda = \int_0^\lambda \left(\frac{dP}{dx}\right) dx \tag{3-33}$$

Solving for the pressure gradient dP/dx in terms of q and substituting into equation 3-33 and using equation 3-28 to relate $\bar{Q}$ and q, the resulting equation gives the relationship between the pressure

rise per wavelength and the time-mean flow rate. This is the desired pump characteristic curve. After performing a number of algebraic manipulations and a change of variables to bring the equation into dimensionless form and defining a dimensionless time-mean flow rate by the expression

$$\Theta = \frac{\overline{Q}}{\pi a^2 c\,(2\phi - \phi^2/2)} \tag{3-34}$$

the equation given by 3-35 results. Θ has a physical significance. The denominator of this expression is the flow that would be transported if all the material in the tube between the radii (a-b) and (a+b) were convected rightwards with speed c. This denominator may be thought of as a "piston displacement" for the pump.

$$\left(\frac{m}{3m+1}\right)^m \frac{\Delta P_\lambda\, a^{m+1}}{2\kappa c^m \lambda} =$$

$$+\int_0^{\eta_1}\left(\frac{-((2\phi-\phi^2/2)\Theta-\phi^2/2+2\phi\sin 2\pi\eta+\phi^2\sin^2 2\pi\eta)}{(1+\phi\sin 2\pi\eta)^{\frac{3m+1}{m}}}\right)^m d\eta$$

$$-\int_{\eta_1}^{\eta_2}\left(\frac{(2\phi-\phi^2/2)\Theta-\phi^2/2+2\phi\sin 2\pi\eta+\phi^2\sin^2 2\pi\eta)}{(1+\phi\sin 2\pi\eta)^{3m+1/m}}\right)^m d\eta \tag{3-35}$$

$$+\int_{\eta_2}^{1.0}\left(\frac{-((2\phi-\phi^2/2)\Theta-\phi^2/2+2\phi\sin 2\pi\eta+\phi^2\sin^2 2\pi\eta)}{(1+\phi\sin 2\pi\eta)^{3m+1/m}}\right)^m d\eta$$

where the limits of integration η_1 and η_2 are the roots of the transcendental equation $-(2\phi-\phi^2/2)\Theta+\phi^2/2 = 2\phi\sin 2\pi\eta+\phi^2\sin^2 2\pi\eta$ (3-36)

and Ⓜ is defined by equation 3-34.

Equation 3-35 establishes the gross pumping performance of the peristaltic pump. It is a pump characteristic curve which allows one to relate the pressure rise produced by the pump to the time-mean flow rate.

Equation 3-35 was integrated numerically by means of a digital computer program in Fortran language using Simpson's rule. (Appendix E) The roots of the transcendental equation 3-36 were found by the Newton-Raphson method. The results of this numerical integration are presented in Section 3.1.5.

Note that the relationship given in equation 3-35 reduces to the relationship presented by Shapiro et al.[34] for a Newtonian fluid when the power law exponent, m, is equal to 1.0.

3.1.5 Energy Considerations

Consider the general viscous energy equation in differential form written for an incompressible Newtonian fluid

$$\rho \frac{De}{Dt} + \nabla \cdot k \nabla T - \nabla \cdot \left(\sum_j \rho D_j h_j \nabla m_j \right) - \mu \Phi - S = 0 \qquad (3\text{-}37)$$

where $\rho \frac{De}{Dt}$ = the rate of internal energy storage per unit volume.

$\nabla \cdot k \nabla T$ = the rate of energy transfer by conduction per unit volume.

$\nabla \cdot \left(\sum_j \rho D_j h_j \nabla m_j \right)$ = the rate of energy transfer by mass diffusion per unit volume.

$\mu \Phi$ = the rate at which the mechanical energy of flow is converted into heat by viscous dissipation per unit volume.

S = the rate of internal energy generation within the fluid per unit volume.

Although the source of the metabolic chemical energy for peristaltic flow may lie within the nerve cell, most investigators feel that this energy is supplied from external sources, possibly from the neighboring Schwann cell. It is assumed in our model that the external peristaltic waves provide the energy for this flow; hence, internal energy sources, S, are neglected.

Mass diffusion associated with the conduction of nerve impulses probably takes place across the boundaries of the nerve fiber. However, this mass flux is assumed to be quite small with respect to axoplasmic flow and mass diffusion is neglected as a significant energy flux.

Thus the energy equation reduces to

$$\rho \frac{De}{Dt} + \nabla \cdot k \nabla T - \mu \Phi = 0 \qquad (3\text{-}38)$$

Equation 3-38 is known as the differential equation of thermal energy, which equates the rate of internal energy storage to the rate of viscous dissipation less the rate of energy conduction.

An order of magnitude estimation of the rate of viscous dissipation indicates that the local temperature gradients within the axoplasm due to peristaltic pumping are entirely negligible. Although the viscosity of the axoplasm is quite large, the velocity gradients within the fluid are sufficiently small such that the local heat generated by viscous friction may be neglected. Because of the large number of nerve fibers in the nervous system ($\sim 10^{10}$), however, the total heat generated within the system is a measurable quantity (~ 0.2 Kcal./day.). Refer to Section 4.5 and Appendix H.

The traveling peristaltic waves act as a pumping mechanism supplying energy to the fluid in the form of mechanical work. Part of this externally supplied work is stored in the fluid as flow work and part is converted into heat by viscous dissipation.

E = Rate of useful energy storage per wavelength = $\int_0^{h(x)} \int_0^{\lambda} U \frac{dP}{dx} dx dy$

$E = Q \Delta P_\lambda$

D = Rate of viscous dissipation per wavelength = $-\int_0^{\lambda} \int_0^{h(x)} \mu \Phi \, dx dy$

where Φ = dissipation function

W = Rate at which mechanical energy must be supplied

Taking the average rates over the period

$$\bar{\omega} = \bar{Q}\,\Delta P_\lambda + D$$

we may define a mechanical efficiency consistent with that commonly used for pumping machinery as

$$\eta = \frac{\bar{E}}{\bar{\omega}} = \frac{\bar{Q}\,\Delta P_\lambda}{\bar{Q}\,\Delta P_\lambda + D}$$

3.1.6 Presentation and Discussion of Results of Theoretical Analysis

Results have been plotted for the axi-symetric case only. The results for the two-dimensional case are similar to the axi-symetric case and the same qualitative discussion applies to both.

The pump characteristic relationships, equations 3-18 and 3-35, express the dimensionless pressure rise versus the dimensionless time-mean flow rate in terms of both the wave and fluid parameters. Since the integrations were not performed directly, the explicit functional relationships between the parameters were not determined in closed form. The results of the numerical integration are shown graphically in terms of two parameters, the amplitude ratio, ϕ , and the power law exponent, m .

In figures (24) and (25), the ordinate is the dimensionless

pressure rise normalized by dividing through by the value of the integral on the right hand side of equation 3-35 when $\Theta = 0.0$. The abscissa is the dimensionless time-mean flow rate defined by equation 3-34. Figure (24) shows a series of curves plotted for different values of the amplitude ratio ϕ and the constant power law exponent m . Figure (25) shows a series of curves plotted at constant amplitude ratio and different values of m .

Since the dimensionless pressure rise contains a function of m , both explicitly and implicitly, and the dimensionless flow rate contains a function of ϕ , it is of limited value to discuss the effects of these parameters on the families of curves. The relationship between ΔP_λ and $\bar{Q}$ is much more of interest. The effect of the parameters on this relationship will become apparent when numerical values are inserted into these expressions in Chapter 4.

A brief discussion concerning the general shape of the curves is of interest. A pseudoplastic fluid is characterized by a decrease in apparent viscosity with increasing shear rate, a shear rate "thinning". For a peristaltic pump operating at constant wave speed, the internal shearing of the fluid is greater at low flow rates because there is more backflow through the pump. Hence the apparent viscosity is lower. At higher flow rates there is less internal shearing and the apparent viscosity is correspondingly higher. But the higher viscosity reduces

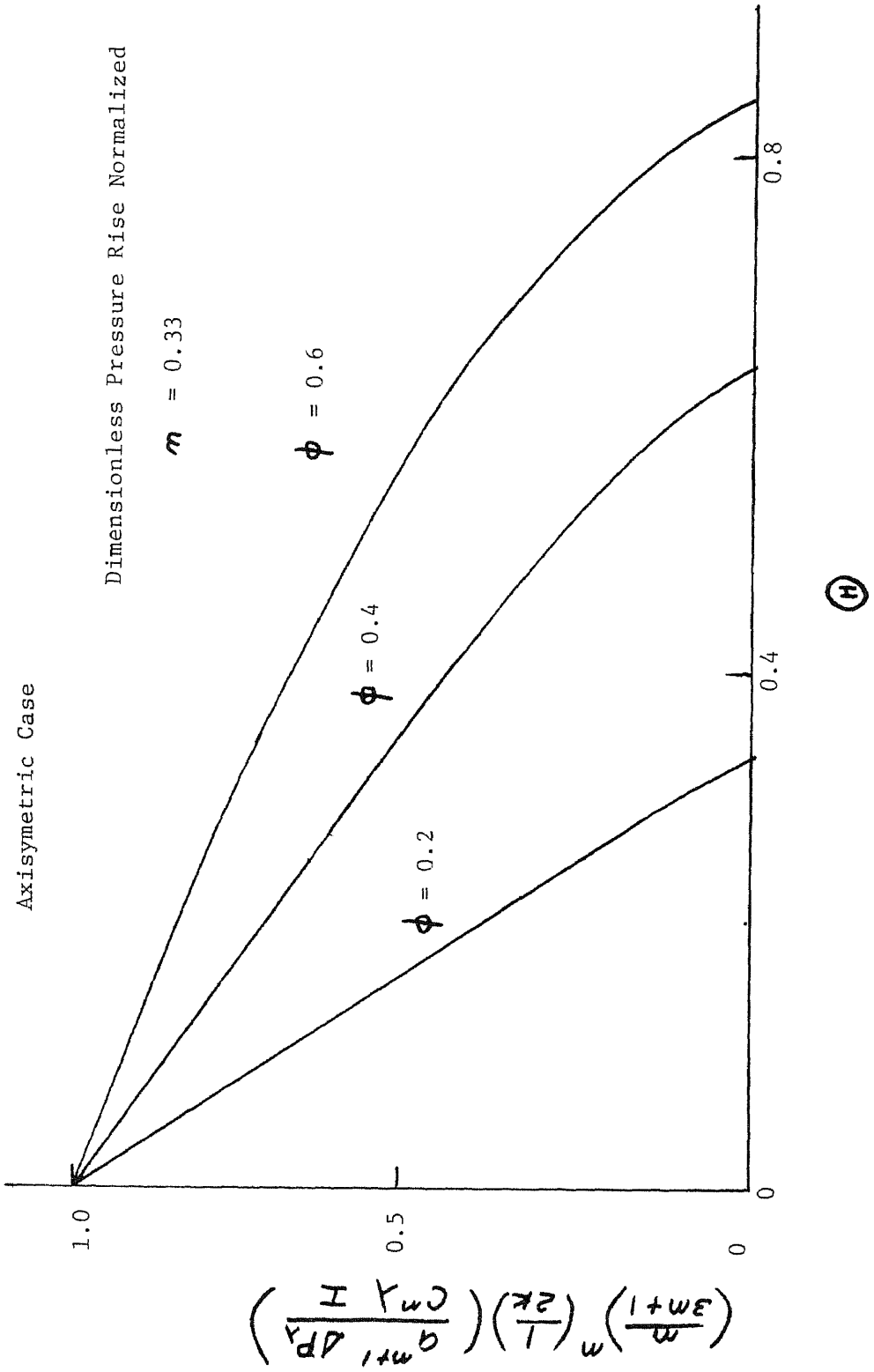

Figure 24 Plot of Theoretical Dimensionless Pressure Rise Versus Dimensionless Time-Mean Flow Rate - Pseudoplastic Fluid

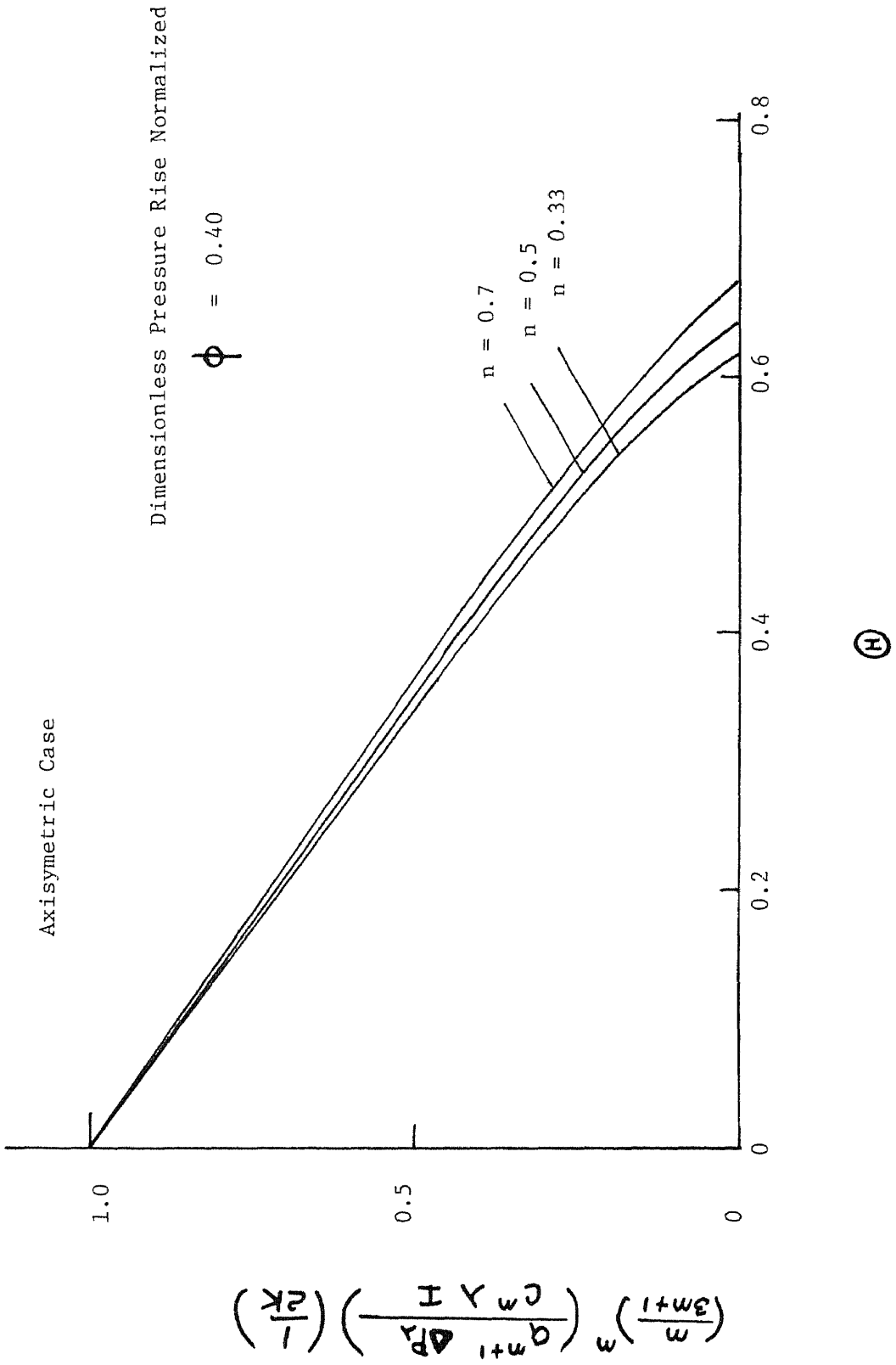

Figure 25 Plot of Theoretical Dimensionless Pressure Versus Dimensionless Time-Mean Flow Rate - Pseudoplastic Fluid

the actual flow rate somewhat. This explains the tendency of the curves to bend downward slightly at higher flow rates.

3.2 EXPERIMENTAL ANALYSIS

3.2.1 Description of the Experimental Apparatus

A two-dimensional model to simulate peristaltic pumping was constructed in the machine shop at the Newark College of Engineering. The model was designed to allow a systematic investigation of the parameters affecting the "gross" pumping performance and to study the fluid motions within the pump. The parameters which may be varied include the wave speed, the wave amplitude, the amplitude ratio, the wavelength, the fluid viscosity, and the type of fluid. The model was constructed of Plexiglas to permit the details of the internal fluid motion to be studied. A photograph of the test model is shown in figure (26).

The model was constructed of an upper and lower Plexiglas surface spaced apart a fixed distance to form a two-dimensional channel. The side walls of the channel were formed of .027" thick rubber sheet. The peristaltic waves were simulated by a series of circular teflon rollers which deformed the rubber side walls of the channel into an approximately sinusoidal shape, figure (27). The rollers were attached to a continuous sprocket and chain assembly which was driven by a low speed motor. As the sprocket and chain assembly rotated, it caused the

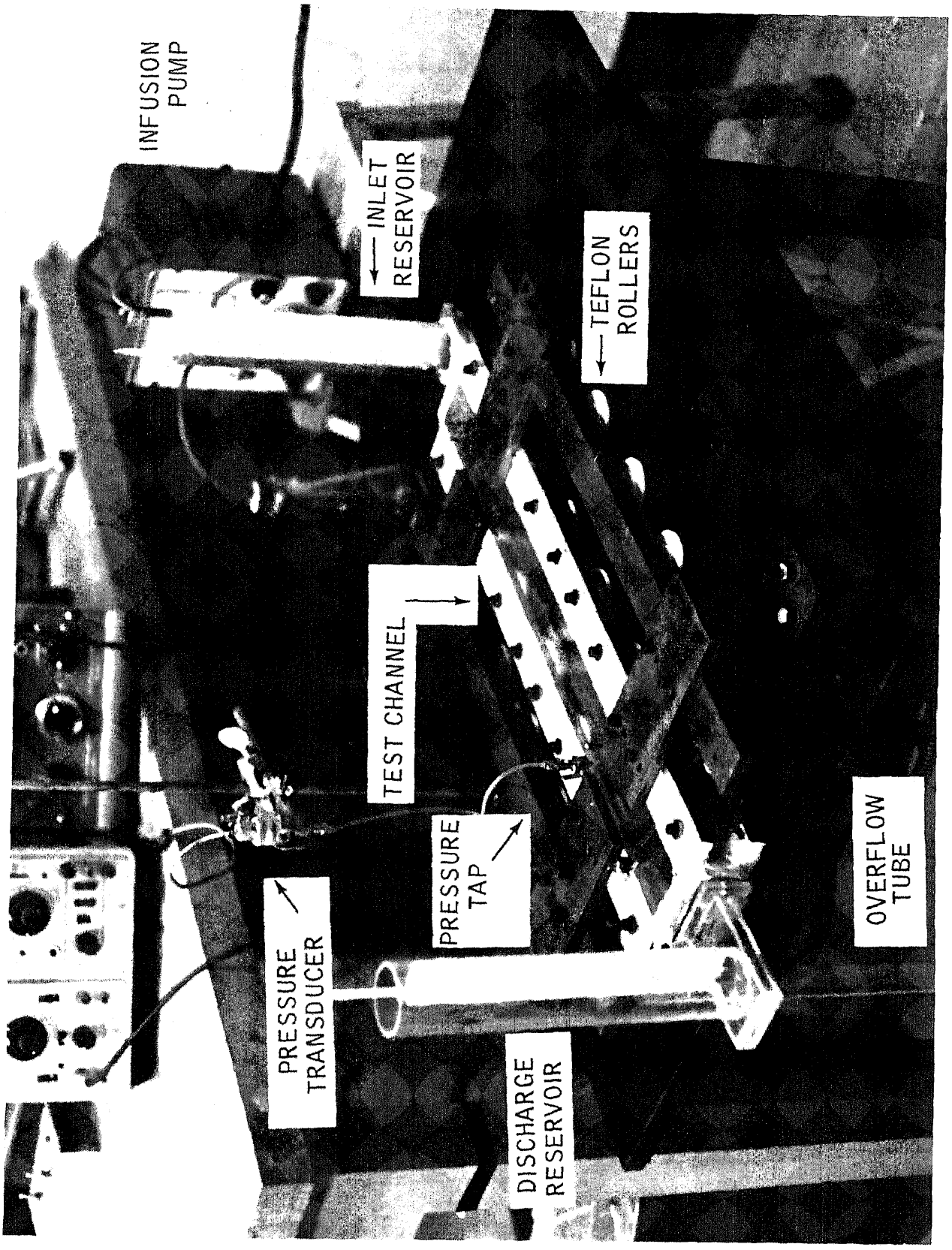

Figure 26 Photograph of Two-Dimensional Test Model

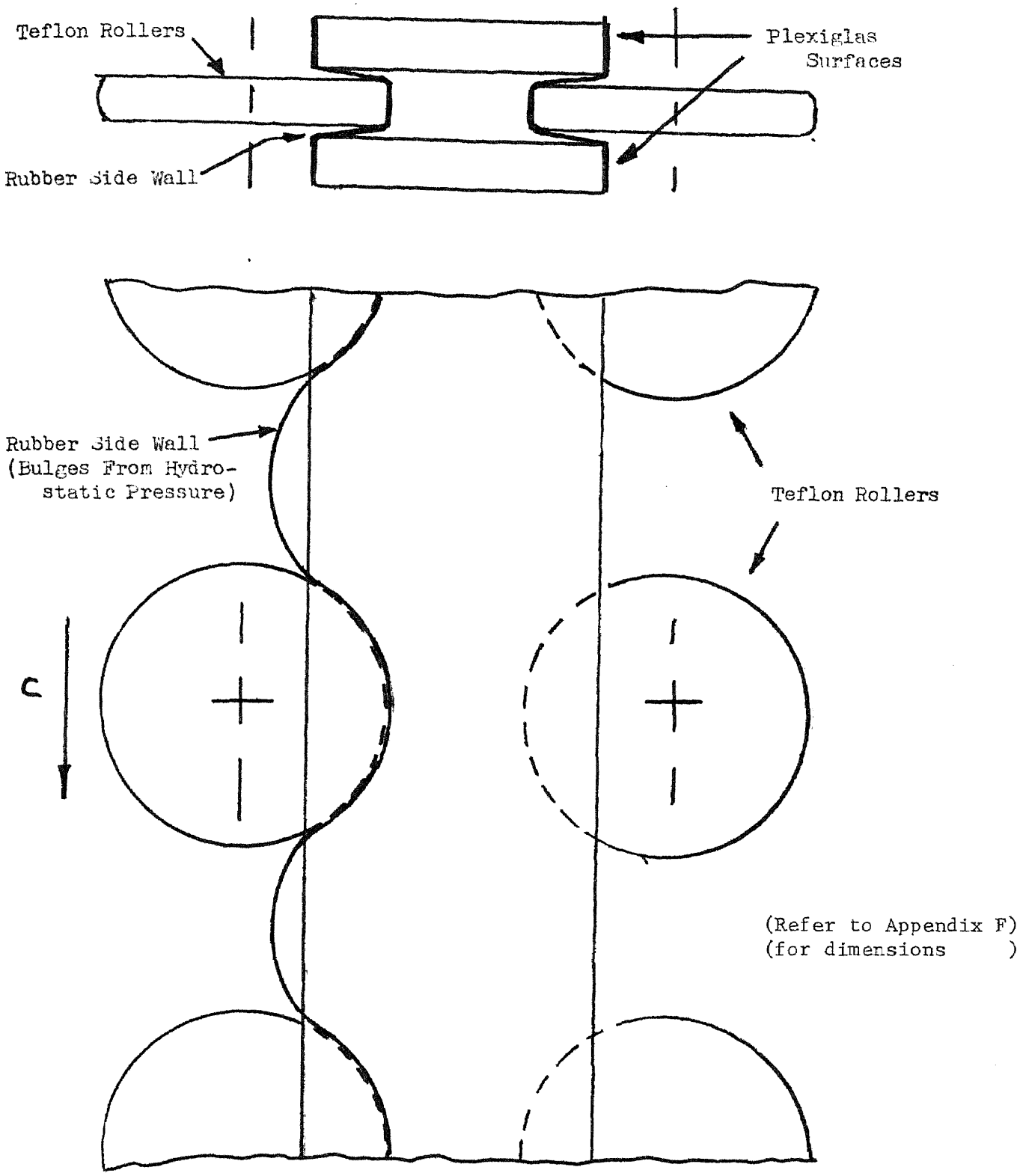

Figure 27 Schematic Of Peristaltic Pump Test Model

teflon rollers to travel lengthwise down the test channel.

Different values of the amplitude, the amplitude ratio, and the wavelength could be obtained by changing the size and spacing of the teflon rollers. The wavespeed could be varied by changing the drive gears on the motor shaft.

The pressure rise produced by the pump and the flow rate were measured by a reservoir attached to each end of the peristaltic pump as shown schematically in figure (28). The difference between the height of the fluid in the "high head" reservoir and the height of the fluid in the "low head" reservoir determined the pressure rise across the pump. The high head reservoir at the discharge end of the pump was supplied with an overflow drain tube. By varying the position of this tube, the peristaltic pump could be operated at different pressure rise conditions. The overflow from the high head reservoir was the net flow. The flow rate was determined by measuring the time required to collect a given quantity of fluid in a graduated cylinder. The height of the fluid in the low head reservoir was maintained constant by adding fluid with a small infusion pump at a rate equal to the flow rate of the peristaltic pump.

Several pressure taps were drilled into the upper plexiglas surface. Using a sensitive pressure transducer, a low noise, high gain,bridge

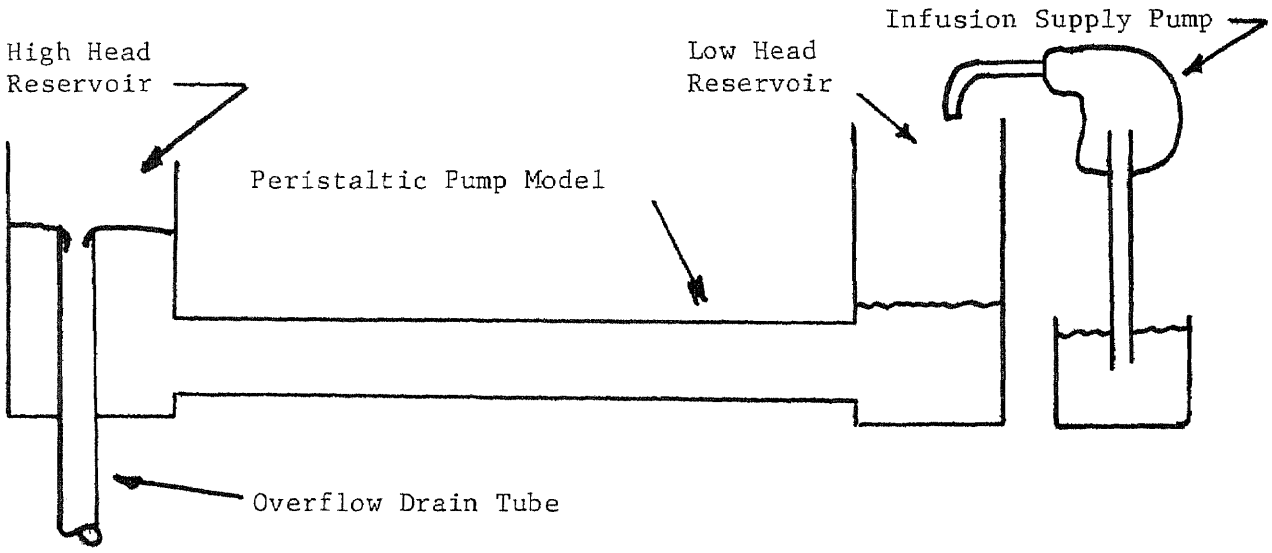

Figure 28 Schematic of Peristaltic Pump Flow Circuit

amplification meter and an oscilloscope, the pressure-time traces could be displayed graphically and photographed with a Polaroid camera.

By introducing small, neutral-density spheres into the fluid, particle path lines could be made visible and motion pictures taken during the passage of a wave.

More detailed information about the model and test equipment including dimensions, operating ranges, specific equipment used, and operating procedure are included in Appendix F.

3.2.2 Presentation of Experimental Results

The two-dimensional model was first used to verify the linear relationship between the dimensionless pressure rise and the dimensionless flow rate predicted by Shapiro [34]. Figure (29) shows the experimental results for the case where ϕ =0.6 and λ =3.5 inches. The dimensionless pressure rise (pressure ratio) is shown on the ordinate and the dimensionless time-mean flow rate (transport ratio) is shown on the abscissa. The theoretical relationship between the pressure ratio and the transport ratio is shown by the solid line in the figure. The variation in Reynolds number is shown by different symbols for the data points. The Reynolds numbers tested ranged from 0.01 to 0.60. Glycerine and Polyethylene Glycol 600 were used as the working fluids and they provided a viscosity range from 0.12 lb.-sec./ft.^{2} to 0.80 lb.-sec./ft.^{2}. The wave speed was varied from 0.211 inches/ sec. to 2.46 inches/sec.

In figure (29), the data appear to be reasonably linear although the transport ratio falls somewhat lower than the theoretical value. However, in light of some of the differences between the theoretical model and the experimental model discussed in Section 3.2.3, the results are in generally good agreement.

The model was next used to verify the theoretical relationship derived in Appendix A for a pseudoplastic fluid. Figure (30) shows

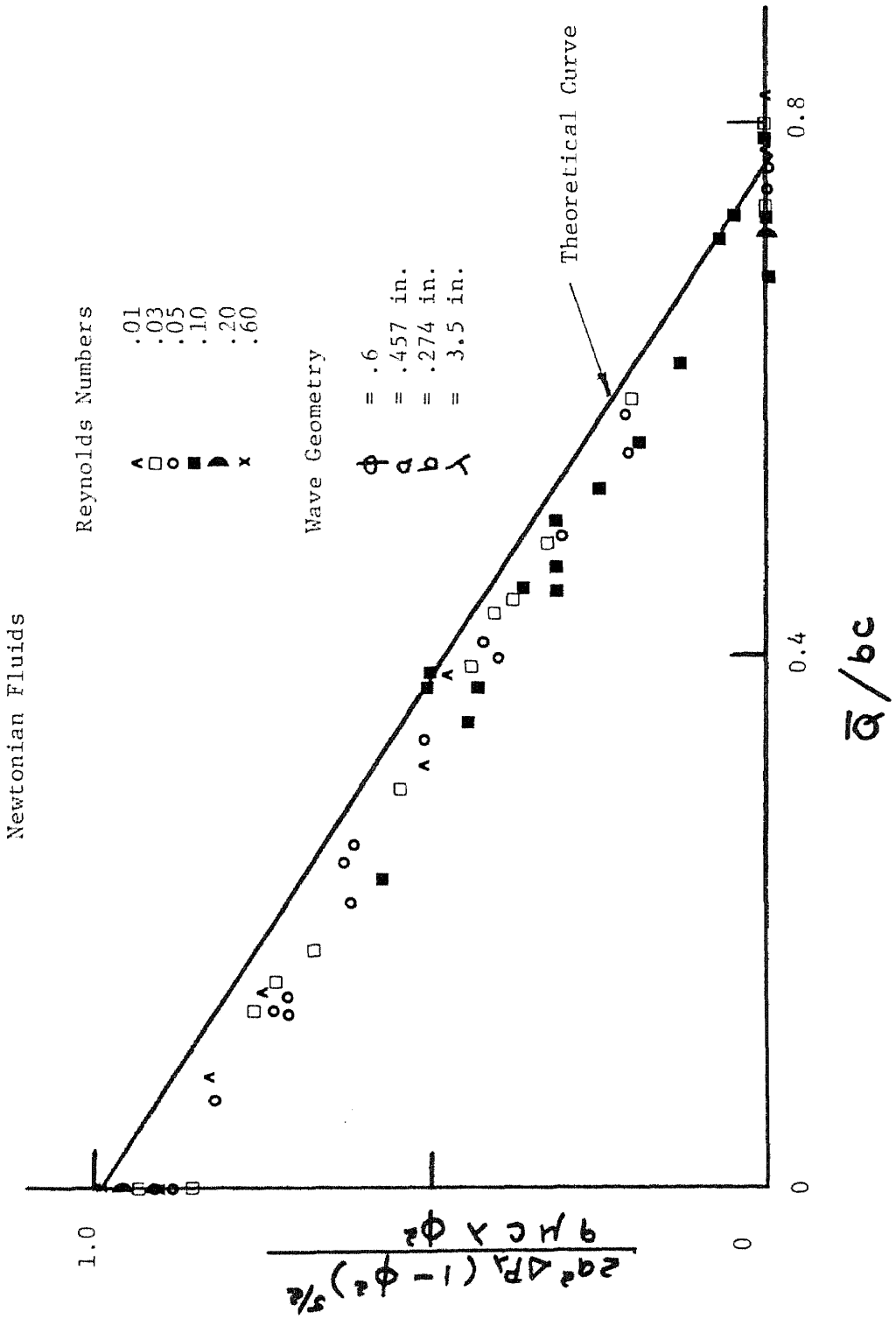

Figure 29 Dimensionless Pressure Rise Versus Dimensionless Time- Mean Flow Rate - Newtonian Fluids (Model Results)

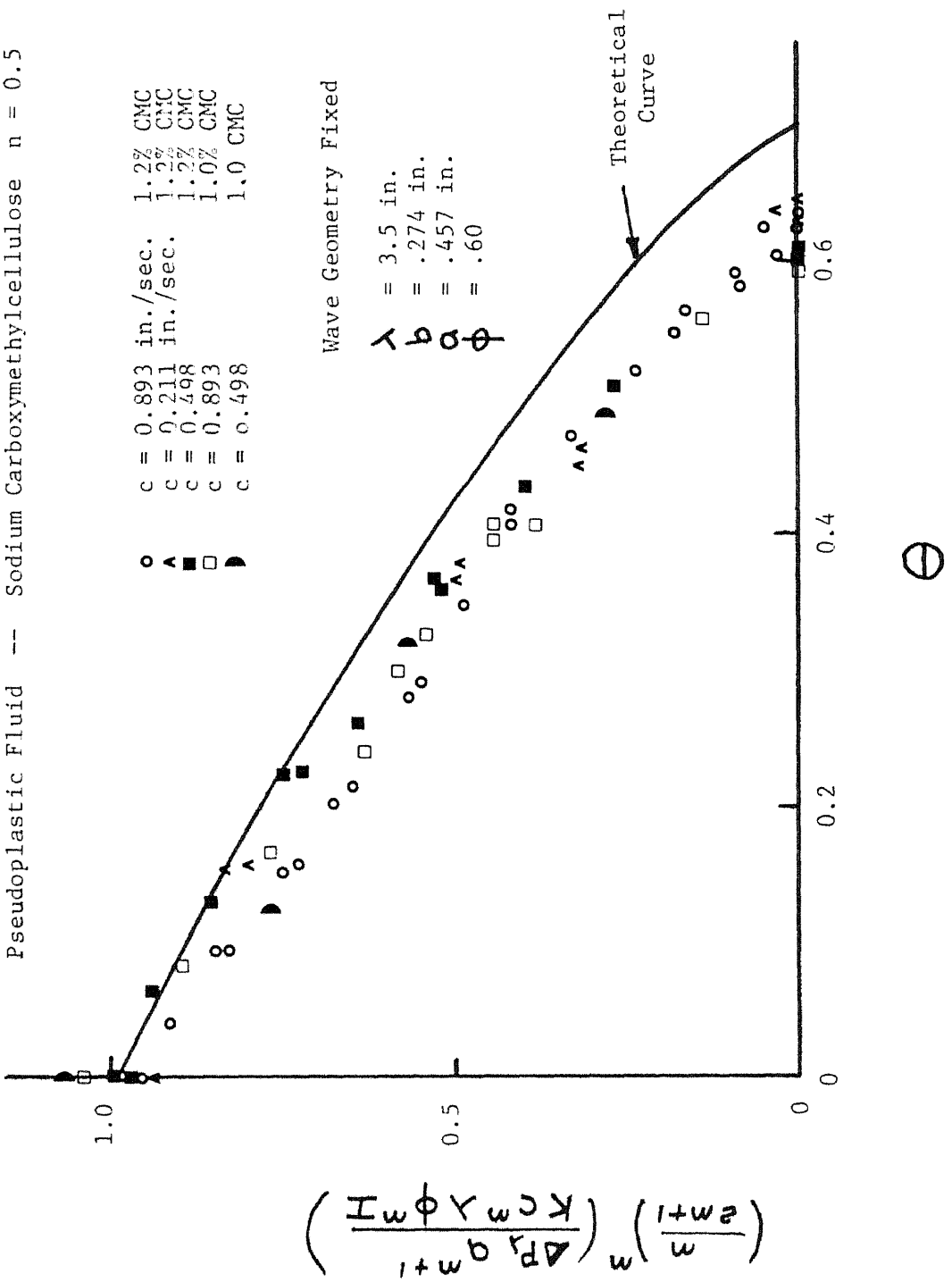

Figure 30 Plot of Dimensionless Pressure Rise Versus Dimensionless Time-Mean Flow Rate - Sodium Carboxymethylcellulose (Model Results)

the experimental results for the case where ϕ =0.6 and λ =3.5 inches. The theoretical relationship between the pressure ratio and the transport ratio is shown as the solid curve in the figure. Sodium Carboxymethylcellulose (Hercule Powder Company 7H3S — C.M.C.) was used as the pseudoplastic test fluid. To establish the viscometric properties of the different concentrations of C.M.C., a series of different Cannon-Fenske capillary tube viscometers were used to determine the flow curves. For concentrations of C.M.C. from 1.0% to 1.2%, the power law exponent, m , was found to be equal to 0.5 while the power law constant, K , varied from 0.054 lb.-sec.^{n}/ft.^{2} to 0.102 lb.-sec.^{n}/ft.^{2}. The wave speed was varied from 0.211 inches/sec. to 2.46 inches/sec.

As may be seen in figure (30), the data appear to follow the general trend of the theoretical curve, although the data points fall somewhat below the theoretical results. In light of some of the differences between the theoretical and experimental model, the results are in generally good agreement.

3.2.3 Discussion of Experimental Results

In the theoretical analysis, it was assumed that the solution was independent of the z coordinate; that is, that the peristaltic tube was infinite in the normal direction. The experimental channel had an upper and lower surface. The effect of these surfaces would be to retard the speed of the fluid near the surfaces and thus to

decrease the mean flow rate.

The theoretical results rest upon the assumption of steady state conditions in the wave coordinate system. This implies that the tube is infinitely long. In the experimental model there were five waves between the ends of the pump. It is reasonable to expect that these end effects would lower the performance of the pump, since, at the discharge end, the fluid is forced into the reservoir and dissipates some kinetic pressure head as turbulence.

Variations in the temperature of the fluid caused the apparent viscosity to vary somewhat during a test run. Although attempts were made to correct for the effects of temperature, this source of error may have contributed to the scatter of the data points. The fact that the wave shape was only approximately sinusoidal may have also contributed another minor source of error.

The theoretical analysis was based on the assumption that the wavelength to diameter ratio was sufficiently large such that the pressure might be considered uniform over the cross section. In order to test the validity of this assumption, a series of pressure versus time traces were recorded for different values of the wave speed. Using a dual beam oscilloscope, the pressure versus time was simultaneously recorded at a point on the centerline of the test channel and at a point where $y/a = 0.8$ during the passage of a wave. Refer to the

sketch in figure (31) for the position of the pressure taps.

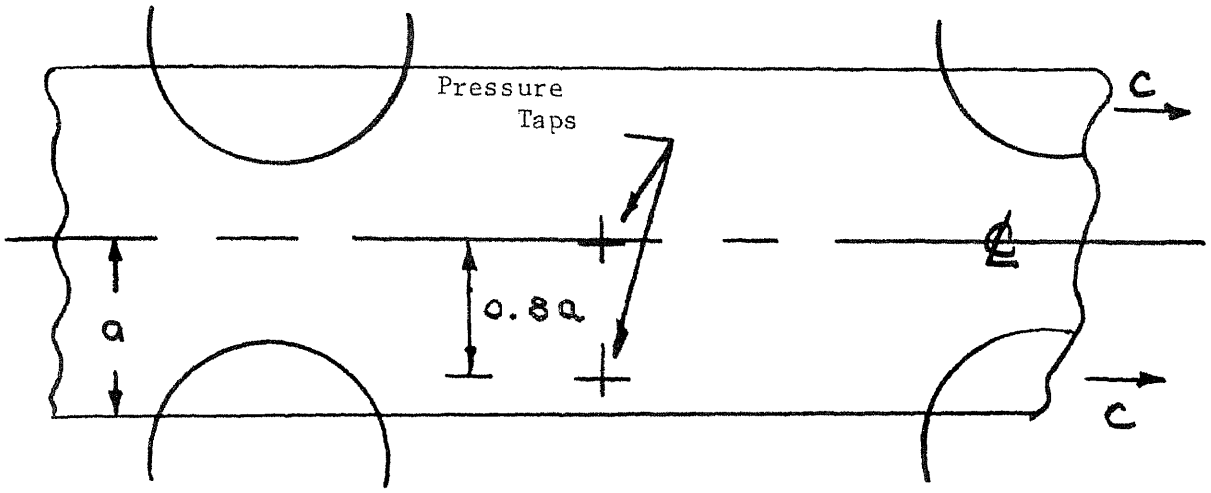

Figure 31 Position of Pressure Taps in Test Model

Figure(32) shows the results of three typical pressure-time traces. The lower curve in each photograph records the pressure at the center-line of the test channel while the upper trace shows the pressure near the wall. From these photographs, the assumption of uniform pressure over the cross section appears to be reasonable.

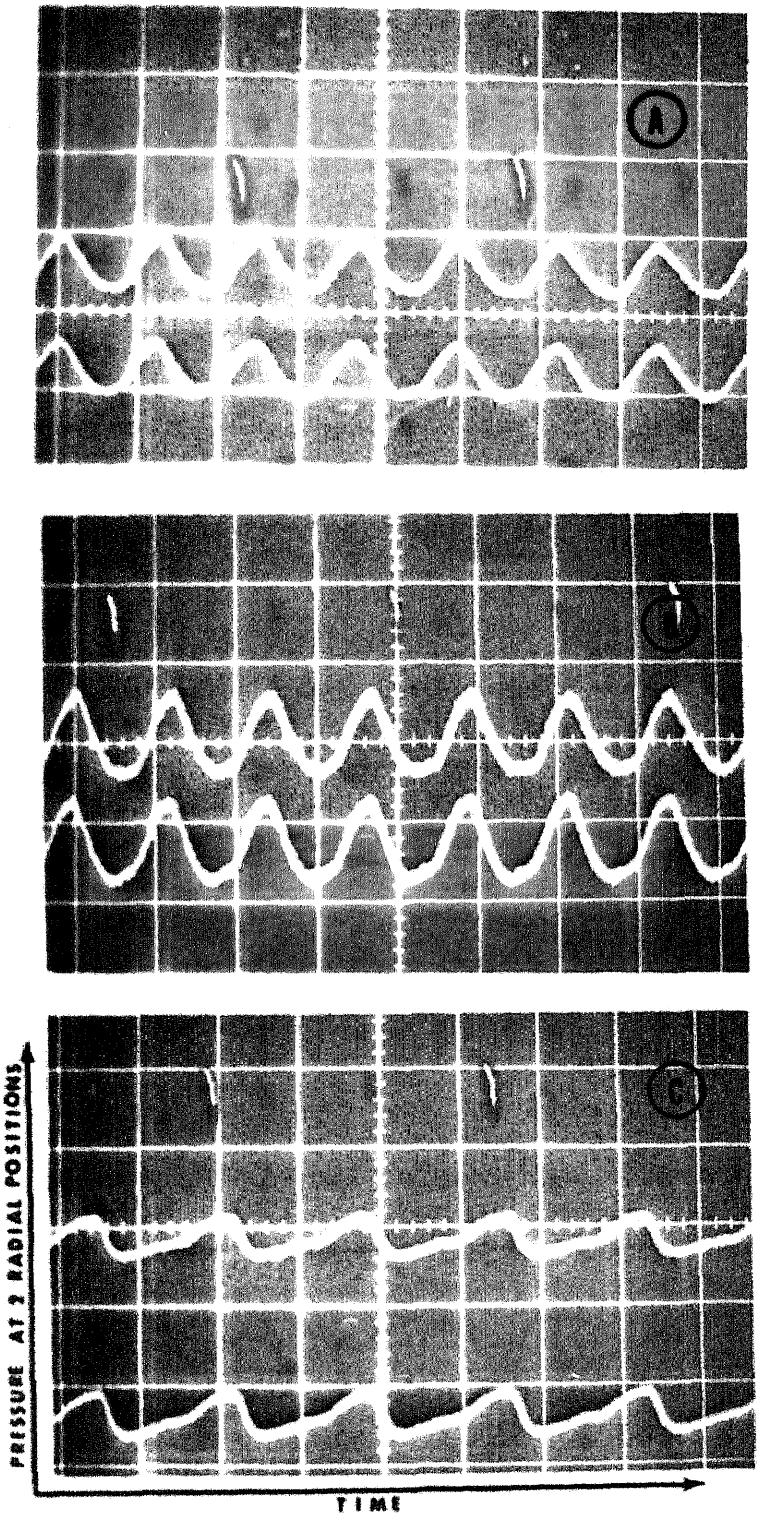

Upper Curves

y = .8a

Lower Curves

y = 0 (centerline)

A. Glycerine-Water

c = 2.4 in./sec.

sweep time 1 sec./cm.

B. Glycerine

c = 2.4 in./sec.

sweep time 1 sec./cm.

C. Glycerine

c = .89 in./sec.

sweep time 2 sec./cm.

Figure 32 Pressure Versus Time Traces Compared at Two Radial Positions

4. PREDICTION OF THEORETICAL AXONAL FLOW SPEED

4.1 Correlation of Pump Characteristic and System Resistance Curves to Determine a System Operating Point

Consider a continuous train of sinusoidal peristaltic waves traveling over the surface of a long tube as shown schematically in figure (33).

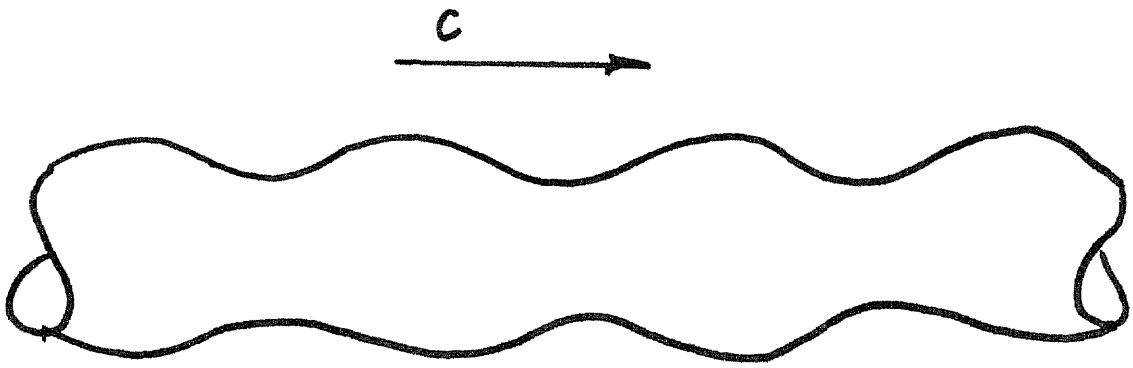

Figure 33 Schematic of a Train of Sinusoidal Peristaltic Waves

If the tube is sufficiently long such that any external resistance at the ends may be neglected or if the ends of the tube are open, the peristaltic mechanism would pump at its theoretical maximum flow rate.

This is specified by the point where the pump characteristic curve intersects the abscissa as shown in figure (34). This is the free discharge condition.

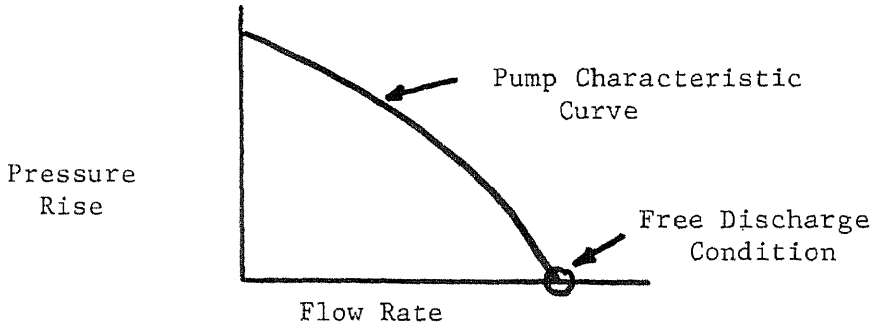

Figure 34 Typical Peristaltic Pump Characteristic Curve for Pseudoplastic Fluid

If, on the other hand, there is an external resistance, the pump will operate at a flow rate somewhat less than the free discharge condition. Specifically, the pump operating point will be determined by the intersection of the pump characteristic curve and the system resistance curve as shown in figure (35).

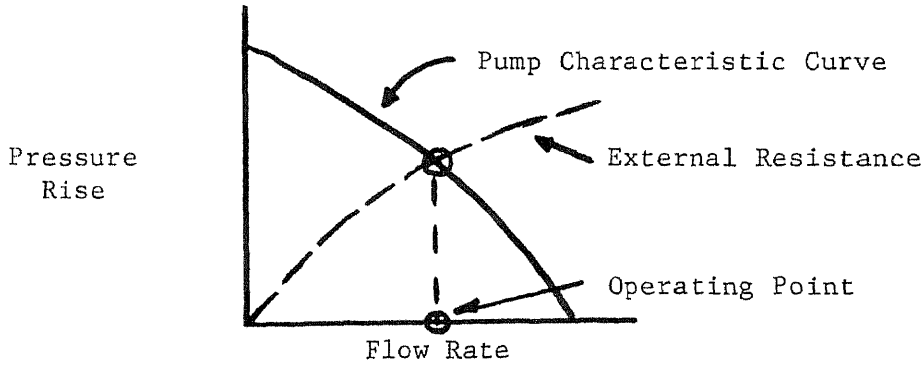

Figure 35 Determination of Operating Point by Intersection of Pump Characteristic and System Resistance Curves

Consider the case where the peristaltic waves are spaced apart from each other a certain distance as shown schematically in figure (36) which represents more accurately the waves observed in the motion pictures of axons in culture. Ideally, each wave may be thought of as an individual pumping mechanism and the region of undeformed tube between two successive waves may be considered to act as an external resistance.

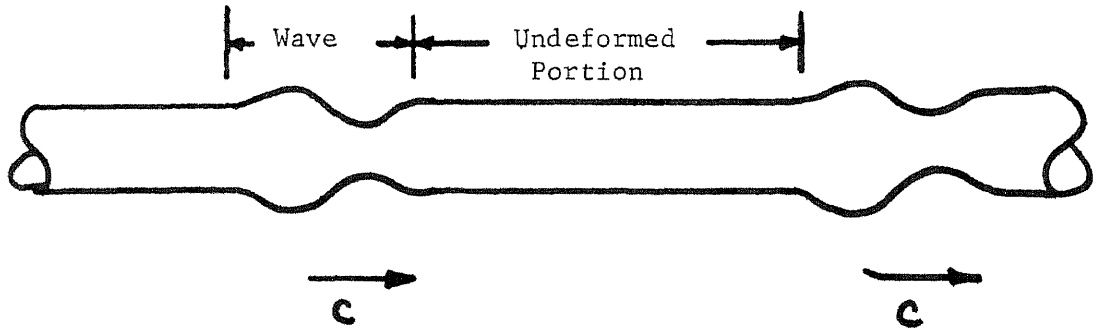

Figure 36 Schematic of Waves Spaced Apart Along the Surface of a Tube

4.2 Simultaneous Solution of Pump Characteristic Curve and System Resistance Curve to Determine Theoretical Flow Rate

Recall equation(3-35)

$$\Delta P_\lambda = \left(\frac{3m+1}{m}\right)^m \left(\frac{2KC^m\lambda}{a^{m+1}}\right) I(\phi, m, \textcircled{a})$$

(3-35)

where $I(\phi, m, \textcircled{a})$ represents the integral on the right hand side of equation (3-35).

If the total length of the tube is L , the total pressure rise is given by

$$\Delta P_T = \Delta P_\lambda (\lambda_o) = \Delta P_\lambda \, m_o L \tag{4-1}$$

where λ_o = total number of waves in the tube

and m_o = number of waves per unit length; therefore

$$\Delta P_T = \left(\frac{3m+1}{m}\right)^m \left(\frac{2KC^m\lambda}{a^{m+1}}\right) I(\phi, m, \Theta)\, m_o L \tag{4-2}$$

Equation (4-2) is the pump characteristic curve.

The system resistance curve for the flow of a pseudoplastic fluid through a uniform cylindrical tube (equation D-20) has been derived in Appendix D.

$$\Delta P = \left(\frac{4L'}{D}\right) k \left(\frac{3m+1}{m}\right)^m \left(\frac{8Q}{\pi D^3}\right)^m \tag{D-20}$$

where L' is the total length of the tube

For the case of the axon, where the waves are spaced apart as shown in figure (36), L' represents the total length of undeformed axon.

$$L' = L(1 - m_o\lambda) \tag{4-3}$$

Thus the system resistance curve for the axon may be determined from the expression

$$\Delta P = \left(\frac{4K}{D}\right)\left(\frac{3m+1}{m}\right)^m \left(\frac{8Q}{\pi D^3}\right)^m \left(L\left(1 - m_0\lambda\right)\right) \tag{4-4}$$

Equations (4-2) and (4-4) may be solved simultaneously for the theoretical operating flow rate or the theoretical mean flow rate. Eliminating the pressure and making the substitution $V = Q/A$, the expression for the mean flow speed V becomes

$$V = c\left[\frac{m_0\lambda}{1 - m_0\lambda}\, I(\phi, m, \Theta)\right]^{\frac{1}{m}} \tag{4-5}$$

Notice that V depends only on the geometrical properties of the peristaltic wave m_0, λ, c, ϕ and the flow behavior index m. Also, V is independent of both the consistency of the fluid K and the radius of the tube a. The biological significance of these two somewhat surprising results will be discussed in Section 4.4.

Equation (4-5) gives an implicit relation for the mean flow speed because the integral $I(\phi, m, \Theta)$ (right hand side of equation 3-35) is a function of Θ and Θ depends on V. Recall that

$$\Theta = \frac{V}{c}\left(\frac{1}{2\phi - \phi^2/2}\right)$$

Knowing the values of the geometrical properties of the wave in

the living system and the value of m from the viscometric experiments, it is possible to evaluate v from equation (4-5) and to compare this value with the average flow speeds observed in living axons. This comparison is discussed in detail in Section 4.4.

4.3 Geometric Properties of the Peristaltic Waves in Axons in Vitro

An experimental procedure for recording the peristaltic surface activity in axons has been developed by Weiss, Taylor and Bock (see Weiss[10]). Intercostal nerves, excised from young mice, were placed in special culture chambers which kept the axons viable for a week or more. Portions of the nerve were stripped of their epineurium and perineurium and the neurons teased apart sufficiently to study the individual fibers under phase contrast microscopy. The microperistaltic surface waves were recorded using time-lapse photographic techniques.

Weiss' motion picture sequences were studied frame by frame in the Vanguard Motion Analyzer. The results of tracking the motion of 41 separate waves in 4 nerve fibers are presented in Table I. The results show a moderate variation in the data in light of the variability of the living system. The mean value and the standard deviation of the three parameters is given in Table I.

Table I

		Mean	Standard Deviation	σ
Amplitude Ratio	ϕ	0.523	0.107	σ_ϕ
Wavelength	λ	38.7 microns	8.46 microns	σ_λ
Wave Speed	c	4.59 mm/day	0.62 mm/day	σ_c

Since the width of the field in any motion picture frame was quite limited, in general from 0 to 2 individual waves could be observed in the length of axon under observation. The number of waves per unit length was determined by averaging, over the time, the number of waves observed and dividing by the length of the axon segment. The average value of was found to be 6.91 waves per mm.

In connection with these measurements, one point should be emphasized. All measurements have been made on nerve fibers teased apart from the nerve bundle. There is no way to estimate to what degree the peristaltic waves are affected when the nerve fibers are separated from the nerve bundle. In addition, there is no assurance that peristaltic motion is possible at all in the tightly packed nerve bundle. If it is assumed that the crest of a wave in one nerve fiber corresponds to the trough of a wave in an adjacent nerve fiber, one may conceive of peristalsis taking place inside a compact nerve bundle. It is feasible, from the standpoint of continuity, for the individual nerve fibers in a

bundle to undergo considerable deformation while the average of all the deformations is constant and the nerve bundle retains its constant dimensions. Resolution of this question is left as an area for future study.

4.4 Theoretical Flow Speed of Axoplasm

Recall equation (4-5).

$$V = c\left(\frac{n_0\lambda}{1-n_0\lambda} I(\phi, n, \omega)\right)^{1/n} \qquad (4\text{-}5)$$

Substituting the mean values of the wave properties presented in Section 4.3 and using the value of the flow behavior index n determined from the viscometric experiments (n =0.41), the value of the axonal flow speed is calculated to be 0.49 mm/day. This calculation procedure was accomplished by first assuming a value of V and evaluating the integral; a new value of V was recomputed from equation 4-5. An iterative technique was used until convergence of the assumed and calculated values of V was achieved.

This value of the theoretical axonal flow speed is in reasonably good agreement with the flow speeds observed in living axons. Published values are generally of the order of 1.0 mm/day. The value of the integral $I(\phi, n, \omega)$ is a strong function of the amplitude ratio ϕ. Substituting the values of $\Phi = \bar{\phi} \pm \sigma_\phi$ into equation (4.5) and keeping the values of the other parameters unchanged, the flow speeds are calculated to be 1.36 and 0.2 mm/day respectively.

Several observations may be made about the theoretical axonal flow speed.

1. Referring to equation (4.5), it is seen that V is independent of the consistency of the axoplasmic material (independent of K). In general the consistency index K is strongly dependent on the temperature of the material whereas the flow behavior index n is essentially independent of the temperature. This implies that the flow speed V is essentially independent of the temperature of the axoplasm. This is particularly significant when one considers cold blooded animals which do not maintain their internal temperature. The supply of axoplasm would evidently proceed at a normal rate independent of the temperature of the animal.

2. It may also be seen (equation 4.5) that the flow speed is independent of the diameter of the axon. In general, axon diameters measure between 2 and 10 microns. Although many investigators have reported axonal flow speeds of the order of 1 mm/day[5,7,37,38,39,40,41,42] there has been little experimental evidence to suggest that the flow speed depends on the diameter of the axon.

4.5 Energy Requirements

Recall that the average rate at which mechanical work must be supplied to the walls per wavelength is given by the equation

$$\bar{W} = \bar{Q}\,\Delta P_\lambda / \eta$$

where $\eta = \eta(\phi, m, \Phi/\Phi_0)$ = mechanical efficiency

The total energy which must be supplied to the nervous system may be estimated by

$$W_T = \bar{Q}\,\Delta P_T\, N$$

where N = total number of nerve cells in system

ΔP_T = total pressure rise (Equation 4.2)

$\bar{Q}$ = average volume flow rate = $\pi a^2 \bar{V}$

$$W_T = \left[\left(\frac{3m+1}{m}\right)^m \left(\frac{2KC^m\lambda}{a^{m+1}}\right)(\pi a^2 \bar{V})(n_0 \bar{L})(N) I(\phi, m, \Phi)\right] / \eta$$

Notice that, unlike the mean flow speed $\bar{V}$, the energy which must be supplied depends both on the consistency of the material K and on the diameter of the tube a. This is consistent with the analogy which has been drawn between the peristaltic pumping mechanism and a positive displacement device.

Using the values of m = 0.41, K = 2.98 lb.-sec.^{n}/ft.^{2} from the microcapillary experiments, the average values of ϕ, λ, C and C given in Section 4.3 with the calculated value of $\bar{V}$ = 0.49 mm/da and assuming N = 7 x 10^9 nerve cells and $\bar{L}$ = 0.2 ft., the total energy requirement is calculated to be

$$W_T \cong 0.01/\eta \quad \text{kcal/day}$$

If a value of η =0.05 is used for the mechanical efficiency [34],

$\bar{w}$ = 0.2 kcal/day

This is an estimate of the total energy which must be supplied from metabolic sources to insure a continuous supply of axoplasm.

4.6 Mathematical Model of the Living System

The differences between the idealized model and the living system should be reiterated. Axoplasm has been treated as a uniform, homogeneous substance in order to study its gross fluid dynamic properties. This simplification disregards the fact that axoplasm may be a composite matrix of materials of different consistencies. The fact that axoplasm is inhomogeneous and may be anisotropic was disregarded in this study. The axon itself was considered to be a long, uniform, cylindrical tube, although its geometry may be quite irregular. In mathematically modeling peristalsis, the peristaltic mechanism has been idealized as a series of uniformly spaced, constant dimension, traveling sinusoidal waves. Average values for the geometrical properties of the waves were used in the numerical calculations.

Although considerable attention was given to minimizing the difference between the physical system and the mathematical model, these differences should be kept in mind when conclusions are applied to the very complex living system.

5. Conclusions

The causes of the proximo-distal flow of axoplasm in nerve fibers has been the subject of much speculation. In this work, engineering techniques were used to study microperistalsis as a possible cause of this flow. Quantitative evidence to support this hypothesis is presented.

An experimental technique for injecting axons (5-10 microns diameter) with micropipettes under visual microscopic control has been perfected. The feasibility of using this technique to study axoplasmic flow in vivo has been shown.

A new technique for microcapillary tube viscometric measurements has been developed. This technique is applicable to any viscous, time-independent biological fluid where the volume of the fluid sample is limited to a few cubic microns. This method was used to obtain a flow curve for axoplasm. The results of these experiments indicate that the gross or overall behavior of axoplasm is characteristic of a highly viscous, pseudoplastic fluid. No evidence of significant time-dependent thixotropic or viscoelastic effects were apparent.

A theoretical analysis of peristaltic pumping of pseudoplastic fluids at low Reynolds numbers by means of an infinite train of sinusoidal peristaltic waves is presented. This work is an extension of the work Shapiro et al. [34] for Newtonian fluids. Data obtained from

experiments performed on a plane, two-dimensional model were used to confirm the theoretical results.

The viscometric data obtained for axoplasm is used to establish system resistance curves for axons idealized as uniform cylindrical tubes containing a homogeneous, pseudoplastic fluid. These data are correlated with the theoretical pump characteristic curves to determine an expected flow rate. A comparison of the theoretical flow rate and the observed axonal flow rates provides quantitative support of the hypothesis that axoplasmic flow is caused by peristalsis. It is shown, in addition, that the pumping of axoplasm depends only on the geometrical properties of the peristaltic waves and the power law exponent. The theoretical flow speed is shown to be both independent of the consistency of the axoplasm and independent of the diameter of the axon.

6. RECOMMENDATIONS FOR FUTURE STUDY

Reasonable estimates of the geometrical properties of the peristaltic waves in the biological system are necessary to describe the peristaltic mechanism. A statistical study of the wave properties was conducted using motion pictures from Weiss' in vitro experiments. Since this study was limited somewhat by the number of usable film sequences, a series of similar experiments should be conducted in order to enlarge the sample on which the statistical analysis is based. Some movies should be made at lower magnification so that larger segments of axons would appear in the field. This would allow a more accurate estimate of the number of waves per unit length, m_o .

Of the film sequences studied, only one was found suitable for tracking the trajectories of cytoplasmic inclusions in the axon during the passage of a wave. Attempts should be made to obtain high magnification movie sequences to study particle paths. The trajectories of fluid particles may be calculated directly from the governing equations. Although this would be a major undertaking, it would allow one to compare the details of the fluid motion in the axon with the expected theoretical motion.

An experimental study of particle path lines might also be undertaken using the plexiglas two-dimensional model. In particular, it would be of interest to study the motion of non-rigid particles, fluid

spheres for example, through a second liquid matrix during the passage of a wave. Such deformable particles could be used to simulate the motion of mitochondria through the axoplasm.

Using techniques developed by the author, in vivo experiments involving the injection of dye or other tracer materials directly into nerve fibers in the living animal appears to be feasible. Preliminary experiments performed on anesthesized frogs appear quite promising. Such experiments would allow the direct visual measurement of the movement of axoplasm over long periods of time in contrast to the more indirect radioactive tracer methods.

REFERENCES

1 Weiss, P., " 'Panta' Rhei' - And so flow our nerves", American Scientist, 57:287, 1969

2 Noback, C. R., The Human Nervous System: Basic Elements Of Structure And Function, McGraw-Hill Book Company, 1967

3 Weiss P., "Endoneurial edema in constricted nerves", Anatomical Record, 86:491, 1943

4 Weiss, P. and H. J. Davis, "Pressure block in nerves provided with arterial sleeves", Journal of Neurophysiology, 6:269, 1943

5 Weiss, P. and H. B. Hiscoe, "Experiments on the mechanism of nerve growth", Journal of Experimental Zoology, 107:315, 1948

6 Weiss P. and M. W. Cavanaugh, "Further evidence of perpetual growth of nerve fibers: recovery of fiber diameter after the release of prolonged constrictions", Journal of Experimental Zoology, 142:461, 1959

7 Weiss, P., "Neuronal dynamics and neuroplasmic ("axonal") flow", in: Cellular Dynamics Of The Neuron, S. H. Barondes, ed., Academic Press, 1969

8 Shepherd, E. H. (1951): "The movement of radioactive phosphorus 32 in peripheral nerve." Ph.D. Dissertation, University of Chicago

9 Samuels, A. J., L. L. Boyarsky, R. W. Gerard, B. Libet, and M. Brust, "Distribution, exchange and migration of phosphate compounds in the nervous system", Americal Journal of Physiology, 164:1, 1951

10 Ochs, S. and E. Burger, "Movement of substance proximo-distally in nerve axons as studied with spinal cord injections of radioactive phosphorus", American Journal of Physiology, 194:499, 1958

11 Waelsch, H. J., "Some aspects of amino acid and protein metabolism of the nervous system", Journal of Nervous and Mental Disease, 126:33, 1958

12 Droz, B. and C. P. Leblond, "Axial migration of proteins in the central nervous system and peripheral nerves as shown by radioautography", Journal of Comparative Neurology, 121:325, 1963

13 Barondes, S. H., ed., Cellular Dynamics Of The Neuron, Academic Press, 1969

14 Weiss, P. and A. Pillai, "Convection and fate of mitochondria in nerve fibers: axonal flow as vehicle", Proceedings of the National Academy of Science, 54:48, 1965

15 Weiss, P., "Self-renewal and proximo-distal convection in nerve fibers", In:Symposium On The Effect Of Use And Disuse Of Neuromuscular Functions, Guttmann, E., ed. Publ. House Czechoslovak Academy of Science, Prague, 1963, pp. 171-183

16 Young, J. Z., "The history of the shape of a nerve fiber", In: Essays On Growth And Form, Legros, C. W. and P. B. Medawar, eds., Clarendon Press, 1945, pp. 41-94

17 Weiss P., A. C. Taylor, and P. A. Pillai, "The nerve fiber as a system in continuous flow: microcinematographic and electron-microscopic demonstrations", Science, 136:330, 1962

18 Weiss P., "Neuronal dynamics", Neurosciences Research Prog. Bulletin, 5:371, 1967

19 Weiss P., "The dynamics of the membrane-bound incompressible body: a mechanism for cellular and subcellular motility", Proceedings Of The National Academy Of Science, 52: 1024, 1964

20 Rosenberg, M. D., "The relative extensibility of cell surfaces", The Journal of Cell Biology, 17:289, 1963

21. deRenyi, G. J., "The structure of cells in tissues as revealed by microdissection", Journal of Comparative Neurology, 47:405, 1929

22 Peterfi, J., In: Handbuch Der Normalen Und Pathologischen Physiologie, A. Bethe, et al., eds., Vol. 9, pp. 79, Springer, Berlin, 1925-1932

23 Weiderheilm, C. A., W. J. Woodbury, S. Kurt, and R. F. Rushmer, "Pulsatile pressures in the microcirculation of the frog's mesentery", American Journal of Physiology, 207:173, 1964

24 Jacobs, H. R., "Meniscal resistances and bubble lengths", Biorheology, 1:229, 1962

25 Jacobs, H. R., "Meniscal resistance in tube viscometry", Biorheology, 3:117, 1966

26 Mardles, E. W. J., "The flow of liquids through fine capillaries and narrow channels: the meniscal resistance (Jamin effect)", Biorheology, 6:10, 1969

27 Fernandez-Moran, H., "Submicroscopic organization of vertibrate nerve fibers", Experimental Cell Research, 3:252, 1952

28 Kamiya, N., "The protoplasmic flow in the myxomycete plasmodium", Protoplasma, 39:344, 1950

29 Kamiya, N. and K. Kuroda, "Studies on the velocity distribution of the protoplasmic streaming in the myxomycete plasmodium", Protoplasma, 49:1, 1958

30 Burns, J. T. and T. Parkes, "Peristaltic motion", Journal of Fluid Mechanics, 29:731, 1967

31 Fung, Y. C. and C. S. Yih, "Peristaltic transport", American Society of Mechanical Engineers - Transactions: Journal of Applied Mechanics, Vol. 35, Series E.: 669, 1968

32 Fung, Y. C., "Fluid transport by peristalsis", Abstract in: Federation Proceedings, Vol. 29#2, E 37, Mar. 1970

33 Hanin, M., "The flow through a channel due to transversely oscillating walls", Israel Journal of Technology, 6:67, 1968

34 Shapiro, A. H., M. Y. Jaffrin and S. L. Weinberg, "Peristaltic pumping with long wavelengths at low Reynolds numbers", Journal of Fluid Mechanics, 37:799, 1969

35 Latham, T. W., "Fluid motions in a peristaltic pump", Master of Science Thesis, Department of Mechanical Engineering, Massachusetts Institute of Technology, June 1966

36 Barton, C. and S. Raynor, "Peristaltic flow in tubes", Bulletin of Mathematical Biophysics, 30:663, 1968

37 Taylor, A. C. and P. A. Weiss, "Demonstration of axonal flow by the movement of tritium-labeled protein in mature optic nerve fibers", Proceedings of the National Academy of Science, 54:1521, 1965

38 Edstrom, A., "Amino acid incorporation in isolated Mauthner nerve fiber components", Journal of Neurochemistry, 13:315, 1966

39 Grafstein, B., "Transport of protein by goldfish optic nerve fibers", Science, 156:196, 1967

40 Weiss, P. and Y. Holland, Neuronal dynamics and axonal flow II.: The olfactory nerve as model test object", Proceedings of the National Academy of Science, 57:258, 1967

41 Lasek, R., "Axoplasmic transport in cat dorsal root ganglion cells as studied with (^{3}H)-L-Leucine", Brain Research, 7:360, 1968

42 McEwen, B. S. and B. Grafstein, "Fast and slow components in axonal transport of protein", Journal of Cell Biology, 38:494, 1968

43 Skelland, A.H.P., Non-Newtonian Flow and Heat Transfer, John Wiley & Son, New York, 1967

A. APPENDIX

A.1 PERISTALTIC PUMPING OF PSEUDOPLASTIC FLUIDS WITH LONG WAVELENGTHS AT LOW REYNOLDS NUMBERS

A.1.1 Two-Dimensional Geometry

Consider an infinite train of sinusoidal peristaltic waves traveling along the walls of a two-dimensional channel. Figure (A-1) shows the nomenclature used for the wave train as observed in the laboratory reference frame (upper case symbols) and in the wave reference frame (lower case symbols).

The transformations between the two reference frames are given by the relations

$$x = X - ct \qquad y = Y \tag{A-1}$$

$$u(x,y) = U(X-ct, Y) - c \qquad v = V \tag{A-2}$$

Since the flow is steady in the reference frame of the wave, the problem is solved initially in this reference frame.

The following assumptions are made:

1. The appropriate Reynolds number is sufficiently small such that the inertial terms in the equations of motion may be neglected;

LABORATORY REFERENCE FRAME

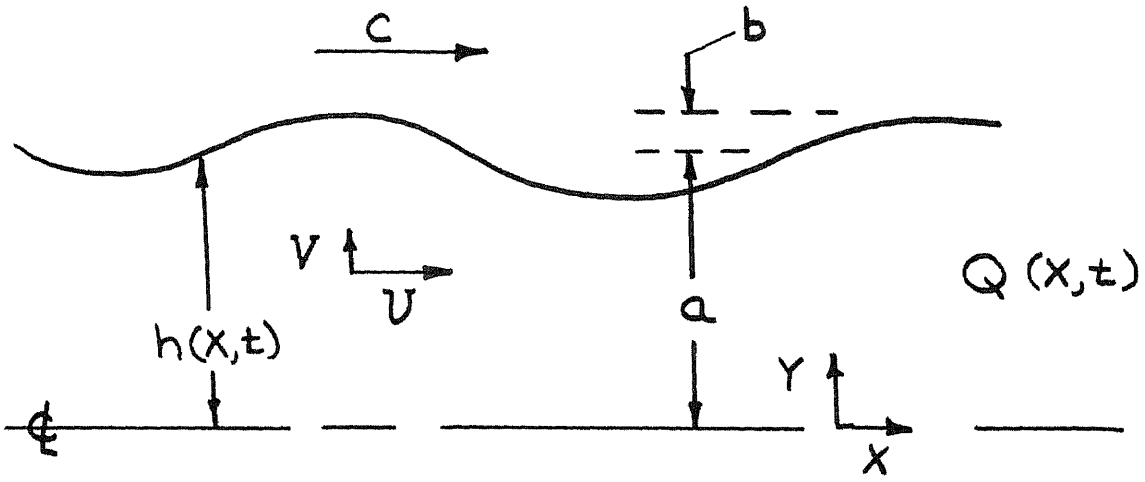

WAVE REFERENCE FRAME

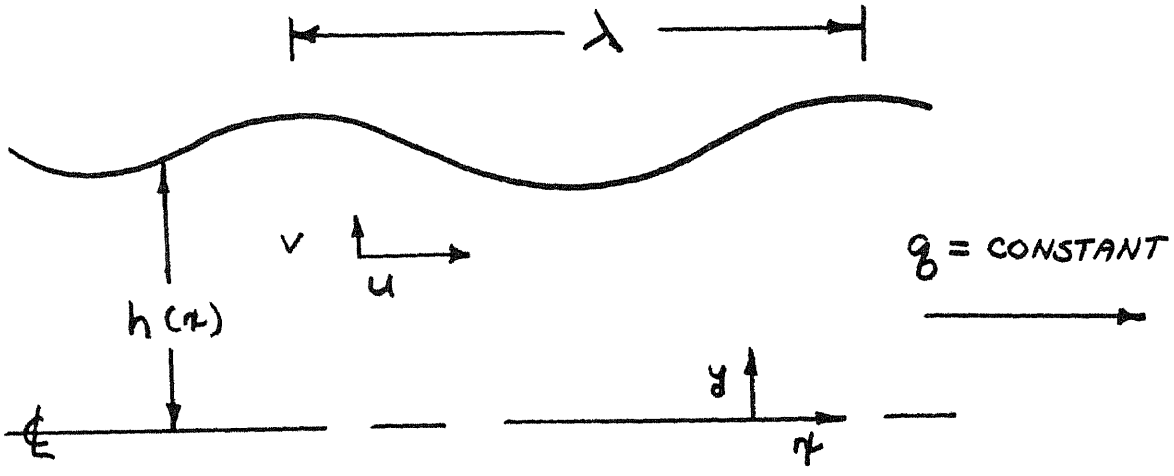

Figure A-1 Nomenclature for Infinite Progressive Train of Sine Waves

2. the ratio of the wavelength to the diameter is sufficiently large such that the pressure may be considered uniform over each cross section;

3. there is an infinite progressive train of sine waves with the wall coordinate following the law

$$h = a + b \sin(2\pi x/\lambda) \tag{A-3}$$

(It may also be shown (ref. 34) that the solution is valid if the train of waves is finite but integral.); and,

4. the fluid is a time-independent pseudoplastic; that is, one which is governed by the shear stress shear rate relationship given by

$$\tau_{yx} = -K \left|\frac{\partial u}{\partial y}\right|^{n-1} \frac{\partial u}{\partial y} \tag{A-4}$$

(The absolute value sign is needed to insure that the shear stress and the shear rate have opposite signs in every region.)

Under these assumptions, the equation of motion in the x direction becomes

$$\frac{dP}{dx} = -\frac{\partial}{\partial y}(\tau_{yx}) \tag{A-5}$$

Since dP/dx depends only on x as a consequence of assumption 2., equation A-5 may be integrated directly with respect to y. Using the boundary conditions that

$$\tau_{yx} = 0 \quad \text{at} \quad y = 0 \tag{A-6}$$

the resulting equation becomes

$$\frac{dP}{dx} y = -\tau_{yx} \tag{A-7}$$

Substituting the expression for the shear stress from equation A-4,

$$\frac{dP}{dx} y = K \left| \frac{\partial u}{\partial y} \right|^{n-1} \frac{\partial u}{\partial y} \tag{A-8}$$

In order to integrate equation A-8, it is necessary to consider the two regions where $\frac{dP}{dx} \geq 0$ and where $\frac{dP}{dx} < 0$.
Equation A-8 may be rewritten as

$$\frac{du}{dy} = (y)^{\frac{1}{n}} \left(\frac{1}{K}\right)^{1/n} \left(\frac{dP}{dx}\right)^{\frac{1}{n}} \quad \text{when} \quad \frac{dP}{dx} \geq 0 \tag{A-9}$$

and

$$\frac{du}{dy} = -(y)^{\frac{1}{n}} \left(\frac{1}{K}\right)^{\frac{1}{n}} \left(-\frac{dP}{dx}\right)^{\frac{1}{n}} \quad \text{when} \quad \frac{dP}{dx} < 0 \tag{A-10}$$

A verification of the validity of breaking equation A-8 into equations A-9 and A-10 is presented in section A.1.2.

Since $\frac{dP}{dx}$ depends only on x , these expressions may be integrated directly with respect to y . Applying the boundary condition

$$u = -c \quad \text{at} \quad y = h(x) \tag{A-11}$$

the expressions for the velocity profiles become

$$u = -c - \left(\left(\frac{n}{n+1}\right)\left(\frac{1}{k}\right)^{\frac{1}{n}} \frac{dp}{dx}^{\frac{1}{n}}\right)\left(h^{\frac{n+1}{n}} - y^{\frac{n+1}{n}}\right) \tag{A-12}$$

when $\frac{dp}{dx} \geq 0$, and,

$$u = -c - \left(\left(\frac{n}{n+1}\right)\left(\frac{1}{k}\right)^{\frac{1}{n}} \left(-\frac{dp}{dx}\right)^{\frac{1}{n}}\right)\left(y^{\frac{n+1}{n}} - h^{\frac{n+1}{n}}\right) \tag{A-13}$$

when $\frac{dp}{dx} < 0$.

In the wave reference frame, the volume flow rate through each cross section, q , is a constant independent of both x and t . It is given by

$$q = \int_0^{h(x)} u \, dy \tag{A-14}$$

Substituting the expressions for u from equations A-12 and A-13,

$$q = -ch - \left(\frac{n}{2n+1}\right)\left(\frac{1}{k}\right)^{\frac{1}{n}} \left(\frac{dp}{dx}\right)^{\frac{1}{n}} h^{\frac{2n+1}{n}} \tag{A-15}$$

when $\frac{dp}{dx} \geq 0$, and,

$$q = -ch + \left(\frac{n}{2n+1}\right)\left(\frac{1}{k}\right)^{\frac{1}{n}} \left(-\frac{dp}{dx}\right)^{\frac{1}{n}} h^{\frac{2n+1}{n}} \tag{A-16}$$

when $\frac{dp}{dx} < 0$.

The instantaneous volume flow rate in the laboratory reference frame, Q , is obtained by integrating the expression

$$Q = \int_0^{h(x)} U(X,Y,t)\,dY \tag{A-17}$$

From equation A-2, recall that $U = c+u$. Thus

$$Q = \int_0^{h} (u+c)\,dy = q+ch \tag{A-18}$$

The time-mean flow rate, $\bar{Q}$, is calculated by integrating the instantaneous volume flow rate over the period T .

$$\bar{Q} = \frac{1}{T}\int_0^{T} Q\,dt \quad \text{From A 13, with } q \text{ constant} \tag{A-19}$$

$$\bar{Q} = q + ac \tag{A-20}$$

The pressure rise per wavelength is defined by the expression

$$\Delta P_\lambda = \int_0^{\lambda} \left(\frac{dP}{dx}\right) dx \tag{A-21}$$

Re-writing equations A-15 and A-16 as

$$\frac{dP}{dx} = \left(\frac{2m+1}{m}\right)^m k \left(\frac{-(q+ch)}{h^{(2m+1)/m}}\right)^m \tag{A-22}$$

when $\frac{dP}{dx} \geq 0$, and,

$$\frac{dP}{dx} = -\left(\frac{2m+1}{m}\right)^m (k) \left(\frac{q+ch}{h^{(2m+1)/m}}\right)^m \tag{A-23}$$

when $\frac{dP}{dx} < 0$, it is apparent that the integral in equation A-21

may be broken up into intervals where $\frac{dP}{d\eta} \geq 0$ and where $\frac{dP}{d\eta} < 0$. The points where $\frac{dP}{d\eta} = 0$ may be determined from equations A-15 or A-16. When $\frac{dP}{d\eta} = 0$,

$$q = -ch = -ac - bc \sin(2\pi\eta/\lambda) \tag{A-24}$$

Recalling that $\bar{Q} = q + ac$ and defining a dimensionless time-mean flow rate, Θ, by the relationship

$$\Theta = \bar{Q}/bc \tag{A-25}$$

the points along the wavelength where $\frac{dP}{d\eta} = 0$ may be determined from the two values of the inverse sine

$$(\eta/\lambda) = \frac{1}{2\pi}\left(\sin^{-1}(-\Theta)\right)_{1,2} \tag{A-26}$$

In the intervals

$$0 \leq \eta/\lambda < \frac{1}{2\pi}\left(\sin^{-1}(-\Theta)\right)_1, \quad \frac{dP}{d\eta} < 0;$$

$$\frac{1}{2\pi}\left[\sin^{-1}(-\Theta)\right]_1 \leq \eta/\lambda \leq \frac{1}{2\pi}\left[\sin^{-1}(-\Theta)\right]_2, \quad \frac{dP}{d\eta} \geq 0;$$

and, $$\frac{1}{2\pi}\left[\sin^{-1}(-\Theta)\right]_2 < \eta/\lambda \leq 1.0, \quad \frac{dP}{d\eta} < 0.$$

The expression for the pressure rise per wavelength is then given by

$$\Delta P_\lambda = -\int_0^{\frac{\lambda}{2\pi}(\sin^{-1}(-\theta))_1} \left(\frac{2m+1}{m}\right)^m K \left(\frac{q+ch}{h^{(2m+1)/m}}\right)^m d\psi$$

$$+\int_{\frac{\lambda}{2\pi}(\sin^{-1}(-\theta))_1}^{\frac{\lambda}{2\pi}(\sin^{-1}(-\theta))_2} \left(\frac{2m+1}{m}\right)^m K \left(\frac{-(q+ch)}{h^{(2m+1)/m}}\right)^m d\psi$$

$$-\int_{\frac{\lambda}{2\pi}(\sin^{-1}(-\theta))_2}^{1.0} \left(\frac{2m+1}{m}\right)^m K \left(\frac{q+ch}{h^{(2m+1)/m}}\right)^m d\psi \qquad \text{(A-27)}$$

where $h = a + b\sin\frac{2\pi\psi}{\lambda}$. Define an amplitude ratio $\phi = b/a$. Recalling that $\theta = \frac{q+ac}{bc}$, multiplying both sides of the equation through by $a^{2m+1}/(bc)^m$ and performing the change of variables $\zeta = \psi/\lambda$ and $d\psi = \lambda\, d\zeta$, one obtains

$$\left(\frac{m}{2m+1}\right)^m \frac{\Delta P_\lambda\, a^{m+1}}{K c^m \lambda \phi^m} =$$

$$-\int_0^{\frac{1}{2\pi}(\sin^{-1}(-\theta))_1} \left(\frac{(\theta+\sin 2\pi\zeta)}{(1+\phi\sin 2\pi\zeta)^{(2m+1)/m}}\right)^m d\zeta \qquad \text{(A-28)}$$

$$+\int_{\frac{1}{2\pi}(\sin^{-1}(-\theta))_1}^{\frac{1}{2\pi}(\sin^{-1}(-\theta))_2} \left(\frac{-(\theta+\sin 2\pi\zeta)}{(1+\phi\sin 2\pi\zeta)^{(2m+1)/m}}\right)^m d\zeta$$

$$-\int_{\frac{1}{2\pi}(\sin^{-1}(-\theta))_2}^{1.0} \left(\frac{(\theta+\sin 2\pi\zeta)}{(1+\phi\sin 2\pi\zeta)^{(2m+1)/m}}\right)^m d\zeta$$

The left hand side of equation A-28 is a dimensionless pressure rise per wavelength. Equation A-28 establishes the relationship between this pressure rise and the dimensionless time-mean flow rate, Θ . This relationship is the desired pump characteristic. Equation A-28 may be integrated numerically and a digital computer program in FORTRAN language to accomplish this integration has been included in Appendix E.

Note that the relationship given in equation A-28 reduces to the relationship presented by Shapiro et al.[34] for a Newtonian fluid when the flow behavior index n is equal to 1.0. (Equation 3-1)

A.1.2 Verification of the Shear Rate Equations For Positive And Negative Values of the Pressure Gradient

We wish to show that both equations A-9 and A-10 reduce to equation A-8. Recall equation A-9.

$$\frac{du}{dy} = y^{\frac{1}{n}} \left(\frac{1}{K}\right)^{\frac{1}{n}} \left(\frac{dP}{d\ell}\right)^{\frac{1}{n}} \qquad \frac{dP}{d\ell} \geq 0 \tag{A-9}$$

$$\left|\frac{du}{dy}\right| = \left| y^{\frac{1}{n}} \left(\frac{1}{K}\right)^{\frac{1}{n}} \left(\frac{dP}{d\ell}\right)^{\frac{1}{n}} \right|$$

$$y \geq 0$$

$$K > 0$$

$$\frac{dP}{d\ell} \geq 0$$

$$\left|\frac{du}{dy}\right| = y^{\frac{1}{n}} \left(\frac{1}{K}\right)^{\frac{1}{n}} \left(\frac{dP}{d\ell}\right)^{\frac{1}{n}}$$

$$\left|\frac{du}{dy}\right|^{n-1} = y^{1-\frac{1}{n}} \left(\frac{1}{K}\right)^{1-\frac{1}{n}} \left(\frac{dP}{d\ell}\right)^{1-\frac{1}{n}}$$

$$\left|\frac{du}{dy}\right|^{n-1} \frac{du}{dy} = y \left(\frac{1}{K}\right) \left(\frac{dP}{d\ell}\right) \tag{A-29}$$

Equation A-29 is identical to equation A-8 which is the desired result.

Similarly, recall equation A-10

$$\frac{du}{dy} = -(y)^{\frac{1}{n}} \left(\frac{1}{K}\right)^{\frac{1}{n}} \left(-\frac{dP}{dx}\right)^{\frac{1}{n}} \qquad \frac{dP}{dx} < 0 \tag{A-10}$$

$$\left|\frac{du}{dy}\right| = \left|-(y)^{\frac{1}{n}} \left(\frac{1}{K}\right)^{\frac{1}{n}} \left(-\frac{dP}{dx}\right)^{\frac{1}{n}}\right|$$

$$y \geq 0$$

$$K > 0$$

$$\left(-\frac{dP}{dx}\right) > 0$$

$$\left|\frac{du}{dy}\right| = + y^{\frac{1}{n}} \left(\frac{1}{K}\right)^{\frac{1}{n}} \left(-\frac{dP}{dx}\right)^{\frac{1}{n}}$$

$$\left|\frac{du}{dy}\right|^{n-1} = y^{1-\frac{1}{n}} \left(\frac{1}{K}\right)^{1-\frac{1}{n}} \left(-\frac{dP}{dx}\right)^{1-\frac{1}{n}}$$

$$\left|\frac{du}{dy}\right|^{n-1} \frac{du}{dy} = -y \left(\frac{1}{K}\right)\left(-\frac{dP}{dx}\right)$$

$$\left|\frac{du}{dy}\right|^{n-1} \frac{du}{dy} = +y \left(\frac{1}{K}\right)\left(\frac{dP}{dx}\right) \tag{A-30}$$

Equation A-30 is identical to equation A-8

B. APPENDIX

B.1 PERISTALTIC PUMPING OF PSEUDOPLASTIC FLUIDS WITH LONG WAVELENGTHS AT LOW REYNOLDS NUMBERS

B.1.1 Axi-symetric Geometry

Consider an infinite train of sinusoidal peristaltic waves traveling over the surface of a long cylindrical tube. Figure B-1 shows the nomenclature used for the wave train as observed in the laboratory reference frame (upper case symbols) and in the wave reference frame (lower case symbols).

The transformations between the two references frames are given by the relations

$$\psi = X - ct \qquad r = R \tag{B-1}$$

$$u(\psi, r) = U(X - ct, R) - c \qquad v = V \tag{B-2}$$

Since the flow is steady in the wave reference frame, the problem is initially solved in this frame.

The following assumptions are made:

1. the appropriate Reynolds number is sufficiently small such that the inertial terms in the equations of motion may be neglected;

2. the ratio of the wavelength to the diameter is sufficiently

LABORATORY REFERENCE FRAME

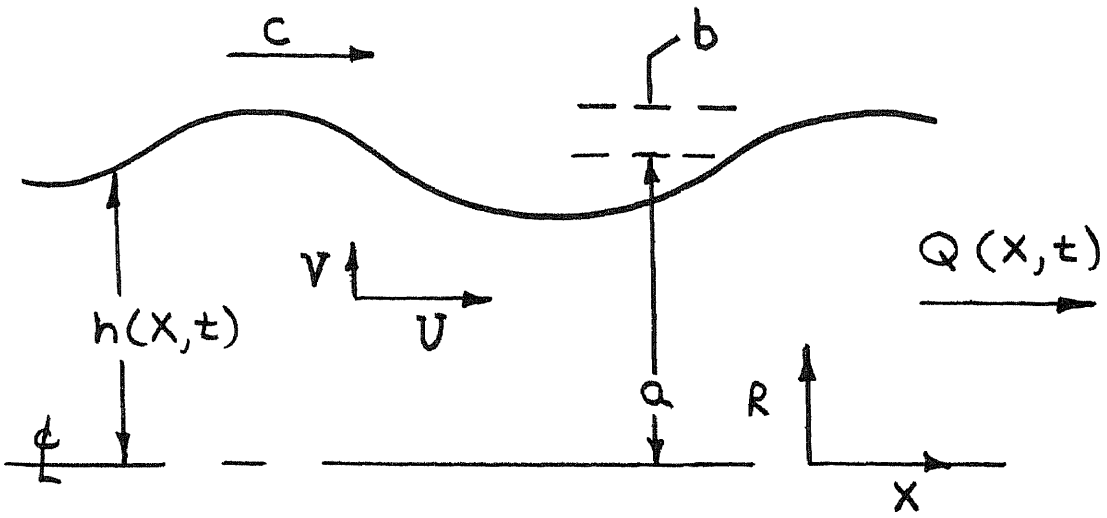

Note a = mean radius of tube

WAVE REFERENCE FRAME

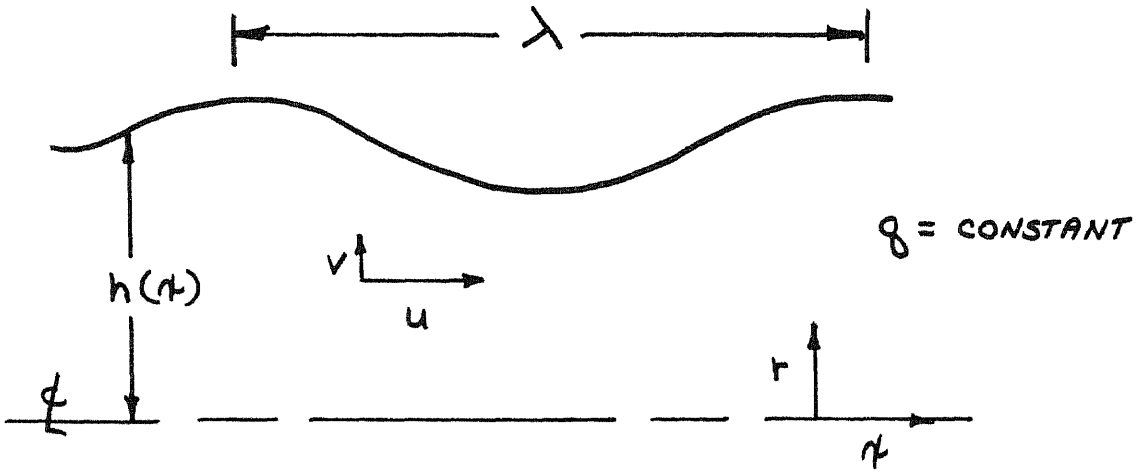

Figure B-1 Nomenclature for Infinite Progressive Train of Sine Waves

large such that the pressure may be considered uniform over the cross section;

3. there is an infinite progressive train of sinusoidal waves with the wall coordinate following the law

$$h = a + b \sin 2\pi x/\lambda \tag{B-3}$$

(It may also be shown (ref.34) that the solution is valid if the number of waves is finite but integral.)

4. the fluid is a time-independent pseudoplastic; that is, one which is governed by the shear stress shear rate relationship given by

$$\tau_{rx} = -K \left| \frac{\partial u}{\partial r} \right|^{n-1} \frac{\partial u}{\partial r} \tag{B-4}$$

(The absolute value sign is needed to insure that the shear stress and the shear rate have opposing signs in every region.)

Under these assumptions, the equation of motion in the axial direction becomes

$$\frac{dP}{dx} = -\frac{1}{r} \frac{\partial}{\partial r} (r \tau_{rx}) \tag{B-5}$$

Since dP/dx depends only on x, as a result of assumption 2, equation B-5 may be integrated directly with respect to r. Using the boundary conditions

$$\tau_{rx} = 0 \qquad \text{at} \qquad r = 0 \tag{B-6}$$

the resulting equation becomes

$$\frac{dP}{dx}\left(\frac{r}{2}\right) = -\tau_{rx} \tag{B-7}$$

Substituting the expression for the shear stress from equation B-4

$$\frac{dP}{dx}\left(\frac{r}{2}\right) = k\left|\frac{\partial u}{\partial r}\right|^{n-1}\frac{\partial u}{\partial r} \tag{B-8}$$

In order to integrate equation B-8, the two distinct regions where $dP/dx < 0$ and where $dP/dx \geq 0$ are considered. Equation B-8 may be re-written as

$$\frac{du}{dr} = r^{\frac{1}{n}}\left(\frac{1}{2k}\right)^{\frac{1}{n}}\left(\frac{dP}{dx}\right)^{\frac{1}{n}} \qquad \frac{dP}{dx} \geq 0 \tag{B-9}$$

and $$\frac{du}{dr} = -(r)^{\frac{1}{n}}\left(\frac{1}{2k}\right)^{\frac{1}{n}}\left(-\frac{dP}{dx}\right)^{\frac{1}{n}} \qquad \frac{dP}{dx} < 0 \tag{B-10}$$

It may be shown that equations B-9 and B-10 are equivalent to equation B-8.

Since dP/dx depends only on x, these expressions may be integrated directly with respect to r. Applying the boundary condition

$$u = -c \qquad \text{at} \qquad r = h \tag{B-11}$$

the expressions for the velocity profiles become

$$u = -c - \left[\frac{n}{n+1}\left(\frac{1}{2k}\right)^{\frac{1}{n}}\left(\frac{dP}{dx}\right)^{\frac{1}{n}}\right]\left[h^{\frac{n+1}{n}} - r^{\frac{n+1}{n}}\right] \tag{B-12}$$

when $\frac{d\rho}{dr} \geq 0$, and,

$$u = -c - \left(\frac{n}{n+1}\left(\frac{1}{2k}\right)^{\frac{1}{n}}\left(-\frac{d\rho}{dr}\right)^{\frac{1}{n}}\right)\left(r^{\frac{n+1}{n}} - h^{\frac{n+1}{n}}\right) \qquad \text{(B-13)}$$

when $\frac{d\rho}{dr} < 0$.

In the reference frame of the wave, the volume flow rate through each cross section, q, is a constant, independent of both r and t. It is given by the relationship

$$q = \int_0^{h(r)} (u)(2\pi r)\, dr \qquad \text{(B-14)}$$

Substituting the expressions for u from equations B-12 and B-13 into equation B-14 and integrating, one obtains

$$q = -\pi h^2 c - \pi\left(\frac{1}{2k}\right)^{\frac{1}{n}}\left(\frac{d\rho}{dr}\right)^{\frac{1}{n}}\left(\frac{n}{3n+1}\right) h^{\frac{3n+1}{n}} \qquad \text{(B-15)}$$

when $\frac{d\rho}{dr} \geq 0$, and,

$$q = -\pi h^2 c + \pi\left(\frac{1}{2k}\right)^{\frac{1}{n}}\left(-\frac{d\rho}{dr}\right)^{\frac{1}{n}}\left(\frac{n}{3n+1}\right) h^{\frac{3n+1}{n}} \qquad \text{(B-16)}$$

when $\frac{d\rho}{dr} < 0$.

The instantaneous volume flow rate in the laboratory reference frame, Q , is obtained by integrating the expression

$$Q = \int_0^{h(r)} U(X, R, t)(2\pi R)\, dR \qquad \text{(B-17)}$$

From equation B-2, recall that $U = u + c$. Thus

$$Q = \int_0^h (2\pi r)(u+c)\,dr = q + \pi h^2 c \tag{B-18}$$

The time-mean flow rate, $\overline{Q}$, is calculated by integrating the instantaneous volume flow rate over the period T .

$$\overline{Q} = \frac{1}{T}\int_0^T Q\,dt \tag{B-19}$$

$$\overline{Q} = q + \pi a^2 c\,(1 + \phi^2/2) \tag{B-20}$$

where $\phi = b/a$.

The pressure rise per wavelength is defined by the expression

$$\Delta P_\lambda = \int_0^\lambda \left(\frac{dp}{dx}\right) dx \tag{B-21}$$

Re-writing equations B-15 and B-16 as

$$\frac{dp}{dx} = \left(\frac{1}{\pi}\right)^m \left(\frac{3m+1}{m}\right)^m (2K) \left(\frac{-(q+\pi h^2 c)}{h^{(3m+1)/m}}\right)^m \tag{B-22}$$

when $\frac{dp}{dx} \geq 0$,and,

$$\frac{dp}{dx} = -\left(\frac{1}{\pi}\right)^m \left(\frac{3m+1}{m}\right)^m (2K) \left(\frac{q+\pi h^2 c}{h^{(3m+1)/m}}\right)^m \tag{B-23}$$

when $dp/dx < 0$, it is apparent that the integral in equation B-21 may be broken up into intervals where $\frac{dp}{dx} \geq 0$ and where $dp/dx < 0$. The points where $dp/dx = 0$ may be determined from equation B-15 or B-16. When $\frac{dp}{dx} = 0$,

$$q = -\pi h^2 C = -\pi C\left(a^2 + 2ab \sin\frac{2\pi\eta}{\lambda} + b^2 \sin^2\frac{2\pi\eta}{\lambda}\right) \tag{B-24}$$

Recall that $\bar{Q} = q + \pi a^2 C\,(1 + \phi^2/2)$ and that $\phi = b/a$. Employing the same nomenclature as Shapiro et al.[34], we define a dimensionless time-mean flow rate, $\textcircled{H}$, by the relationship

$$\textcircled{H} = \frac{\bar{Q}}{\pi a^2 C\,(2\phi - \phi^2/2)} \tag{B-25}$$

Introducing these quantities into equation B-24, this relationship becomes

$$-(2\phi - \phi^2/2)\textcircled{H} + \phi^2/2 = 2\phi \sin\frac{2\pi\eta}{\lambda} + \phi^2 \sin^2\frac{2\pi\eta}{\lambda} \tag{B-26}$$

when $\frac{dp}{d\eta} = 0$.

This equation may be solved by the Newton-Raphson method to obtain the two points η_1/λ and η_2/λ along the wave where $dp/d\eta = 0$. Note that, unlike the two-dimensional case, η_1/λ and η_2/λ depend not only on $\textcircled{H}$ but also on ϕ. Note also that when the quantity $-(2\phi - \phi^2/2)\textcircled{H} + \phi^2/2$ is positive, the points where $\frac{dp}{d\eta} = 0$ lie in the first and second quadrants whereas when $-(2\phi - \phi^2/2)\textcircled{H} + \phi^2/2$ is negative, the points lie in the third and fourth quadrants. It is also possible to solve the quadratic in B-26 directly.

The expression for the pressure rise per wavelength may then be written. Substituting the values for $\frac{dp}{d\eta}$ from equations B-22 and B-23 into the expression for the pressure rise per wavelength given by B-21

Case I $\left(-(2\phi - \phi^2/2)\,\textcircled{H} + \phi^2/2\right) < 0$

$$\Delta P_\lambda = \int_0^{\eta_1} \left(\frac{dP}{d\eta}\right) d\eta + \int_{\eta_1}^{\eta_2} (dP/d\eta)\, d\eta + \int_{\eta_2}^{1} (dP/d\eta)\, d\eta \qquad \text{(B-27)}$$

$dP/d\eta \geq 0$ $\quad$ $dP/d\eta < 0$ $\quad$ $dP/d\eta \geq 0$

Case II $\left(-(2\phi - \phi^2/2)\,\textcircled{H} + \phi^2/2\right) \geq 0$

$$\Delta P_\lambda = \int_0^{\eta_1} \left(\frac{dP}{d\eta}\right) d\eta + \int_{\eta_1}^{\eta_2} (dP/d\eta)\, d\eta + \int_{\eta_2}^{1} \left(\frac{dP}{d\eta}\right) d\eta \qquad \text{(B-28)}$$

<0 $\quad$ ≥ 0 $\quad$ <0

where η_1 and η_2 are found from equation B-26.

Consider case I

$$\Delta P_\lambda = +\int_0^{\eta_1} \left(\frac{1}{\pi}\right)^m \left(\frac{3m+1}{m}\right)^m (2K) \left(\frac{(-1)(\beta + \pi h^2 C)}{h^{(3m+1)/m}}\right)^m d\eta$$

$$- \int_{\eta_1}^{\eta_2} \left(\frac{1}{\pi}\right)^m \left(\frac{3m+1}{m}\right)^m (2K) \left(\frac{\beta + \pi h^2 C}{h^{(3m+1)/m}}\right)^m d\eta \qquad \text{(B-29)}$$

$$+ \int_{\eta_2}^{1} \left(\frac{1}{\pi}\right)^m \left(\frac{3m+1}{m}\right)^m (2K) \left(\frac{(-1)(\beta + \pi h^2 C)}{h^{(3m+1)/m}}\right)^m d\eta$$

where $h = a + b \sin 2\pi t/\lambda$ and $\phi = b/a$.

Recall that $\textcircled{H} = \bar{Q}/\pi a^2 c\,(2\phi - \phi^2/2)$. Multiplying both sides of the equation through by $a^{3m+1}/(\pi a^2 c)^m$ and performing the change of variables $\zeta = t/\lambda$, $dt = \lambda\, d\zeta$, one obtains

$$\left(\frac{m}{3m+1}\right)^m \frac{\Delta P_\lambda\, a^{m+1}}{2K c^m \lambda} =$$

$$+ \int_0^{\zeta_1} \left(\frac{-((2\phi - \phi^2/2)\textcircled{H} - \phi^2/2 + 2\phi \sin 2\pi\zeta + \phi^2 \sin^2 2\pi\zeta}{(1 + \phi \sin 2\pi\zeta)^{\frac{3m+1}{m}}} \right)^m d\zeta$$

$$- \int_{\zeta_1}^{\zeta_2} \left(\frac{((2\phi - \phi^2/2)\textcircled{H} - \phi^2/2 + 2\phi \sin 2\pi\zeta + \phi^2 \sin^2 2\pi\zeta)}{(1 + \phi \sin 2\pi\zeta)^{\frac{3m+1}{m}}} \right)^m d\zeta \qquad \text{(B-30)}$$

$$+ \int_{\zeta_2}^{1.0} \left(\frac{-((2\phi - \phi^2/2)\textcircled{H} - \phi^2/2 + 2\phi \sin 2\pi\zeta + \phi^2 \sin^2 2\pi\zeta)}{(1 + \phi \sin 2\pi\zeta)^{\frac{3m+1}{m}}} \right)^m d\zeta$$

where ζ_1 and ζ_2 are found from equation B-26.

A similar relation may be derived for case II. The left hand side of equation B-30 is a dimensionless pressure rise per wavelength. Equation B-30 establishes the relationship between this dimensionless pressure rise per wavelength and the dimensionless time-mean flow rate $\textcircled{H}$, the pump characteristic relationship. Equation B-30 has been integrated numerically and a digital computer program in FORTRAN language to accomplish this integration has been included in Appendix E.

Note that the relationship given in equation B-30 reduces to the relationship presented by Shapiro et al.[34] for a Newtonian fluid when the flow behavior index, m , is equal to 1.0.

C. APPENDIX

C.1 Reynolds Number

In the analyses presented in Appendices A and B, the Reynolds number was assumed small enough such that the inertial terms in the equations of motion might be neglected. It is of interest, therefore, to determine an appropriate Reynolds number for the peristaltic pumping of a pseudoplastic fluid.

The Reynolds number measures the ratio of the inertial forces to the viscous forces within the fluid. From the equation of motion, this ratio is given by

$$Re_y = \frac{\rho u \left(du/dx\right)}{\frac{\partial}{\partial y}\left(\tau_{yx}\right)} \qquad \text{(c-1)}$$

Under conditions where the peristaltic wave acts like a pump, the longitudinal velocity as observed in the wave reference frame, is of order c. The coordinate x may be considered to be of order λ and the coordinate y of order a. Thus a typical inertia term $\rho u \partial u/dx$ is of order $\rho c^2 \lambda$. The shear stress τ_{yx} is defined for a pseudoplastic fluid by the relationship

$$\tau_{yx} = k\left(\frac{\partial u}{\partial y}\right)^n \qquad \text{(C-2)}$$

The shear stress is of order kc^n/a^n and the viscous term

$\frac{\partial}{\partial y}(\tau_{yx})$ is of order Kc^n/a^n. Thus the Reynolds number defined by equation C-1 is of order $\left(\frac{\rho a^n c^{2-n}}{K}\right)(a/\lambda)$. For n = 1.0, this relationship reduces to the Reynolds number derived by Shapiro et al.[34] for the peristaltic pumping of Newtonian fluids.

D. APPENDIX

D.1 Derivation of the Rabinowitsch-Mooney Equations

Consider the flow in a uniform cylindrical tube of radius R as shown in figure D-1. The following assumptions are made:

1. the fluid is in steady laminar flow;
2. the fluid is time-independent (this assumption rules out thixotropic and viscoelastic fluids.);
3. there is no slip between the fluid and the walls of the tube; and,
4. body forces may be neglected.

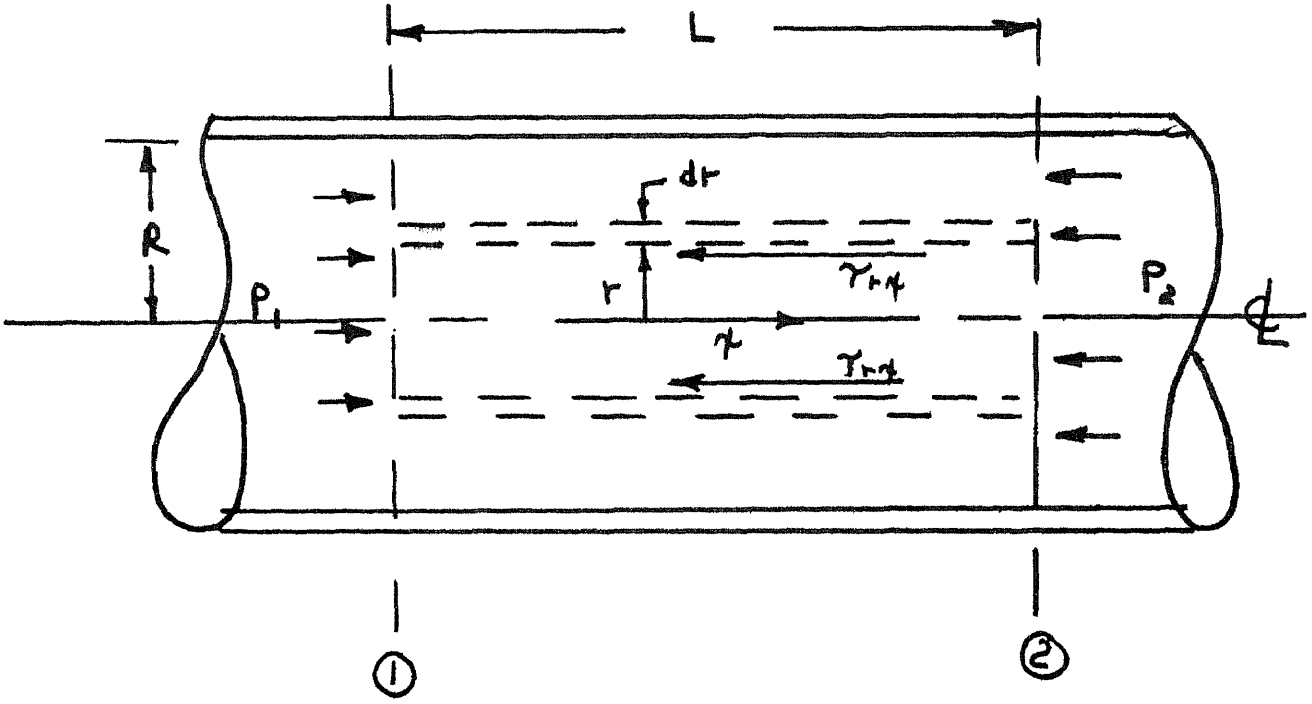

Figure D-1 Stresses Acting on a Cylindrical Element of Fluid

Making a force balance on a cylindrical element of radius r between sections 1 and 2

$$\pi r^2 P_1 - \pi r^2 P_2 - 2\pi r L \tau_{rx} = 0 \qquad \text{(D-1)}$$

$$\tau_{rx} = \frac{r \Delta P}{2L} \qquad \text{(D-2)}$$

The volumetric flow rate through the differential annulus between r and $r+dr$ is

$$dQ = u (2\pi r) dr \qquad \text{(D-3)}$$

$$Q = \pi \int_0^{R^2} (u)\, d(r^2) \qquad \text{(D-4)}$$

This expression may be integrated by parts

$$Q = \pi u r^2 \Big|_0^{R^2} - \pi \int_0^{R^2} r^2 du \qquad \text{(D-5)}$$

Applying the non-slip condition of assumption 3 ($u = 0$ at $r = R$), the first term of equation D-5 is zero.

$$Q = -\pi \int_0^{R^2} r^2 du \qquad \text{(D-6)}$$

In general we may write

$$du = -f(\tau_{rx})\, dr \qquad \text{(D-7)}$$

where $f(\tau_{r\phi})$ is some arbitrary function of the shear stress.

From a force balance on a cylindrical element of radius R ,

(Equation D-2 with $r = R$)

$$\tau_w = R \Delta P / 2L \tag{D-8}$$

and

$$\tau_{r\phi} = (r/R)\, \tau_w \tag{D-9}$$

Re-writing equation D-9 as

$$r^2 = \frac{R^2 \tau_{r\phi}^2}{\tau_w^2} \quad \text{and} \quad dr = \frac{R}{\tau_w} d(\tau_{r\phi}) \tag{D-10}$$

and substituting into equation D-6

$$Q = \pi \int_0^{\tau_w} \frac{R^2 \tau_{r\phi}^2}{\tau_w^2} f(\tau_{r\phi}) \frac{R}{\tau_w} d\tau_{r\phi} \tag{D-11}$$

$$\frac{Q}{\pi R^3} = \frac{1}{\tau_w^3} \int_0^{\tau_w} \tau_{r\phi}^2 f(\tau_{r\phi})\, d\tau_{r\phi} \tag{D-12}$$

Multiply equation D-12 through by τ_w^3 and differentiate both sides with respect to τ_w using Leibnitz's rule for differentiating the integral

$$3\left(\frac{Q}{\pi R^3}\right)\tau_w^2 + \tau_w^3 \frac{d}{d\tau_w}\left(\frac{Q}{\pi R^3}\right) = \tau_w^2 f(\tau_w) \tag{D-13}$$

$$3\left(\frac{8Q}{\pi D^3}\right) + \tau_\omega \frac{d}{d\tau_\omega}\left(\frac{8Q}{\pi D^3}\right) = f(\tau_\omega) \qquad \text{(D-14)}$$

Recall that $f(\tau_\omega) = -\left(\frac{du}{dr}\right)_\omega$ and that $\tau_\omega = \frac{D\,\Delta P}{4L}$.

Substituting into equation D-14

$$3\left(\frac{8Q}{\pi D^3}\right) + \frac{D\,\Delta P}{4L}\left(\frac{d(8Q/\pi D^3)}{d(D\Delta P/4L)}\right) = -\left(\frac{du}{dr}\right)_\omega \qquad \text{(D-15)}$$

$$\tau_\omega = \frac{D\,\Delta P}{4L} \qquad \text{(D-16)}$$

Equations D-15 and D-16 allow us to relate the shear stress at the wall to the shear rate at the wall in terms of measurable quantities. Equations D-15 and D-16 are known as the Rabinowitsch-Mooney equations.

D.2 Laminar Flow of a Pseudoplastic Fluid Through a Uniform Cylindrical Tube

Recall the general Rabinowitsch-Mooney relationship for a time-independent fluid given by equation D-12

$$\frac{Q}{\pi R^3} = \frac{1}{\tau_\omega^3} \int_0^{\tau_\omega} \tau_{r\theta}^2 f(\tau_{r\theta}) \, d\tau_{r\theta} \tag{D-12}$$

For a pseudoplastic fluid

$$f(\tau_{r\theta}) = -\frac{dv}{dr} = \left(\frac{1}{k}\right)^{\frac{1}{n}} (\tau_{r\theta})^{\frac{1}{n}} \qquad (\tau_{r\theta} \geq 0) \tag{D-17}$$

Substituting equation D-17 into D-12

$$\frac{Q}{\pi R^3} = \frac{1}{\tau_\omega^3} \left(\frac{1}{k}\right)^{\frac{1}{n}} \int_0^{\tau_\omega} \tau_{r\theta}^2 (\tau_{r\theta})^{\frac{1}{n}} \, d\tau_{r\theta} \tag{D-18}$$

Equation D-18 may be integrated directly to yield

$$\tau_\omega = k \left(\frac{3n+1}{n}\right)^n \left(\frac{8Q}{\pi D^3}\right)^n \tag{D-19}$$

Recall that

$$\tau_\omega = \frac{D \Delta P}{4L} \tag{D-8}$$

The pressure flow relationship then becomes

$$\Delta P = \left(\frac{4L}{D}\right)(K)\left(\frac{3n+1}{n}\right)^n \left(\frac{8Q}{\pi D^3}\right)^n \qquad \text{(D-20)}$$

E. APPENDIX (Numerical Integration-Axisymetric Case)

```
*JOB  AXISYM
*NOLIST
    8 READ 10,  EN,PHI,  N1,  N2,  N3,  TH1,  TH2,  THINC
   10 FORMAT(2F10.0,3I10,2F10.0,F9.0)
      IF (EN)   650,  650,  12
   12 THETA = TH1
   14 X1 = -(2.0*PHI-PHI*PHI/2.0)   * THETA  + PHI*PHI/2.0
      XPRIM = -X1
      IF (X1) 20,  100, 120
   20 Z = 3.1415926
      D = Z
   25 Z=Z-((2.0*PHI*SIN(Z))+PHI*PHI*SIN(Z)*SIN(Z)-X1)/(2.0*PHI*COS(Z)+
     1   2.0*PHI*PHI*SIN(Z)*COS(Z))
      IF (ABS(    Z-D)-0.001)40,  40,  30
   30 D=Z
      GO TO 25
   40 ZLIM1 = Z
      ZLIM2 = (3.0*3.1415926)-Z
      FN1=N1
      H1=ZLIM1/FN1
      SUM4=0.0
      SUM2=0.0
      I=1
      Y=H1
   41 ALPHA =       XPRIM+2.0*PHI*SIN(Y)+PHI*PHI*SIN(Y)*SIN(Y)
      BETA = 1.0+PHI*SIN(Y)
      BETA = BETA**(((3.0*EN)+1.0)/EN)
      GAMMA=ALPHA/BETA
      GAMMA=GAMMA**EN
      SUM4=SUM4+GAMMA
      DELTA=XPRIM+2.0*PHI*       SIN(Y+H1)+PHI*PHI*SIN(Y+H1)*SIN(Y+H1)
       EPS=1.0+PHI*SIN(Y+H1)
      EPS=EPS**(((3.0*EN)+1.0)/EN)
      ZETA=DELTA/EPS
      ZETA=ZETA**EN
      SUM2=SUM2+ZETA
      IF(I-N1+3)45,50,50
   45 I=I+2
      Y=Y+2.0*H1
      GO TO 41
   50 ALP=XPRIM+2.0*PHI*SIN(ZLIM1-H1)+PHI*PHI*SIN(ZLIM1-H1)*
     1   SIN(ZLIM1-H1)
      BET=1.0+PHI*SIN      (ZLIM1-H1)
      BET=BET**(((3.0*EN)+1.0)/EN)
      GAM=ALP/BET
      GAM=GAM**EN
      VAL1=(H1/(3.0*6.2831852))*(4.0*SUM4+2.0*SUM2+4.0*GAM+XPRIM**EN)
      VAL1=-VAL1
      FN2=N2
      H2=       (ZLIM2-ZLIM1)/FN2
      SUM4=0.0
      SUM2=0.0
      I=1
      Y=(ZLIM1+H2)
   51  ALPH2=XPRIM+2.0*SIN(Y)*PHI+PHI*PHI*SIN(Y)*SIN(Y)
```

```
      ALPH2=-ALPH2
      BETA2=1.0+PHI*SIN(Y)
      BETA2=BETA2**(((3.0*EN)+1.0)/EN)
      GAMM2=ALPH2/BETA2
      GAMM2=GAMM2**EN
      SUM4=SUM4+GAMM2
      DELT2=XPRIM+2.0*PHI*SIN(Y+H2)+PHI*PHI*SIN(Y+H2)*SIN(Y+H2)
      DELT2=-DELT2
      EPS2=1.0+PHI*SIN(Y+H2)
      EPS2=EPS2**(((3.0*EN)+1.0)/EN)
      ZETA2=DELT2/EPS2
       ZETA2=ZETA2**EN
      SUM2=SUM2+ZETA2
      IF (I-N2+3)   55, 60,  60
55    I=I+2
      Y=Y+2.0*H2
      GO TO 51
60    ALP2=XPRIM+2.0*PHI*SIN(ZLIM2-H2)+PHI*PHI*SIN(ZLIM2-H2)*SIN(ZLIM2-
     1    H2)
      ALP2=-ALP2
      BET2=1.0+PHI*SIN(ZLIM2-H2)
      BET2=BET2**(((3.0*EN)+1.0)/EN)
      GAM2=ALP2/BET2
      GAM2=GAM2**EN
      VAL2=(H2/(3.0*6.2831852))*(4.0*SUM4+2.0*SUM2+4.0*GAM2)
      FN3=N3
      H3=(6.2831852-ZLIM2)/FN3
      SUM4=0.0
       SUM2=0.0
      I=1
      Y=ZLIM2+H3
61    ALPH3=XPRIM+2.0*SIN(Y)*PHI+PHI*PHI*SIN(Y)*SIN(Y)
      BETA3=1.0+PHI*SIN(Y)
      BETA3=BETA3**(((3.0*EN)+1.0)/EN)
      GAMM3=ALPH3/BETA3
      GAMM3=GAMM3**EN
      SUM4=SUM4+GAMM3
      DELT3=XPRIM+2.0*PHI*SIN(Y+H3)+PHI*PHI*SIN(Y+H3)*SIN(Y+H3)
      EPS3=1.0+PHI*SIN(Y+H3)
      EPS3=EPS3**(((3.0*EN)+1.0)/EN)
      ZETA3=DELT3/EPS3
      ZETA3=ZETA3**EN
      SUM2=SUM2+ZETA3
      IF(I-N3+3)65,70,70
65    I=I+2
      Y=Y+2.0*H3
      GO TO 61
70    ALP3=XPRIM+2.0*PHI*SIN(6.2831852-H3)+PHI*PHI*SIN(6.2831852-H3)*
     1    SIN(6.2831852-H3)
      BET3=1.0+PHI*SIN(6.2831852-H3)
      BET3=BET3**(((3.0*EN)+1.0)/EN)
      GAM3=ALP3/BET3
      GAM3=GAM3**EN
      VAL3=(H3/(3.0*6.2831852))*     (4.0*SUM4+2.0*SUM2+4.0*GAM3+
     1    XPRIM**EN          )
      VAL3=-VAL3
```

```
      VALUE=VAL1+VAL2+VAL3
      GO TO 500
  100 PRINT 110,X1
  110 FORMAT(1X,&X1=&,F10.5)
      THETA=THETA+THINC
      IF(THETA-TH2)  14,14,8
  120 Z=0.0
      D=Z
  125 Z=Z-((2.0*PHI*SIN(Z))+PHI*PHI*SIN(Z)*SIN(Z)-X1)/(2.0*PHI*COS(Z)+
     1    2.0*PHI*PHI*SIN(Z)*COS(Z))
      IF(ABS(Z-D)-0.001)  140,140,130
  130 D=Z
      GO TO 125
  140 ZLIM1=Z
      ZLIM2=3.1415926-Z
      FN1=N1
      H1=ZLIM1/FN1
      SUM4=0.0
      SUM2=0.0
      I=1
      Y=H1
  141 ALPHA=XPRIM+2.0*PHI*SIN(Y)+PHI*PHI*SIN(Y)*SIN(Y)
      ALPHA=-ALPHA
      BETA=1.0+PHI*SIN(Y)
      BETA=BETA**(((3.0*EN)+1.0)/EN)
      GAMMA=ALPHA/BETA
      GAMMA=GAMMA**EN
      SUM4=SUM4+GAMMA
      DELTA=XPRIM+2.0*PHI*SIN(Y+H1)+PHI*PHI*SIN(Y+H1)*SIN(Y+H1)
      DELTA=-DELTA
      EPS=1.0+SIN(Y+H1)*PHI
      EPS=EPS**(((3.0*EN)+1.0)/EN)
      ZETA=DELTA/EPS
      ZETA=ZETA**EN
      SUM2=SUM2+ZETA
      IF(I-N1+3)  145,150,150
  145 I=I+2
      Y=Y+2.0*H1
      GO TO 141
  150 ALP=XPRIM+2.0*PHI*SIN(ZLIM1-H1)+PHI*PHI*SIN(ZLIM1-H1)*SIN(ZLIM1-
     1    H1)
      ALP=-ALP
      BET=1.0+PHI*SIN(ZLIM1-H1)
      BET=BET**(((3.0*EN)+1.0)/EN)
      GAM=ALP/BET
      GAM=GAM**EN
      VAL1=(H1/(3.0*6.2831852))*(4.0*SUM4+2.0*SUM2+4.0*GAM+
     1 ((-1.0)*(XPRIM))**EN)
      FN2=N2
      H2=          (ZLIM2-ZLIM1)/FN2
      SUM4=0.0
      SUM2=0.0
      I=1
       Y=ZLIM1+H2
  151 ALPH2=XPRIM+2.0*PHI*SIN(Y)+PHI*PHI*SIN(Y)*SIN(Y)
      BETA2=       1.0+PHI*SIN(Y)
```

```
      BETA2=BETA2**(((3.0*EN)+1.0)/EN)
      GAMM2=ALPH2/BETA2
      GAMM2=GAMM2**EN
      SUM4=SUM4+GAMM2
       DELT2=XPRIM+2.0*PHI*SIN(Y+H2)+PHI*PHI*SIN(Y+H2)*SIN(Y+H2)
      EPS2=   1.0+PHI*SIN(Y+H2)
       EPS2=EPS2**(((3.0*EN)+1.0)/EN)
       ZETA2=DELT2/EPS2
      ZETA2=ZETA2**EN
      SUM2=SUM2+ZETA2
      IF(I-N2+3)          155,160,160
155   I=I+2
      Y=Y+2.0*H2
      GO TO 151
160   ALP2=XPRIM+      2.0*PHI*SIN(ZLIM2-H2)+PHI*PHI*SIN(ZLIM2-H2)*
     1    SIN(ZLIM2-H2)
      BET2=1.0+PHI*SIN(ZLIM2-H2)
      BET2=BET2**(((3.0*EN)+1.0)/EN)
      GAM2=ALP2/BET2
      GAM2=GAM2**EN
      VAL2=(H2/(3.0*6.2831852))*(4.0*SUM4+2.0*SUM2+4.0*GAM2)
      VAL2=-VAL2
      FN3=N3
      H3=       (6.2831852-ZLIM2)/FN3
      SUM4=0.0
      SUM2=0.0
      I=1
      Y=ZLIM2+H3
161     ALPH3=XPRIM+2.0*PHI*SIN(Y)+PHI*PHI*SIN(Y)*SIN(Y)
       ALPH3=-ALPH3
      BETA3=1.0+PHI*SIN(Y)
      BETA3=BETA3**(((3.0*EN)+1.0)/EN)
      GAMM3=ALPH3/BETA3
      GAMM3=GAMM3**EN
      SUM4=SUM4+GAMM3
      DELT3=XPRIM+2.0*PHI*SIN(Y+H3)+PHI*PHI*SIN(Y+H3)*SIN(Y+H3)
      DELT3=-DELT3
      EPS3=1.0+PHI*SIN(Y+H3)
      EPS3=EPS3**(((3.0*EN)+1.0)/EN)
      ZETA3=DELT3/EPS3
      ZETA3=ZETA3**EN
      SUM2=SUM2+ZETA3
      IF(I-N3+3)        165,170,170
165   I=I+2
      Y=Y+2.0*H3
       GO TO 161
170   ALP3=XPRIM+ 2.0*PHI*SIN(6.2831852-H3)+PHI*PHI*SIN(6.2831852-H3)*
     1     SIN(6.2831852-H3)
       ALP3=-ALP3
      BET3=1.0+PHI*SIN(6.2831852-H3)
      BET3=BET3**(((3.0*EN)+1.0)/EN)
       GAM3=ALP3/BET3
      GAM3=GAM3**EN
      VAL3=(H3/(3.0*6.2831852))*(4.0*SUM4+2.0*SUM2+4.0*GAM3+
     1   ((-1.0)*(XPRIM))**EN)
      VALUE=VAL1+VAL2+VAL3
```

```
      GO TO 500
  500 PRINT 550,VALUE,THETA,EN,PHI
  550 FORMAT(1X,%VALUE=%,F10.5,%THETA=%,F10.5,%EN=%,F10.5,%PHI=%F10.5 )
      THETA=THETA+THINC
      IF(THETA-TH2)  14,14,8
  650 STOP
      END
```

(Two-Dimensional Case)

```
*JOB     SIMRUL
    8 READ 10,  EN,  PHI,  N1,  N2,  N3,  TH1,  TH2,  THINC
   10 FORMAT (2F10.0,3I10,2F10.0,F9.0)
      IF (EN)   250,  250,  12
   12 THETA = TH1
   20 X1 = THETA+THETA**3/6.0+(3.0*THETA**5)/40.0+       (5.0*THETA
     1  **7)/112.0+(35.0*THETA**9)/1152.0+(63.0*THETA**11)/2816.0
     2  +(231.0*THETA**13)/13312.0+(429.0*THETA**15)/30720.0
     3  +(6435.0*THETA**17)/557056.0+(12155.0*THETA**19)/1245184.0
      ZLIM1  =0.5 + X1/(2.0*3.1415926)
      ZLIM2 = 1.0 - X1/(2.0*3.1415926)
      FN1  =  N1
      H1  =  ZLIM1/FN1
      SUM4  =  0.0
      SUM2  =  0.0
      I  =  1
      Z  =  H1
   30 SUM4=SUM4+((THETA+SIN (6.2831852*Z))/(1.0+PHI*
     1 SIN (6.2831852*Z))**(((2.0*EN)+1.0)/EN))**EN
      SUM2=SUM2+((THETA+SIN (6.2831852*(Z+H1)))/(1.0+PHI*
     1SIN (6.2831852*(Z+H1)))**(((2.0*EN)+1.0)/EN))**EN
      IF (I - N1 +3)  40,  50,  50
   40 I = I + 2
      Z = Z + H1 + H1
      GO TO 30
   50 VAL1 = (H1/3.0)*((4.0*SUM4)+(2.0*SUM2)+1.0*(0.0001+THETA)**EN
     1  +4.0*((THETA + SIN (6.2831852*(ZLIM1 - H1)))/(1.0
     2  +PHI*SIN (6.2831852*(ZLIM1 - H1)))**(((2.0*EN) +1.0)/EN))**EN)
      VAL1= -VAL1
      FN2 = N2
      H2 = (ZLIM2 - ZLIM1)/FN2
      SUM4 = 0.0
       SUM2 = 0.0
      I = 1
      Z = ZLIM1 + H2
   60 GAMMA = THETA + SIN(6.2831852*Z)
      GAMMA = -GAMMA
      BETA = 1.0 + PHI*SIN(6.2831852*Z
      BETA = BETA**(((2.0*EN)+1.0)/EN)
```

```
      ALPHA = GAMMA/BETA
      ALPHA = ALPHA**EN
      SUM4 = SUM4 + ALPHA
      DELTA = THETA + SIN(6.2831852*(Z+H2)      )
      DELTA = -DELTA
       EPS = 1.0 + PHI*SIN (6.2831852*(Z+  H2))
      EPS = EPS**(((2.0*EN)+1.0)/EN)
       ZETA = DELTA/EPS
      ZETA = ZETA**EN
      SUM2 = SUM2 + ZETA
       IF (I - N2 + 3) 70,  80,  80
 70   I = I + 2
      Z = Z + H2 + H2
      GO TO 60
 80   AVAL = (H2/3.0)*((4.0*SUM4) + (2.0*SUM2)                    )
      BVAL = THETA + SIN(6.2831852*(ZLIM2 - H2))
      BVAL = -BVAL
      CVAL = 1.0 + SIN     (6.2831852*(ZLIM2 - H2))*PHI
      CVAL = CVAL**(((2.0*EN) + 1.0)/EN)
      DVAL = BVAL/CVAL
      DVAL = 4.0*DVAL**EN
      DVAL=DVAL*(H2/3.0)
      VAL2 = AVAL + DVAL
      FN3 = N3
      H3 = (       1.0 - ZLIM2) / FN3
      SUM4 = 0.0
      SUM2 = 0.0
      I = 1
      Z = ZLIM2 + H3
      ALPHA=0.0
      BETA=0.0
      GAMMA =0.0
       DELTA=0.0
      EPS=0.0
      ZETA = 0.0
 90   GAMMA=THETA + SIN(6.2831852*Z)
      BETA = 1.0+PHI*SIN(6.2831852*Z)
      BETA=BETA**(((2.0*EN)+1.0)/EN)
      ALPHA = GAMMA/BETA
      ALPHA = ALPHA**EN
      SUM4=SUM4+ALPHA
      DELTA = THETA + SIN      (6.2831852*(Z+H3))
      EPS = 1.0 + PHI*SIN(6.2831852*(Z+H3))
      EPS=EPS**(((2.0*EN)+1.0)/EN)
      ZETA = DELTA/EPS
      ZETA = ZETA**EN
       SUM2=SUM2 + ZETA
      IF (I - N3 + 3 )   100,   150,   150
100   I = I + 2
      Z = Z + H3 + H3
      GO TO 90
150   VAL3= (H3/3.0)*((4.0*SUM4)+(2.0*SUM2)+(1.0*THETA**EN) + 4.0*
     1  ((THETA +SIN (6.2831852*(1.0-H3)))/(1.0+PHI*SIN (6.2831852*
     2  (1.0 - H3)))**(((2.0*EN)+1.0)/EN))**EN)
       VAL3 = -VAL3
      VALUE = VAL1 + VAL2 + VAL3
```

```
      PRINT       200,   VALUE,  THETA,  EN,  PHI
  200 FORMAT(1X,&VALUE=&,F10.5,&THETA=&,F10.5,&EN=&, F10.5,&PHI=&,F10.5)
      THETA = THETA + THINC
      IF (THETA - TH2)       20,  20,  8
  250 STOP
      END
/$
```

F. APPENDIX

Table II shows the equipment used for the viscometric experiments

Table II

Photographic Equipment		
	Movie Camera	Bolex-Paillard H-16 Reflex 16 mm
	Camera Lens	Carl Zeiss 751756 f = 2.5 cm
	Camera Motor	Bolex-Paillard MCE 17 B
	Voltage Reg.	Bolex BXE 70 A
	Movie Film	Kodak Tri-X Reversal 16 mm B/W
Microscope and Micromanipulator		
	Microscope	Carl Zeiss Phase Contrast 4273712
	Objective lens	Carl Zeiss 16x l.w.d. 4411480
	Ocular lens	Carl Zeiss 12.5x
	Micromanipulator	L.P.C. distributed by Eric Sobotka Co., Inc. Farmingdale, New York
Pressure Recording Equipment		
	Transducer	Type 4-313 200psia Consolidated Engineering Corp. Pasadena, California
	Bridge Amplifier	Model BAM-1 Ellis Associates, Pelham, New York
	Oscilloscope	Tektronix Single Beam Storage Oscilloscope
Photographic Measurement Equipment		
	Film Analyzer	Vanguard Motion Analyzer, Vanguard Equipment Corp., New York

Table III lists information about the peristaltic wave model, including the type of fluids used, overall dimensions of the test channel and the ranges of the variables tested.

Table III

Test Fluids Used in Model

Glycerine	Merck Inc. Reagent Grade
Polyethylene Glycol 600	J. T. Baker co. P.E.G. 600
Sodium Carboxy-methyl cellulose	Hercules Powder Co. 7H3S

Dimensions and Ranges of Variables

Channel length	22"
Channel Width	2"
Channel Depth	0.25"
Wavespeed	0.211 - 2.46 in./sec.
Amplitude Ratio	0.3 - 0.6
Wavelength	3.5"

Additional Equipment

Capillary Viscometers	Cannon-Fenske sizes 100, 200, 300, 350, 400
Infusion Pump	Sigmamotor Inc., Middleport, New York, Model TM- 204
Pressure Transducer	Type 4-313 $\pm$ 5 psia Consolidated Eng. Corp., Pasadena, California

Mercury Thermometers, Stopwatch (0.01 min./div.), Graduated Cylinders

G. APPENDIX

Consider the experiment of drawing axoplasm up into a micropipette as discussed in section 2.3. Two quantities were calculated, the wall shear stress $\frac{D\Delta P}{4L}$ and the apparent shear rate at the wall $\frac{8V}{D} = \frac{8\Delta X}{D\Delta t}$. It may be shown that

$$\varepsilon_\tau = \left(\varepsilon_D^2 + \varepsilon_{\Delta P}^2 + \varepsilon_L^2\right)^{1/2}$$

$$\varepsilon_{S.R.} = \left(\varepsilon_{\Delta X}^2 + \varepsilon_{\Delta t}^2 + \varepsilon_D^2\right)^{1/2}$$

where ε_τ = relative error in determining the shear stress

$\varepsilon_{S.R.}$ = relative error in determining the apparent shear rate

ε_D = relative error in measuring the diameter D

ε_L = relative error in measuring the capillary length L

$\varepsilon_{\Delta P}$ = relative error in measuring the pressure difference across the capillary ΔP

$\varepsilon_{\Delta X}$ = relative error in measuring the movement of the meniscus ΔX

$\varepsilon_{\Delta t}$ = relative error in measuring the time interval Δt

It was assumed that the relative error in measuring the diameter D is independent of the error in measuring L or ΔX. This may be a reasonable assumption because ε_D depends on the accuracy of the measuring instrument whereas the accuracy in measuring L or ΔX is limited by the ability to visually establish the location of the meniscus and the location of the tip of the micropipette. Since axoplasm is relatively opaque, these were the most difficult measurements.

From experience in recording the data, the following estimates are made. $\varepsilon_D \sim \pm .1$, $\varepsilon_{\Delta P} \sim \pm .02$, $\varepsilon_L \sim \pm .01$, $\varepsilon_{\Delta t} \sim \pm .02$, $\varepsilon_{\Delta \gamma} \sim \pm .2$. Thus $\varepsilon_T = \pm .103$ and $\varepsilon_{S.R.} = \pm .225$. It was found that 92% of the data fell within these limits.

H. APPENDIX

H.1 Estimation of the Rate of Viscous Dissipation

The viscous dissipation term in the energy equation is given by

$$\Phi_v = \tau : \vec{V} \qquad \text{(scalar product)} \qquad \text{(H-1)}$$

where τ = Stress Tensor

$\vec{V}$ = Velocity Vector

The viscous dissipation per unit volume may be estimated by

$$\Phi_v \sim -\tau_{rx}\left(\frac{\partial U}{\partial R}\right) \qquad \text{(H-2)}$$

Recall that, for a pseudoplastic, the shear stress is related to the shear rate by

$$\tau_{rx} = -K\left(\frac{\partial U}{\partial R}\right)^n \qquad \left(\frac{\partial U}{\partial R} \geq 0\right) \qquad \text{(H-3)}$$

Thus,

$$\Phi_v \sim K\left(\frac{\partial U}{\partial R}\right)^{n+1} \qquad \text{(H-4)}$$

An estimate of the velocity gradient $\frac{\partial U}{\partial R}$ may be made. The longitudinal velocity in the laboratory reference frame may be expressed by

$$U = \left(\frac{3n+1}{n+1}\right) c \left(1 + Q/\pi h^2 c\right)\left(1 - (R/h)^{\frac{n+1}{n}}\right) \qquad \text{(H-5)}$$

The velocity gradient $\frac{\partial U}{\partial R}$ is given by

$$\frac{\partial U}{\partial R} = -\left(\frac{3n+1}{n}\right)(c)\left(1 + Q/\pi h^2 c\right)\left(R^{1/n}/h^{\frac{n+1}{n}}\right) \qquad \text{(H-6)}$$

At any given position X and time t, the maximum value of the velocity gradient occurs at the tube wall ($R = a$)

$$\left(\frac{\partial U}{\partial R}\right)_{\omega} = -\left(\frac{3n+1}{n}\right)\left(1 + \frac{q}{\pi a^2 c H^2}\right)\left(\frac{c}{(a)(H^{\frac{n+1}{n}})}\right) \qquad \text{(H-7)}$$

where $H = h/a = 1 + \phi \sin 2\pi\left(\frac{X - ct}{\lambda}\right)$

Recall that $$q/\pi a^2 c = (2\phi - \phi^2/2)\textcircled{H} - (1 + \phi^2/2) \qquad \text{(H-8)}$$

Thus the velocity gradient at the wall may be written

$$\left(\frac{\partial U}{\partial R}\right)_{\omega} = -\left(\frac{3n+1}{n}\right)\left(\frac{c}{a}\right)\left[1 + \frac{1}{H^2}\left((2\phi - \phi^2/2)\textcircled{H} - (1 + \phi^2/2)\right)\right]\left[\frac{1}{H^{\frac{n+1}{n}}}\right] \qquad \text{(H-9)}$$

The maximum value of $\left(\frac{\partial U}{\partial R}\right)_{\omega}$ occurs when $H = (1 - \phi)$.

$$\left(\frac{\partial U}{\partial R}\right)_{max} = -\left(\frac{3n+1}{n}\right)\left(\frac{c}{a}\right)\left[1 + \frac{1}{(1-\phi)^2}\left((2\phi - \phi^2/2)\textcircled{H} - (1 + \phi^2/2)\right)\right]\left[\frac{1}{(1-\phi)^{\frac{n+1}{n}}}\right] \qquad \text{(H-10)}$$

Substituting the values of $\phi = 0.523$, $c = 4.59$ mm/day, $n = 0.41$, $a = 5.0$ microns, $\textcircled{H} = \frac{V}{c}\left(\frac{1}{(2\phi - \phi^2/2)}\right) = 0.1174$ into equation H-10,

$$\left(\frac{\partial U}{\partial R}\right)_{max} = 2.6 \text{ sec.}^{-1}$$

Using equation H-4 and the value of $K = 3.38$ lb.-sec.^{n}/ft.^{2}

$$\Phi_{V_{max}} \sim 13.0 \frac{\text{ft.-lb.}}{\text{ft.}^3\text{-sec.}} = 0.148 \times 10^{-21} \frac{\text{Kcal.}}{\mu^3\text{-sec.}}$$

This is an estimate of the maximum rate of instantaneous viscous heat generation per unit volume. The time-average value at any point will be a considerably smaller quantity.

Assuming that all the heat generated by viscous friction must be conducted radially to the surrounding medium, and assuming, further, that this heat is generated uniformly at the maximum rate of viscous dissipation (actual generation will be considerably less), we may write

$$k \nabla^2 T = k \left(\frac{d^2 T}{dR^2} + \frac{1}{R} \frac{dT}{dR} \right) = - \Phi_{V_{max}}$$

ΔT = temperature difference between center and periphery of axon

$$= \Phi_{V_{max}} a^2 / 4k$$

Using the values of $\Phi_{V_{max}} = 13.0 \frac{\text{ft.-lb.}}{\text{ft.}^3\text{-sec.}}$, $a = 5$ microns $= 3.04 \times 10^{-5}$ ft., $k \cong$ thermal conductivity of water $= 0.065 \frac{\text{ft.-lb.}}{\text{ft.-sec.-}^\circ\text{F}}$

$$\Delta T \cong 1.35 \times 10^{-8} \, ^\circ\text{F}$$

It is apparent that the temperature differences due to viscous heat generation may be neglected.

VITA

Author: Robert John Biondi

Education:	1960-1964	Stevens Institute of Technology, M.E.
	1964-1967	Syracuse University, M. S. M. E.
	1967-Present	Newark College of Engineering
Professional Experience:	1964-1967	Design Engineer, Carrier Corporation Syracuse, New York
	1967-1968	Research Engineer, Worthington Air Conditioning Company, East Orange, New Jersey

Dissertation Research:

This dissertation is the result of more than two years full-time research in the Laboratory of Developmental Biology of Professor Paul A. Weiss, The Rockefeller University, New York, New York and in the Biomedical Engineering Laboratory of Professor Martin J. Levy, The Newark College of Engineering, Newark, New Jersey.